DEVELOPMENT AND EVALUATION OF A PROCEDURE FOR SIMULATING A RANDOM DIRECTIONAL SECOND ORDER SEA SURFACE AND ASSOCIATED WAVE FORCES

by

J. N. Sharma and R. G. Dean
Department of Civil Engineering
University of Delaware

Ocean Engineering Report No. 20

July, 1979

ACKNOWLEDGMENT

This report represents the dissertation of the first author. Financial support and encouragement for his work was provided by the following companies: Amoco Production Company, Continental Oil Company, Earl and Wright Consulting Engineers, Gulf Oil Corporation, J. Ray McDermott Company, Inc., Lloyd's Registry of Shipping, Marathon Oil Company, Mobil Research and Development Corporation, Phillips Petroleum Company, Shell Oil Company and Union Oil Company of California. Special appreciation is expressed to the Amoco Production Company which coordinated the industry support and to Dr. Frank Hsu who served as the Amoco representative for that effort. The support for the computer time was provided by the University of Delaware Computer Center and is gratefully acknowledged.

TABLE OF CONTENTS

LIST OF FIGURES

LIST OF TABLES

LIST OF SYMBOLS

$a_i, a_j, a_{ij}, a_m, a_n$	wave amplitudes
b_m, b_n	normalized wave amplitudes
$b_{ij}^{(2)}$	second order normalized amplitudes
$B(\ )$	function of frequency, spectral density and water depth
B_{ij}^{+}, B_{ij}^{-}	functions of wave numbers $\vec{k}_i$ and $\vec{k}_j$
C	$= \cos\theta$
C_1, C_2	constants
C_{ij}^{+}, C_{ij}^{-}	functions of wave numbers $\vec{k}_i$ and $\vec{k}_j$
C_D	coefficient of drag
C_M	inertia coefficient
C_ν	normalizing constant in directional distribution function
$D(\theta)$	directional spreading function
D_{ij}^{+}, D_{ij}^{-}	functions of $\vec{k}_i$, $\vec{k}_j$, R_i, R_j and h
D_x, D_y	horizontal drag force components
E, E_f	total energy in feet^2
F_x, F_y	horizontal force components
F_{NL}	wave force computed by a nonlinear wave theory

g	acceleration due to gravity
h	water depth in feet
H	wave height in feet
i	a subscript
I_x, I_y	horizontal inertia force components
j	a subscript
k, k_i, k_j, k_m, k_n	wave numbers in feet^{-1}
k_{ij}^{+}, k_{ij}^{-}	second order wave numbers
$\vec{k}, \vec{k}_i, \vec{k}_j, \vec{k}_m, \vec{k}_n$	horizontal vector wave numbers
$\vec{k}_{ij}^{+}, \vec{k}_{ij}^{-}, \vec{k}_{ij}^{(2)}$	second order horizontal vector wave numbers
k_3	skewness coefficient in feet^3
K	skewness kernel values in feet^{-1}
ℓ	dimensionless parameter derived from wave numbers
m	a subscript
M	a number
n	a subscript
$\vec{n}$	unit normal vector
N	a number
NU	a positive number characterizing directional spread of wave energy
$Q(t)$	Bernoulli term
Re	Reynolds number

R, R_i, R_j, R_n	$= k_n \tanh k_n h$, reduced wave numbers
s	elevation above the bottom
$S(\sigma)$	spectral density of water surface displacement
$S(\sigma,\theta), S_{\eta\eta}(\sigma,\theta)$	directional spectral densities of water surface displacement
$S_{ff}(\sigma,\theta)$	spectral density of wave forces
t	time in seconds
T	wave period in seconds
T_{LDS}	pseudo-transfer cofficient
$T_{\eta f}$	linearized transfer function for computing forces from water surface displacement
u	velocity in x direction
$\dot{u}$	acceleration in x direction
v	velocity in y direction
$\dot{v}$	acceleration in y direction
w	velocity in z direction
$\vec{x}, \vec{x}_m, \vec{x}_n$	horizontal Cartesian vectors
$\epsilon, \epsilon_1, \epsilon_2, \epsilon_i, \epsilon_j, \epsilon_{ij}$	random phases drawn from uniform distribution between $(0, 2\pi)$
η	water surface displacement
η_1, η_2	two random variables
$\eta^{(1)}$	first order water surface

displacement

$\eta^{(2)}$ second oreder water surface displacement

θ angle in radians

θ_o principal direction

θ_* the most forceful direction

ν a positive number characterizing directional spread of wave energy

ρ mass density of water in slugs/feet

$\rho_{uv}, \rho_{u\dot{v}}, \rho_{u\dot{u}}, \rho_{\dot{u}v}, \rho_{v\dot{v}}, \rho_{\dot{u}\dot{v}}$ correlations amongst horizontal water particle kinematics

σ σ_i, σ_j , σ_n frequency in radians/second

σ_o frequency corresponding to a peak in spectral density

$\sigma_{ij}^{(2)}$ second order frequency

$\sigma_u, \sigma_{\dot{u}}$, σ_v, $\sigma_{\dot{v}}$ standard deviations of horizontal water particle kinematics

τ duration of simulated realizations

Φ scalar velocity potential

$\Phi^{(1)}$ first order velocity potential

$\Phi^{(2)}$ second order velocity potential

$\Psi_i, \Psi_j, \Psi_m, \Psi_n, \Psi_{mn}$ functions of frequency, horizontal location vector, time and random phases

ABSTRACT

The boundary value problem with the appropriate boundary conditions for the three dimensional nonlinear random wave field is reviewed. Using perturbation techniques, the nonlinear problem is converted into a series of linear (in the unknowns of that order) boundary value problems. These are solved to the second order for the finite depth case in terms of finite Fourier sums, including relationships for the second order interaction components. The results obtained are verified with available solutions for more special cases.

Formulas are developed for:

(i) the correlations and probability density for the water particle kinematics, and distribution of force per unit length of a pile,

(ii) a closed form solution for the joint probability density of the inline and the cross forces for the drag dominant case and a three dimensional random sea, and

(iii) the effects of finite time simulation on the mean

square value of a random realization, and on the correlations amongst the simulated variables.

Wave forces due to a directional nonlinear random sea are simulated via the following steps:

(i) a linear short-crested sea is represented by a number of Fourier components propagating in many directions;

(ii) second order correction components are computed by the formulas developed;

(iii) water particle kinematics and sea surface displacement are computed by the superposition of the linear and nonlinear components;

(iv) wave forces are computed by the Morison formula; and

(v) total forces on a pile are computed up to the free surface.

Some of the more notable features of the present method are that it :

(i) correctly models the intercorrelations and skewnesses of the variables in the wave field;

(ii) includes nonlinearity correct up to second order;

(iii) preserves the phases of the nonlinear corrections;

(iv) provides the capability to model any directional energy spectrum; and

(v) computes total force up to the actual free surface.

The above method is applied to simulate linear and nonlinear random realizations of the sea surface for the Bretschneider spectrum and four different directional spreads. The nonlinearity represented by the skewness is computed in each case and it is found that the skewness is greatest for a narrow directional spread because for any given two wave numbers the skewness kernel is largest for small included angles. The reasons for this phenomenon and the possible occurrence of negative skewness in the field are discussed.

The simulation method is further applied to compute total wave forces on a single pile and a multiple pile group. The total force on a pile reduces by a factor of 1 to 0.61 with increase in the directional spread of the energy spectrum from unidirectional to omnidirectional. For the four pile group with 60 feet separation the reduction factors are similar to those for the single pile case. These results are the same as those obtained by a so-called hybrid method (Dean 1977) for a drag dominant case. For a four pile group with one pile at each corner of a 300 feet square the reduction factor varies from 0.79 to 0.39 for the directional spectrum varying from unidirectional to omnidirectional.

These results suggest that considerable economy can be realized in the design of large structures by incorporating the directional effects of a real sea.

CHAPTER 1

INTRODUCTION

The storm characteristics to be considered in developing design wave forces for offshore structures differ substantially depending on the area in which the structure is to be installed. Some design storms may be fairly distant from the site of interest, in which case the effects of dispersion result in a fairly periodic and long-crested design wave. A more common situation in many cases is that in which the structure is located near to or in the storm generating area. In this case realistic design waves, particularly those due to hurricanes, should include the following three important characteristics:

(1) Nonlinearity:- waves with peaked crests and shallow troughs;

(2) Randomness:- lack of order or regularity in the wave motion; and

(3) Directionality:- waves approaching from many directions resulting in short-crestedness.

Nonlinear and random aspects of the ocean waves have recieved considerable attention (see Hudspeth, 1974 for bibliography). The methodologies presently in use for calculating wave forces on offshore structures depend heavily on the stream function method (Dean, 1965; Dalrymple, 1974) for extreme nonlinear wave analysis and linear spectral methods for compliant structures (Borgman, 1967; Malhotra and Penzien, 1970).

1.1 Directional Effects

In the absence of definitive measured directional spectra and economical calculation procedures, the directional characteristics of ocean waves have been ignored in the inline force methods of design and analysis of ocean structures. The inline force methods seem to yield reasonably good results. However, the consideration of multidirectional seas can substantially affect the wave forces as discussed below:

(1) Dean (1977) showed that the forces on four piles could be reduced significantly (upto 23%) for a directional sea state compared to a unidirectional sea condition.

(2) In and near hurricanes, waves travel in many directions resulting in a short-crested condition. Partial instantaneous standing waves may form resulting in high particle velocities below relatively low water elevations and low particle velocities below high sea surface displacements.

(3) The drag component of the total wave force is a quadratic function of the water particle velocity. In a random sea state associated with strong hurricane winds there may be large velocity components normal to the inline (predominant) force direction. Thus the resultant velocity and the wave forces differ considerably for a directional sea.

(4) Nonlinear effects generate sums and differences of the frequencies associated with the linear spectrum. Conceivably these frequencies could coincide with the natural period of a structure causing a relatively large response.

(5) Total second order components are less in the directional sea state compared to the unidirectional sea condition. For example a wave of amplitude a, frequency σ and wave number k travelling in water of

depth h has a second order Stokes amplitude

$$\frac{ka^2}{4} \frac{\cosh kh}{\sinh^3 kh} \left(\cosh 2kh + 2\right) \tag{1-1}$$

Now instead of one wave at 90 degrees, consider 3 waves of amplitudes $a/\sqrt{3}$ coming from directions 30, 90 and 150 degrees with respect to x axis. In this case the amplitude of the second order Stokes component is

$$\frac{1}{3} \frac{ka^2}{4} \frac{\cosh kh}{\sinh^3 kh} \left(\cosh 2kh + 2\right) \tag{1-2}$$

In addition there will be three more second order components, with amplitudes less than a/100, in directions 60, 90 and 120 degrees with respect to the x axis.

Thus the directional aspects of ocean waves may be as important as the nonlinear and random aspects, which have received considerable attention in the past.

1.2 Objectives

In the present study the nonlinearity, randomness and directionality, all important elements of ocean waves, have been retained. The twofold nonlinearity, one due to the nonlinear boundary condition at the surface and the second due to the drag force relationship, prevent a closed form solution for the wave forces from being obtained. Therefore, in the present study, the wave forces due to a nonlinear directional random sea have been simulated via the following steps:

(i) A linear directional sea has been represented by a number of discrete frequencies and at each frequency there are several wave components with independent phases propagating in several directions;

(ii) Second order perturbation components including all fundamental interactions have been computed according to the analytical formulation developed for the finite depth case;

(iii) Water particle kinematics have been computed from the linear and the nonlinear second order perturbation components;

(iv) The wave forces have been computed from the water particle kinematics and the Morison formula using suitable drag and inertia coefficients suggested by Dean and Aagaard (1970).

The above simulation method has been implemented for several directional spreads and compared with the results of the hybrid method proposed by Dean (1977).

The present study also includes the following theoretical investigations:

(i) Formulas for the second order perturbation components of a directional random sea in finite depth have been developed.

(ii) Since the most important single measure of nonlinearity is the skewness, the related kernels for the finite depth case have been studied in detail. Kernels for the finite depth case have been compared with those given by Longuet-Higgins (1963) for infinite depth.

(iii) A possible mechanism has been suggested to explain some of the observed negative skewnesses.

(iv) Formulas for intercorrelations and probability densities of the water particle kinematics in a linear random wave field have been derived.

(v) The joint distribution for the components of drag force has been derived from the given joint Gaussian distribution for the components of water particle kinematics for the directional sea.

(vi) Formulas have been presented to explain the effects of finite time simulation on the mean square value of a random realization and on the correlations amongst the simulated variables.

The present dissertation has been organized as follows:

(i) A brief review of the pertinent previous studies is presented in Chapter 2.

(ii) In Chapter 3 the theoretical relations for the second order perturbation solutions for finite depth have been derived. Formulas for the three dimensional simulation of the nonlinear random sea surface and associated water particle kinematics have been developed.

(iii) Statistical relations for linear random directional sea have been derived in Chapter 4.

(iv) Chapter 5 contains the methodology of simulation used in this study.

(v) The simulation method has been implemented and example results presented in Chapter 6.

(vi) The summary of results and conclusions are contained in the seventh chapter.

CHAPTER 2

BACKGROUND AND REVIEW OF RELATED LITERATURE

As discussed in the previous chapter, the problem of computing design wave forces is complicated due to the nonlinearity of the waves and the complexities of the random and directional sea surface. Two essentially different but complementary approaches have developed in an attempt to establish realistic design wave loadings.

2.1 Extreme Nonlinear Wave Models

One approach is to represent nonlinearities of the motion for a single wave composed of a characteristic fundamental period and its higher harmonics. A number of such theories have been developed (Skjelbreia and Hendrickson, 1961; Chappelear, 1961; Dean, 1965; Von Schwind and Reid, 1972; Laitone, 1960). Dalrymple (1974) extended the stream function approach of Dean to the waves on a shear current. Some of these theories can be shown to account for the nonlinearities adequately; however, they avoid the random and directional characteristics of the sea surface.

2.2 Linear Random Models

The second approach exploits the principle of linear superposition of infinitely many waves having given frequencies, amplitudes and directions of propagation, but independent phases. The total energy is distributed over a continuum of frequencies and directions. In this manner, a three dimensional random Gaussian sea can be represented fully. However, ignoring the nonlinearities makes the random Gaussian model unrealistic, especially for large waves.

Following Rice (1944), both Rudnick (1951) and Birkhoff and Kotik (1951) suggested that the random sea can be modelled as a Gaussian process. Birkhoff and Kotik (1951) elaborated on the principle of random phases as applicable to ocean wave problems. Pierson (1955) developed the Gaussian model further, applying it to several oceanographic problems. In this model the sea surface is represented by the following pseudo-integral

$$\eta(\vec{x}, t) = \int_0^\infty \int_{-\pi}^{\pi} \sqrt{S(\sigma,\theta)\, \Delta\sigma\, \Delta\theta}\; \cos\left\{\vec{k}\,\vec{x} - \sigma t + \epsilon(\sigma,\theta)\right\} \qquad (2\text{-}1)$$

in which

σ is angular frequency

k is wave number related to σ by the dispersion relation

$$\sigma^2 = gk \tanh kh \tag{2-2}$$

h is depth of water

g is acceleration due to gravity

θ is direction of propagation

$S(\sigma,\theta)$ is the energy density associated with the frequency σ and wave direction θ such that the unidirectional spectrum is

$$S(\sigma) = \int_{-\pi}^{\pi} S(\sigma,\theta)\, d\theta \tag{2-3}$$

and the total energy E is

$$E = \int_0^{\infty}\int_{-\pi}^{\pi} S(\sigma,\theta)\, d\theta\, d\sigma \tag{2-4}$$

$\epsilon(\sigma,\theta)$ is the random phase lying between $(-\pi, \pi)$ and independent of all the other phases.

Pierson (1955) has given a proof that Equation (2-1) represents a three dimensional stationary Gaussian process.

Longuet-Higgins in a series of articles (1956,1957,1961) presented a comprehensive account of a random moving surface, including derivations of the following statistical properties:

(i) the probability distribution of the surface elevation and the magnitude and orientation of the gradient;

(ii) the average number of zero crossings per unit distance along a line in an arbitrary direction;

(iii) the average length of the contours per unit area, and the distribution of their directions;

(iv) the average density of maxima and minima per unit area of the surface, and the average density of specular points (i.e. points where the two components of gradient take given values);

(v) the probability distribution of the velocities of zero-crossing along a line;

(vi) the probability distribution of the velocities of contours and of specular points;

(vii) the probability distribution of the envelope and phase angle; and

(viii) when the spectrum is narrow, the probability distribution of the heights of maxima and minima and the distribution of the intervals between successive zero-crossings along an arbitrary line.

All the results are expressed in terms of the two-dimensional energy spectrum of the surface, and have been found to involve the moments of the spectrum up to a finite order only. Properties (i) and (iii) to (vi) have been discussed in detail for the special case of a narrow band spectrum. The converse problem, given certain statistical properties of the surface, to find a convergent sequence of approximation to the energy spectrum, has also been studied and solved (Longuet-Higgins, 1957, 1961)

Borgman (1969) has given relations between the variables of interests such as water particle velocity, water surface elevation etc. in a directional spectra model for design use.

2.3 Wave Force Probability and Spectral Density

Pierson and Holmes (1965) and Borgman (1967) have applied a linear unidirectional Gaussian model to derive the probability density of wave forces obtained from the Morison formula. From the joint Gaussian distribution of velocity and acceleration, Pierson and Holmes have derived the probability density of force as an integral to be evaluated numerically. For zero mean velocity Borgman (1967) has expressed the integral in terms of parabolic cylindrical functions.

Borgman (1967) has also developed the linearized spectral density of wave forces on a pile due to a random Gaussian sea. The drag force component has been approximated in the simplest form by a linear relation. He has also presented relationships for cubic and quintic approximations. These and other statistical models for waves and wave forces have been summarized by Borgman (1973).

The influence of current on random wave forces has been studied by Tung and Huang (1972,1973). They extended the results of Borgman (1967) to include the presence of steady current and the effects of wave-current interactions. They have reported that for forces on members near the surface the interactions are more important than for forces on members near the bottom. The wave-current interactions have mild effects on the statistical distribution of the maxima of sea surface elevation. The various aspects of wave-current interactions have been reviewed by Peregrine (1976).

2.4 Linear Filter Models

Reid (1958) developed a method for linear filtering of a sea surface record to obtain the kinematics required to compute forces on a pile by the Morison formula. Wheeler (1969) used this technique to compute force coefficients from measured hurricane wave records and reported very little difference between the measured and the predicted peak forces at different elevations of an instrumented piling. Hudspeth et.el. (1974) applied this technique using hurricane records and reported mean square errors for forces computed over the crest portion of the records which compared favorably with mean square errors from pressure forces computed using Dean's stream function method (1965). In another application Hudspeth (1974,1975) used the linear filtering method to obtain the water particle kinemtics from the nonlinear random sea simulation.

2.5 Nonlinear Random Models

Stokes' perturbation method has been extended to random waves by Tick (1959,1961), Phillips (1960,1961), Hasselman (1962,1963) and Longuet-Higgins (1962,1963). The first three authors have assumed a first order stationary Gaussian solution in terms of the Fourier-Stieltje's integral. Tick's derivation extended to the second order, and was illustrated by an example of a nonlinear realization in deep water (1963). The same paper included the nonlinear interaction kernel for the finite depth case. Phillips, Hasselman and Longuet-Higgins have carried out the perturbation scheme to higher order and shown that at higher orders, certain combinations of wave numbers interact resonantly and there is considerable energy transfer from one wave number to another. However, such resonant interactions and transfer of energy take place rather slowly and are of primary importance in the study of wave generation, wave transmission and swell propagation over long distances.

Tick restricted his perturbation derivation to the second order for unidirectional spectra. In search for a mechanism of wave generation, propagation and interactions, Phillips (1961) and Longuet-Higgins (1962) carried out the perturbation to the third order and Hasselman (1962-63) to the sixth order in energy spectrum, but restricted their derivation to the deep water case partly due to the fact that: (1) the relations for the deep water case are simpler and still bring out the underlying theory without the complexities of the finite depth equations, and (2) the physical processes of wave generation, propagation and interaction which they had in mind to model are primarily deep water phenomena. Unlike Tick their derivation is for directional seas, because unidirectional spectral models do not present interesting solutions even at higher perturbation than second order. Also wave generation, propagation and interaction take place in all directions on an ocean surface.

Longuet-Higgins (1963) developed a perturbation solution assuming the first order solution as the sum of large number of waves having different frequencies and wave numbers but independent phases. He used his solution to compute skewness coefficients for surface elevation and compared with the skewness computed by Kinsman (1960) from field data. The agreement between the skewnesses predicted by theory and those computed from the field data is remarkable particularly in light of the fact that the theory does not take into account the random fluctuating pressure due to the wind blowing over the water surface.

2.6 Nonlinear Random Model in Deep Water

The theoretical derivation of Longuet-Higgins (1963) is reviewed here because the theoretical derivations of this study follow the functional approximation approach of Longuet-Higgins and not the measure theory approach of Tick and others.

A random homogeneous surface displacement on water of infinite depth has been represented to the first approximation by

$$z = \eta^{(1)} \qquad (2\text{-}5)$$

where

$$\eta^{(1)} = \sum_{n=1}^{N} a_n \cos\psi_n \,, \quad \psi_n = \vec{k}_n \cdot \vec{x} - \sigma_n t + \epsilon(\vec{k}_n) \qquad (2\text{-}6)$$

in which

$\vec{x}$ is the horizontal vectorial Cartesian coordinate

t is time

$\vec{k}_n$ is a horizontal vector wave number

σ_n is angular frequency related to $\vec{k}_n$ by the following dispersion relation

$$\sigma_n^2 = g\,|\vec{k}_n| \qquad (2\text{-}7)$$

g being the acceleration due to gravity

a_n and $\epsilon(\vec{k}_n)$ are amplitudes and random phases so that $a_n \cos\epsilon$ and $a_n \sin\epsilon$ are jointly normal with ϵ uniformly distributed and

$$\sum_{\vec{k}_n \ni d\vec{k}} \tfrac{1}{2} a_n^2 = E(\vec{k})\, d\vec{k} \quad . \qquad (2\text{-}8)$$

Corresponding to the free surface elevation $\eta^{(1)}$ there is a velocity potential

$$\phi^{(1)} = \sum_{n=1}^{N} b_n \, e^{k_n z} \sin\psi_n \; ; \quad b_n = \frac{a_n \sigma_n}{k_n} \tag{2-9}$$

However, $\eta^{(1)}$ and $\phi^{(1)}$ are only the first approximation to the solution of Laplace equation. To satisfy the nonlinear boundary condition at the free surface, terms of higher order are considered in the series expansion

$$\eta = \eta^{(1)} + \eta^{(1)} + \eta^{(3)} + \cdots\cdot \tag{2-10}$$

$$\phi = \phi^{(1)} + \phi^{(2)} + \phi^{(3)} + \cdots\cdot \tag{2-11}$$

in which $\eta^{(2)}$ and $\phi^{(2)}$ contain terms proportional to the product of the linear amplitudes, $\eta^{(3)}$ and $\phi^{(3)}$ contain terms proportional to the third order products of the amplitudes, and so on. The equations for $\phi^{(2)}$ and $\eta^{(2)}$ are

$$\nabla^2 \phi^{(2)} = 0 \tag{2-12}$$

$$\nabla \phi^{(2)} \to 0 \quad , \quad z \to -\infty \tag{2-13}$$

After Taylor Series expansion about z=0,

$$\left(\frac{\partial^2}{\partial t^2}+g\frac{\partial}{\partial z}\right)\phi^{(2)}=-\frac{\partial}{\partial t}\left(\nabla\phi^{(1)}\right)^2-\eta^{(1)}\frac{\partial}{\partial z}\left(\frac{\partial^2}{\partial t^2}+g\frac{\partial}{\partial z}\right)\phi^{(1)};\ z=0 \qquad (2\text{-}14)$$

$$\eta^{(2)}=-\frac{1}{g}\left[\frac{\partial\phi^{(2)}}{\partial t}+\frac{1}{2}(\nabla\phi^{(1)})^2+\eta^{(1)}\frac{\partial^2\phi^{(1)}}{\partial z\,\partial t}\right];\quad z=0 \qquad (2\text{-}15)$$

It is assumed that the mean level $\overline{\eta^{(2)}}$ is zero. Substituting $\phi^{(1)}$ in Equation (2-14) and after some reduction we obtain

$$\left(\frac{\partial^2}{\partial t^2}+g\frac{\partial}{\partial z}\right)\phi^{(2)}$$
$$=-\sum_{i=1}^{N}\sum_{j=1}^{N} b_i\, b_j\, \left[(\sigma_i-\sigma_j)(\vec{k}_i\cdot\vec{k}_j+k_i\,k_j)\ \sin(\psi_i-\psi_j)\right.$$
$$\left.+(\sigma_i+\sigma_j)\ (\vec{k}_i\cdot\vec{k}_j-k_i\,k_j)\sin(\psi_i+\psi_j)\right] \qquad (2\text{-}16)$$

To satisfy the above and Equation (2-13), $\phi^{(2)}$ is of the form

$$\phi^{(2)}=\sum_{i=1}^{N}\sum_{j=1}^{N}\left[C_{ij}^{-}\ e^{|\vec{k}_i-\vec{k}_j|z}\ \sin(\psi_i-\psi_j)\right.$$
$$\left.+\ C_{ij}^{+}\ e^{|\vec{k}_i+\vec{k}_j|z}\ \sin(\psi_i+\psi_j)\right. \qquad (2\text{-}17)$$

substituting in the above, $\phi^{(2)}$ is found as

$$\phi^{(2)} = \sum_{i=1}^{N} \sum_{j=1}^{N} b_i b_j \left[\frac{(\sigma_i - \sigma_j)(\vec{k}_i \cdot \vec{k}_j + k_i k_j)}{(\sigma_i - \sigma_j)^2 - g|\vec{k}_i - \vec{k}_j|} e^{|\vec{k}_i - \vec{k}_j| z} \sin(\psi_i - \psi_j) \right.$$

$$\left. + \frac{(\sigma_i + \sigma_j)(\vec{k}_i \vec{k}_j - k_i k_j)}{(\sigma_i + \sigma_j)^2 - g|\vec{k}_i + \vec{k}_j| z} e^{|\vec{k}_i + \vec{k}_j| z} \sin(\psi_i + \psi_j) \right] \qquad (2\text{-}18)$$

Inserting this in Equation (2-15)

$$\eta^{(2)} = \sum_{i=1}^{N} \sum_{j=1}^{N} a_i a_j \left[\left\{ \frac{B_{ij}^- - B_{ij}^+ - k_i k_j}{\sqrt{k_i k_j}} \right\} \sin\psi_i \sin\psi_j \right.$$

$$\left. + \left\{ \frac{B_{ij}^- + B_{ij}^+ - \vec{k}_i \vec{k}_j}{\sqrt{k_i k_j}} + (k_i + k_j) \right\} \cos\psi_i \cos\psi_j \right] \qquad (2\text{-}19)$$

in which

$$B_{ij}^- = \frac{(\sqrt{k_i} - \sqrt{k_j})^2 (\vec{k}_i \vec{k}_j + k_i k_j)}{(\sqrt{k_i} - \sqrt{k_j})^2 - |\vec{k}_i - \vec{k}_j|} \qquad (2\text{-}20)$$

$$B_{ij}^+ = \frac{(\sqrt{k_i} + \sqrt{k_j})^2 (\vec{k}_i \vec{k}_j + k_i k_j)}{(\sqrt{k_i} + \sqrt{k_j})^2 - |\vec{k}_i + \vec{k}_j|} \qquad (2\text{-}21)$$

The kernel in the skewness formula

$$k_3 = 6 \iiiint K(\vec{k}_i, \vec{k}_j)\; E(\vec{k}_i)\; E(\vec{k}_j)\; d\vec{k}_i\, d\vec{k}_j \qquad (2\text{-}22)$$

is

$$K(\vec{k}_i, \vec{k}_j) = \frac{B^{-}_{ij} + B^{+}_{ij} - k_i k_j + \sqrt{k_i k_j}\,(k_i + k_j)}{\sqrt{k_i k_j}} \qquad (2\text{-}23)$$

This skewness kernel has been further examined by Longuet-Higgins. The kernel has been expressed in terms of θ, the angle between the wave number vectors $\vec{k}_i$ and $\vec{k}_j$, and a dimensionless parameter ℓ

$$\ell = \frac{k_i + k_j}{2\,(k_i k_j)^{\frac{1}{2}}} \geq 1 \qquad (2\text{-}24)$$

such that

$$K(\vec{k}_i, \vec{k}_j) = (k_i\, k_j)^{\frac{1}{2}}\, f(\ell, \theta) \qquad (2\text{-}25)$$

in which

$$f(\ell, \theta) = \frac{(\ell-1)\,(1+c)}{(\ell-1) - \left(\ell^2 - \frac{1}{2} - \frac{c}{2}\right)^{\frac{1}{2}}} - \frac{(\ell+1)\,(1-c)}{(\ell+1) - \left(\ell^2 - \frac{1}{2} + \frac{c}{2}\right)^{\frac{1}{2}}} + (2\ell - c) \qquad (2\text{-}26)$$

and

$$c \equiv \cos\theta$$

It has been further shown that $f(\ell,\theta) > 0$. From this it immediately follows that the skewness coefficient is positive. The function $f(\ell,\theta)$ as given by Longuet-Higgins has been reproduced as Figure (2.1). In Chapter 6 this will be compared with a similar computation for the finite depth case.

2.7 Nonlinear Random Sea Simulation

Hudspeth (1974,1975) has solved the nonlinear boundary value problem for the propagation of random surface gravity waves in an ocean of finite depth. He has introduced a nonlinear interaction matrix facilitating the use of the Fast Fourier Transform in digital simulation of the nonlinear random sea correct to the second order. The second order correction to the linear first order wave spectrum has been computed and added to the linear spectral components. The time sequence of the random nonlinear waves is efficiently obtained by the inverse Fast Fourier Transform. This time sequence of the nonlinear random sea surface was filtered by a linear digital filter modified by a vertical coordinate stretching function. The water particle kinematics thus computed have been used in the Morison formula to compute the wave forces. Force spectra and normalized cumulative

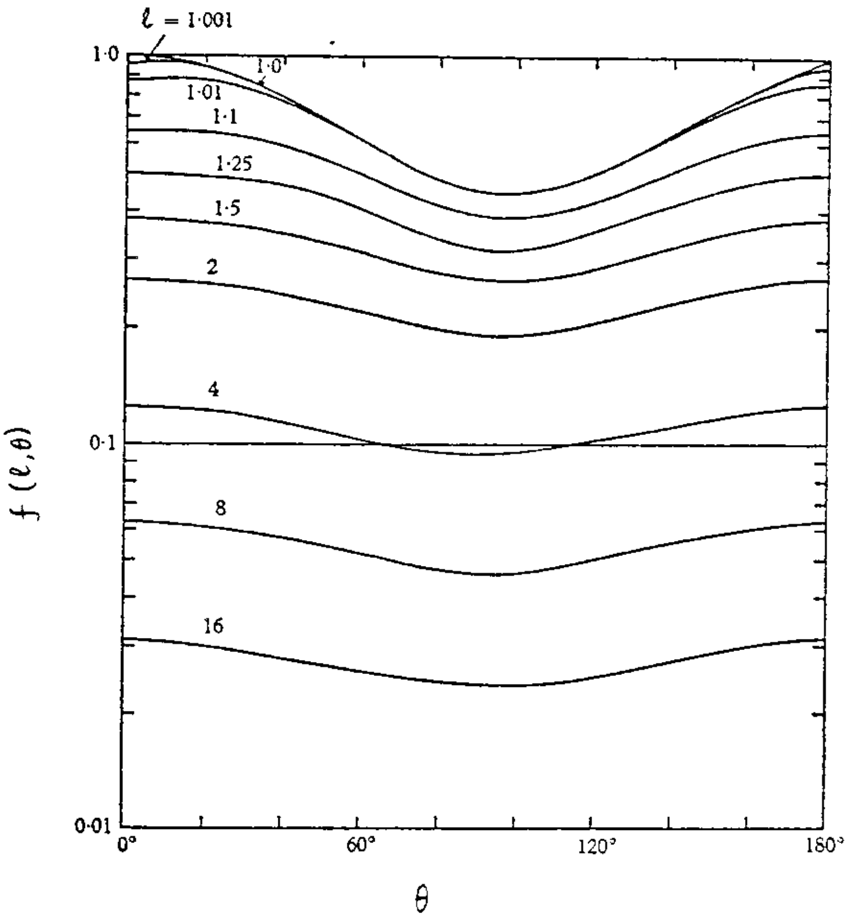

Figure 2-1. Graph of f(ℓ , θ) defined by Equation 2-26, for Various Values of ℓ (After Longuet-Higgins 1963).

probability distributions were computed from the pressure force realizations obtained by filtering simulated nonlinear random sea surface realizations. These simulated results were compared with the spectra and normalized cumulative probability distributions of the forces recorded during Hurricane Carla, by Wave Force Project II dynamometer at a distance of 55.3 feet above the ocean floor on an instrumented platform in a water depth of approximately 100 feet in the Gulf of Mexico. Hudspeth's simulation was restricted to unidirectional spectra and his comparison with measurements was limited to the measured inline forces.

2.8 Hybrid Method

Dean (1977) proposed a hybrid method for computing design wave force and moment loading on an offshore structure. The hybrid method is a combination of linear and nonlinear wave theories incorporating the most significant features of the real sea, i.e. the nonlinearities and the directional spectrum. Wave loading due to nonlinear waves with energy present over a continuum of frequencies and directions is represented by the product of a nonlinear wave force and a linearized force transfer coefficient, the latter representing the effect of the directional spectrum. The force, F_{NLDS}, due to a nonlinear directional sea is presented as

$$F_{NLDS} = F_{NL} \cdot T_{LDS} \tag{2-27}$$

in which

F_{NL} is the wave force computed by a wave theory applicable for nonlinear waves of a single fundamental period propagating in a single direction

T_{LDS} is a pseudo-transfer coefficient based on linear wave theory.

The following directional spreading function was used

$$\begin{aligned} D_\nu(\theta) &= C_\nu \cos^{2\nu}(\theta - \theta_0) \quad , \ |\theta - \theta_0| < \frac{\pi}{2} \\ &= 0 \quad , \ |\theta - \theta_0| > \frac{\pi}{2} \end{aligned} \tag{2-28}$$

in which

θ_0 is the principal direction

ν is a positive real number

C_ν is a coefficient such that

$$\int_{-\pi}^{\pi} D_\nu(\theta)\, d\theta = 1 \tag{2-29}$$

For a wave of single frequency acting on a single piling, it has been shown that

$$T_{LDS} = \sqrt{\frac{C_\nu}{C_{\nu+1}}} \tag{2-30}$$

in an inertia-dominant case and

$$T_{LDS} = \frac{C_\nu}{C_{\nu+1}} \tag{2-31}$$

in a drag-dominant case.

For a complete directional spectrum of the form

$$S_{\eta\eta}(\sigma, \theta) = S_{\eta\eta}(\sigma) \cdot D_\nu(\theta) \tag{2-32}$$

the spectrum of the total linearized force in the direction θ_* is

$$S_{ff}(\sigma, \theta_*) = \int_{-\pi}^{\pi} T_{\eta f}(\sigma)\, S_{\eta\eta}(\sigma)\, C_\nu \cdot$$

$$\cos^{2\nu}(\theta - \theta_o)\cos^2(\theta - \theta_*)\, d\theta \tag{2-33}$$

in which

$$T_{\eta f} = \left(\frac{8}{\pi}\, \overline{u^2}\, c_1^2 + c_2^2 \sigma^2\right) \sigma^2 \frac{\cosh^2 kS}{\sinh^2 kS} \tag{2-34}$$

S is elevation above bottom

h is depth of water

$$c_1 = \frac{c_D \rho}{2} D \tag{2-35}$$

$$C_2 = \frac{C_m \rho \pi D^2}{4} \tag{2-36}$$

T_{LDS} in the above case has been derived as

$$T_{LDS} = \frac{\int_0^{\infty} \int_0^{2\pi} S_{\eta\eta}(\sigma, \theta_*)\, d\sigma\, d\theta_*}{\int_0^{\infty} S_{\eta\eta}(\sigma)\; T_{\eta f}(\sigma)\, d\sigma} \tag{2-37}$$

Examples of single and multiple pile presented show force reduction upto 23%. In Chapter 6 the results of the hybrid method will be compared with the results of the methods used in the present study.

CHAPTER 3

THEORY OF DIRECTIONAL NONLINEAR RANDOM WAVE INTERACTIONS

Random functions can be represented by either Fourier-Stieltjes integrals or Fourier integrals. Although the Fourier-Stieltjes integral representation does not require an a priori assumption regarding the existence of a density function and is therefore a much more powerful tool, the Fourier integral representation gives identical results for many practical situations, is more easily understood, and is readily computed. For these reasons, the finite Fourier approximations of the Fourier integral have been used in the present study.

The boundary value problem with the appropriate boundary conditions for the three dimensional nonlinear random wave field is defined and using perturbation techniques, the nonlinear problem is converted into linear (in the unknowns of that order) boundary value problems. These are solved for the finite depth case in terms of finite Fourier sums. Relationships for the second order interaction components are derived and the results obtained here compared with solutions due to Longuet-Higgins (1963) and Chappelear (1961) for more specialized conditions.

3.1 Fundamentals of Boundary Value Problem

If viscous and turbulence effects can be regarded as small (more precisely, if the motion is irrotational), incompressible flows can be well described by a potential function or stream function. The velocity potential ϕ can be defined in terms of the gradients of the velocity components:

$$u = \frac{\partial \phi}{\partial x}$$
$$v = \frac{\partial \phi}{\partial y} \tag{3-1}$$
$$w = \frac{\partial \phi}{\partial z}$$

The mass conservation equation for an incompressible fluid is

$$\frac{\partial u}{\partial x} + \frac{\partial v}{\partial y} + \frac{\partial w}{\partial z} = 0 \tag{3-2}$$

which yields

$$\frac{\partial^2 \phi}{\partial x^2} + \frac{\partial^2 \phi}{\partial y^2} + \frac{\partial^2 \phi}{\partial z^2} = 0$$

$$0 \le z \le h+\eta \, , \; -\infty \le x, y \le \infty \tag{3-3}$$

The appropriate boundary conditions (Figure 3.1) for the problem are presented below:

(1) Bottom Boundary Condition (BBC)

At the bottom boundary, the velocity normal to the boundary is equal to zero i.e. $\vec{v}.\vec{n}=0$. For the present case of a horizontal boundary at depth h

$$\frac{\partial \phi}{\partial z} = 0 \quad , \quad z = -h \, , \, -\infty \leq x, y \leq \infty \qquad (3\text{-}4)$$

(2) Kinematic Free Surface Boundary Condition (KFSBC)

The water particle on the free surface remains on the free surface i.e. the vertical velocity at the free surface is equal to the total rate of change of water elevation.

$$\frac{\partial \eta}{\partial t} + u\frac{\partial \eta}{\partial x} + v\frac{\partial \eta}{\partial y} = w \, , \quad z = \eta(x, y, t) \qquad (3\text{-}5)$$

(3) Dynamic Free Surface Boundary Condition (DFSBC)

At the free surface the pressure is equal to the atmospheric pressure. In the present case, the uniform surface pressure is taken as zero without loss of generality.

$$g\eta + \frac{1}{2}(u^2+v^2+w^2) + \frac{\partial \phi}{\partial t} = -Q(t) \, , \quad z = \eta(x, y, t) \qquad (3\text{-}6)$$

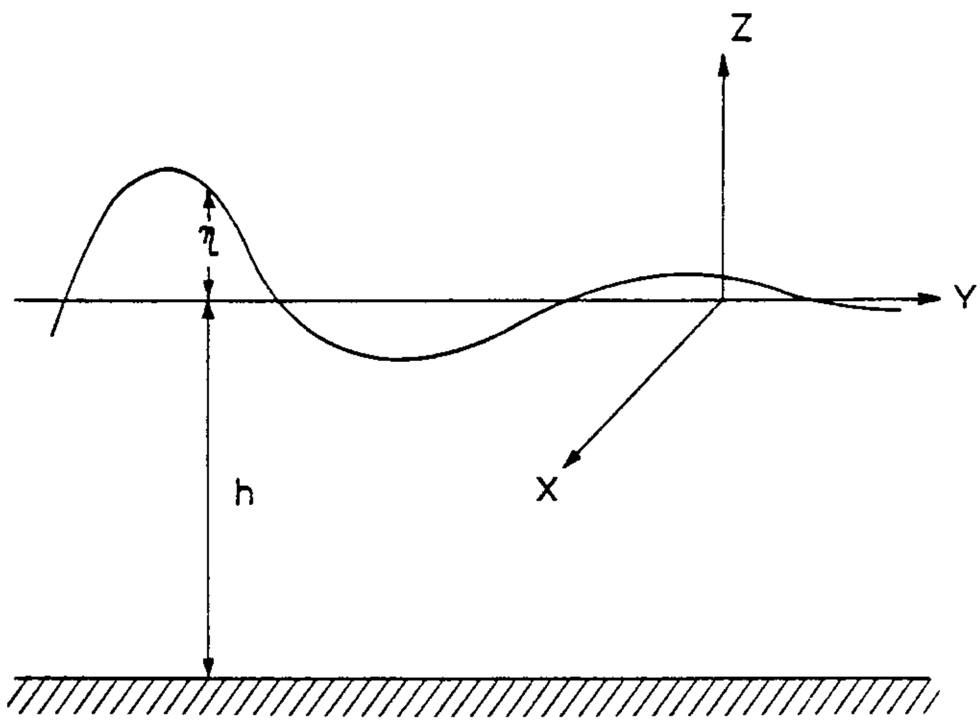

Figure 3-1. Definition of Boundary Value Problem.

which is recognized as an unsteady form of the Bernoulli equation with the so-called Bernoulli term, Q(t).

(4) Combined Free Surface Boundary Condition (CFSBC)

This is an alternative form of (2) and (3) above in which, by eliminating η, involves only ϕ and its derivatives. The total derivative of the Bernoulli equation after some reduction is

$$-\frac{\partial^2\phi}{\partial t^2} - g\frac{\partial\phi}{\partial z} - \frac{\partial Q}{\partial t}$$

$$-\left(\frac{\partial}{\partial t} + \frac{1}{2}\vec{\nabla}\phi\cdot\vec{\nabla}\right)|\vec{\nabla}\phi|^2 = 0$$

$$z = \eta(x,y,t) \qquad (3\text{-}7)$$

3.2 Method of Solution

The perturbation method is adopted here for solution of the boundary value problem formulated in the preceding section. This method assumes that:

(i) all variables can be expanded as a convergent power series of a small parameter such as water surface slope, and

(ii) the nonlinear CFSBC can also be expanded in a convergent Maclaurin series about the still water level z=0 with some parameter.

The random velocity potential ϕ, random sea surface η and the Bernoulli term Q(t) may be represented in the following manner with the perturbation parameter absorbed into the function:

$$\phi(x,y,z,t) = \phi^{(1)}(x,y,z,t) + \phi^{(2)}(x,y,z,t) + \cdots \qquad (3\text{-}8)$$

$$\eta(x,y,t) = \eta^{(1)}(x,y,t) + \eta^{(2)}(x,y,t) + \cdots \qquad (3\text{-}9)$$

$$Q(t) = Q^{(1)}t + Q^{(2)}(t) + \cdots \qquad (3\text{-}10)$$

Substituting into Laplace's equation we find

$$\nabla^2 \phi^{(1)}(x,y,z,t) = 0 \; ; \; \nabla^2 \phi^{(2)}(x,y,z,t) = 0 \; ; \cdots \qquad (3\text{-}11)$$

The bottom boundary condition becomes

$$\frac{\partial \phi^{(1)}}{\partial z} = 0 \; ; \; \frac{\partial \phi^{(2)}}{\partial z} = 0 \; ; \cdots \qquad z = -h \qquad (3\text{-}12)$$

Since the CFSBC is satisfied at the unknown free surface, it presents an additional difficulty. However, for small perturbation parameters the CFSBC can be expanded in a Maclaurin series about the mean water level z=0 to give

$$\sum_{n=0}^{\infty} \eta^n \frac{\partial^n}{\partial z^n}\left[\frac{\partial^2 \phi}{\partial t^2} + g\frac{\partial \phi}{\partial z} + \frac{\partial Q}{\partial t} + \left(\frac{\partial}{\partial t} + \frac{1}{2}\vec{\nabla}\phi\cdot\vec{\nabla}\right)\left|\vec{\nabla}\phi\right|^2\right] = 0 \; ; \; z = 0 \qquad (3\text{-}13)$$

Substituting the perturbation expansions for ϕ , η, and Q we find after some reduction

$$
\begin{aligned}
0 = & \frac{\partial^2}{\partial t^2}\left(\phi^{(1)} + \phi^{(2)} + \phi^{(3)} + \cdots\right) + g\frac{\partial}{\partial z}\left(\phi^{(1)} + \phi^{(2)} + \cdots\cdots\right) \\
& + \frac{\partial}{\partial t}\left(Q^{(1)} + Q^{(2)} + \cdots\cdots\right) + \frac{\partial}{\partial t}\left\{\left|\vec{\nabla}\left(\phi^{(1)} + \phi^{(2)} + \cdots\right)\right|^2\right\} \\
& + \frac{1}{2}\vec{\nabla}\left(\phi^{(1)} + \phi^{(2)} + \cdots\cdots\right)\cdot\vec{\nabla}\left\{\left|\vec{\nabla}\left(\phi^{(1)} + \phi^{(2)} + \cdots\right)\right|^2\right\} \\
& + \left(\eta^{(1)} + \eta^{(2)} + \cdots\right)\left[\frac{\partial^3}{\partial t^2 \partial z}\left(\phi^{(1)} + \phi^{(2)} + \cdots\right) + g\frac{\partial^2}{\partial z^2}\left(\phi^{(1)} + \phi^{(2)} + \cdots\right)\right] \\
& + \frac{1}{2}\frac{\partial}{\partial z}\left\{\vec{\nabla}\left(\phi^{(1)} + \phi^{(2)} + \cdots\right)\cdot\vec{\nabla}\left|\vec{\nabla}\left(\phi^{(1)} + \phi^{(2)} + \cdots\right)\right|^2\right\},
\end{aligned}
$$

$$z = 0 \qquad (3\text{-}14)$$

Terms of the same order are separated for later convenience.

$$
\begin{aligned}
0 = & \frac{\partial^2 \phi^{(1)}}{\partial t^2} + g\frac{\partial \phi^{(1)}}{\partial z} + \frac{\partial Q^{(1)}}{\partial t} \\
& + \frac{\partial^2 \phi^{(2)}}{\partial t^2} + g\frac{\partial \phi^{(2)}}{\partial z} + \frac{\partial Q^{(2)}}{\partial t} \\
& + \frac{\partial}{\partial t}\left|\vec{\nabla}\phi^{(1)}\right|^2 + \eta^{(1)}\left(\frac{\partial^3 \phi^{(1)}}{\partial t^2 \partial z} + g\frac{\partial^2 \phi^{(1)}}{\partial z^2}\right) \\
& + \text{terms of third and higher order}, \quad z = 0 \qquad (3\text{-}15)
\end{aligned}
$$

The dynamic free surface boundary condition is also expanded in a Maclaurin series about the mean water level to yield

$$\sum_{n=0}^{\infty} \eta^n \frac{\partial^n}{\partial z^n} \left\{ g\eta + \frac{1}{2}(u^2+v^2+w^2) + \frac{\partial \phi}{\partial t} + Q(t) \right\} = 0 \; , \quad z = 0 \qquad (3\text{-}16)$$

Substituting perturbation expansions for ϕ, η, and Q, and separating terms of the same order we obtain

$$0 = g\eta^{(1)} + \frac{\partial \phi^{(1)}}{\partial t} + F^{(1)} + g\eta^{(2)} + \frac{\partial \phi^{(2)}}{\partial t} + Q^{(2)}(t)$$
$$+ \frac{1}{2}|\vec{\nabla}\phi^{(1)}|^2 + \eta^{(1)} \frac{\partial^2 \phi^{(1)}}{\partial z \, \partial t}$$
$$+ \text{terms of third and higher order} \qquad (3\text{-}17)$$

The nonlinear boundary value problem posed earlier reduces to the following sets of linear (in the unknown of that order) boundary value problems :

(1) First Order Equations

$$\nabla^2 \phi^{(1)} = 0 \tag{3-18}$$

$$\frac{\partial \phi^{(1)}}{\partial z} = 0 \quad , \qquad z = -h \tag{3-19}$$

$$\frac{\partial^2 \phi^{(1)}}{\partial t^2} + g \frac{\partial \phi^{(1)}}{\partial z} + \frac{\partial Q^{(1)}}{\partial t} = 0 \quad , \qquad z = 0 \tag{3-20}$$

$$\eta^{(1)} = -\frac{1}{g}\left(\frac{\partial \phi^{(1)}}{\partial t} + Q^{(1)}(t)\right) \quad , \qquad z = 0 \tag{3-21}$$

(2) Second Order Equations

$$\nabla^2 \phi^{(2)} = 0 \tag{3-22}$$

$$\frac{\partial \phi^{(2)}}{\partial z} = 0 \quad , \qquad z = -h \tag{3-23}$$

$$\frac{\partial^2 \phi^{(2)}}{\partial t^2} + g \frac{\partial}{\partial z} \phi^{(2)} + \frac{\partial Q^{(2)}}{\partial t}$$

$$= -\frac{\partial}{\partial t} \left|\vec{\nabla} \phi^{(1)}\right|^2 - \eta^{(1)} \frac{\partial}{\partial z}\left(\frac{\partial^2 \phi^{(1)}}{\partial t^2} + g \frac{\partial \phi^{(1)}}{\partial z}\right) , \quad z = 0 \tag{3-24}$$

$$\eta^{(2)} = -\frac{1}{g}\left(\frac{\partial \phi^{(2)}}{\partial t} + \frac{1}{2}\left|\vec{\nabla} \phi^{(1)}\right|^2 + Q^{(2)} + \eta^{(1)} \frac{\partial^2 \phi^{(1)}}{\partial z \partial t}\right) , \; z = 0 \tag{3-25}$$

3.3 First Order Solution in Finite Depth

Assuming a velocity potential of the form

$$\phi^{(1)} = \sum_{n=1}^{\infty} b_n \frac{\cosh k_n(h+z)}{\cosh k_n h} \sin\left(\vec{k}_n \cdot \vec{x} - \sigma_n t + \epsilon_n\right) \tag{3-26}$$

satisfying

$$\begin{aligned} &\nabla^2 \phi^{(1)} = 0 \\ &\frac{\partial \phi^{(1)}}{\partial z} = 0 \quad , \quad z = -h \end{aligned} \tag{3-27}$$

we obtain for the free surface

$$\eta^{(1)} = \frac{1}{g} \sum b_n \sigma_n \cos\left(\vec{k}_n \cdot \vec{x} - \sigma_n t + \epsilon_n\right) \tag{3-28}$$

$$= \sum_{n=1}^{\infty} a_n \cos \psi_n \tag{3-29}$$

in which

$$a_n = \frac{b_n \sigma_n}{g} \tag{3-30}$$

$$\sigma_n^2 = g|\vec{k}_n| \tanh |\vec{k}_n| h \tag{3-31}$$

As shown by Birkhoff and Kotik (1951) and Pierson (1955) the above represents a Gaussian random sea surface if the phases are independent.

3.4 Second Order Solution in Finite Depth

Now assume the second order velocity potential to be represented as

$$\phi^{(2)} = \sum_{i=1}^{\infty} \sum_{j=1}^{\infty} b_{ij}^{(2)} \frac{\cosh |\vec{k}_{ij}^{(2)}| (h+z)}{\cosh |\vec{k}_{ij}^{(2)}| h} \sin\left(\vec{k}_{ij}^{(2)} \cdot \vec{x} - \sigma_{ij}^{(2)} t + \epsilon_{ij}^{(2)}\right) \quad (3\text{-}32)$$

satisfying $\nabla^2 \phi^{(2)} = 0$ and the bottom boundary condition; $\vec{k}_{ij}^{(2)}$ and $\sigma_{ij}^{(2)}$ are given by sums and differences of the fundamental vector wave numbers and frequencies. In order to evaluate $b_{ij}^{(2)}$, $k_{ij}^{(2)}$ and $\sigma_{ij}^{(2)}$, the second order potential represented by Equation (3-32) is substituted in the left hand hand side of Equation (3-24) and the first order velocity potential $\phi^{(1)}$ and water elevation $\eta^{(1)}$, represented by Equations (3-26), and (3-26) are substituted in the right hand side of Equation (3-24). The first term on the right hand side of Equation (3-24) is found to be

$$\begin{aligned} &-\frac{\partial}{\partial t} \left| \vec{\nabla} \phi^{(1)} \right|^2 \\ &= \sum_{i=1}^{\infty} \sum_{j=1}^{\infty} b_i b_j \sigma_j \Big[\left(\vec{k}_i \cdot \vec{k}_j + R_i R_j \right) \sin(\psi_i - \psi_j) \\ &\qquad - \left(\vec{k}_i \cdot \vec{k}_j - R_i R_j \right) \sin(\psi_i + \psi_j) \Big] \end{aligned} \quad (3\text{-}33)$$

in which $R_i = k_i \tanh k_i h = \dfrac{\sigma_i^2}{g}$

Reversing the roles of i and j

$$-\frac{\partial}{\partial t}\left|\vec{\nabla}\phi^{(1)}\right|^2$$

$$=\sum_{i=1}^{\infty}\sum_{j=1}^{\infty} b_i\, b_j\, \sigma_i\Big[(\vec{k}_i\cdot\vec{k}_j+k_i k_j)\sin(\psi_i-\psi_j)$$

$$-(\vec{k}_i\cdot\vec{k}_j-k_i k_j)\sin(\psi_i+\psi_j) \qquad (3\text{-}34)$$

Adding and dividing by two we obtain

$$-\frac{\partial}{\partial t}\left|\vec{\nabla}\phi^{(1)}\right|^2$$

$$=\sum_{i=1}^{\infty}\sum_{j=1}^{\infty}\frac{1}{2}\, b_i b_j\Big[(\sigma_i-\sigma_j)(\vec{k}_i\cdot\vec{k}_j+k_i k_j)\sin(\psi_i-\psi_j)$$

$$+(\sigma_i+\sigma_j)(\vec{k}_i\cdot\vec{k}_j-k_i k_j)\sin(\psi_i+\psi_j)\Big] \qquad (3\text{-}35)$$

The second term on the right hand side of Equation (3-24) is

$$-\eta^{(1)}\frac{\partial^3\phi^{(1)}}{\partial z\,\partial t^2}\bigg|_{z=0}=\frac{1}{2}\sum_{i=1}^{\infty}\sum_{j=1}^{\infty} b_i\, b_j\, \sigma_i\, k_j^2\left\{\sin(\psi_i+\psi_j)-\sin(\psi_i-\psi_j)\right\} \quad (3\text{-}36)$$

Similarly the last term on the right hand side of Equation (3-24) is

$$-\eta^{(1)} g\,\frac{\partial^2\phi^{(1)}}{\partial z^2}\bigg|_{z=0}$$

$$=-\frac{1}{2}\sum_{i=1}^{\infty}\sum_{j=1}^{\infty}\sigma_i\, k_j^2\left\{\sin(\psi_i+\psi_j)-\sin(\psi_i-\psi_j)\right\} \qquad (3\text{-}37)$$

Combining the last two equations we obtain

$$-\eta^{(1)} \frac{\partial}{\partial z}\left(\frac{\partial^2}{\partial t^2} + g\frac{\partial}{\partial z}\right)\phi^{(1)}\Big|_{z=0}$$

$$= -\frac{1}{2}\sum_{i=1}^{\infty}\sum_{j=1}^{\infty} \sigma_i\left(k_j^2 - R_j^2\right)\left\{\sin(\psi_i+\psi_j) - \sin(\psi_i-\psi_j)\right\} \quad (3\text{-}38)$$

Reversing the roles of i and j

$$-\eta^{(1)} \frac{\partial}{\partial z}\left(\frac{\partial^2}{\partial t^2} + g\frac{\partial}{\partial z}\right)\phi^{(1)}\Big|_{z=0}$$

$$= \frac{1}{2}\sum_{i=1}^{\infty}\sum_{j=1}^{\infty} b_i b_j \sigma_j\left(k_i^2 - R_i^2\right)\left\{\sin(\psi_i+\psi_j) - \sin(\psi_i-\psi_j)\right\} \quad (3\text{-}39)$$

Adding and dividing by two we obtain finally

$$-\eta^{(1)} \frac{\partial}{\partial z}\left(\frac{\partial^2}{\partial t^2} + g\frac{\partial}{\partial z}\right)\phi^{(1)}\Big|_{z=0}$$

$$= -\frac{1}{4}\sum\sum b_i b_j\left[\left(\sigma_i k_j^2 + \sigma_j k_i^2\right) - \left(\sigma_i R_j^2 + \sigma_j R_i^2\right)\right]\sin(\psi_i+\psi_j)$$

$$+\frac{1}{4}\sum_{i=1}^{\infty}\sum_{j=1}^{\infty} b_i b_j\left[\left(\sigma_i k_j^2 - \sigma_j k_i^2\right) - \left(\sigma_i R_j^2 - \sigma_j R_i^2\right)\right]\sin(\psi_i-\psi_j) \quad (3\text{-}40)$$

Equation (3-24) reduces to the following

$$\sum_{i=1}^{\infty}\sum_{j=1}^{\infty}\left\{-\left(\sigma_{ij}^{(2)}\right)^2+g\,k_{ij}^{(2)}\tanh k_{ij}^{(2)}h\right\} b_{ij}^{(2)}\sin\psi_{ij}^{(2)}$$

$$=\sum_{i=1}^{\infty}\sum_{j=1}^{\infty}-\tfrac{1}{2}b_i b_j\Big[(\sigma_i-\sigma_j)\left(\vec{k}_i\cdot\vec{k}_j+R_iR_j\right)\sin(\psi_i-\psi_j)$$

$$+(\sigma_i+\sigma_j)\left(\vec{k}_i\vec{k}_j-R_iR_j\right)\sin(\psi_i+\psi_j)\Big]$$

$$-\frac{1}{4}\sum_{i=1}^{\infty}\sum_{j=1}^{\infty}b_ib_j\left[(\sigma_ik_j^2+\sigma_jk_i^2)-(\sigma_iR_j^2+\sigma_jR_i^2)\right]\sin(\psi_i+\psi_j)$$

$$+\sum_{i=1}^{\infty}\sum_{j=1}^{\infty}b_ib_j\left[(\sigma_ik_j^2-\sigma_jk_i^2)-(\sigma_iR_j^2-\sigma_jR_i^2)\right]\sin(\psi_i-\psi_j) \quad (3\text{-}41)$$

From inspection $\phi^{(2)}$ has a solution of the form sin($\psi_i-\psi_j$) and sin($\psi_i+\psi_j$). Based on the preceding equation the solution of $\phi^{(2)}$ is obtained as

$$\phi^{(2)}=\frac{1}{2}\sum_{i=1}^{\infty}\sum_{j=1}^{\infty}b_ib_j\,\frac{\cosh k_{ij}^-(h+z)}{\cosh k_{ij}^-h}\,\frac{(\sigma_i-\sigma_j)(\vec{k}_i\cdot\vec{k}_j+R_iR_j)}{(\sigma_i-\sigma_j)^2-g\,k_{ij}^-\tanh k_{ij}^-h}\sin(\psi_i-\psi_j)$$

$$-\frac{1}{4}\sum_{i=1}^{\infty}\sum_{j=1}^{\infty}b_ib_j\,\frac{\cosh k_{ij}^-(h+z)}{\cosh k_{ij}^-h}\,\frac{(\sigma_ik_j^2-\sigma_jk_i^2)-(\sigma_iR_j^2-\sigma_jR_i^2)}{(\sigma_i-\sigma_j)^2-g\,k_{ij}^-\tanh k_{ij}^-h}\sin(\psi_i-\psi_j)$$

$$+\frac{1}{2}\sum_{i=1}^{\infty}\sum_{j=1}^{\infty}b_ib_j\,\frac{\cosh k_{ij}^+(h+z)}{\cosh k_{ij}^+h}\left\{\frac{(\sigma_i+\sigma_j)(\vec{k}_i\vec{k}_j-R_iR_j)}{(\sigma_i+\sigma_j)^2-g\,k_{ij}^+\tanh k_{ij}^+h}\sin(\psi_i+\psi_j)\right.$$

$$\left.+\frac{1}{2}\,\frac{(\sigma_ik_j^2+\sigma_jk_i^2)-(\sigma_iR_j^2+\sigma_jR_i^2)}{(\sigma_i+\sigma_j)^2-g\,k_{ij}^+\tanh k_{ij}^+h}\sin(\psi_i+\psi_j)\right\} \quad (3\text{-}42)$$

in which

$$k_{ij}^{-} = \left| \vec{k}_i - \vec{k}_j \right| \qquad (3\text{-}43)$$

$$k_{ij}^{+} = \left| \vec{k}_i + \vec{k}_j \right| \qquad (3\text{-}44)$$

A compact form of Equation (3-42) is

$$\phi^{(2)} = \frac{1}{4}\sum_{i=1}^{\infty}\sum_{j=1}^{\infty} b_i b_j \frac{\cosh k_{ij}^{-}(h+z)}{\cosh k_{ij}^{-} h} \frac{D_{ij}^{-}}{(\sigma_i - \sigma_j)} \sin(\psi_i - \psi_j)$$

$$+ \frac{1}{4}\sum_{i=1}^{\infty}\sum_{j=1}^{\infty} b_i b_j \frac{\cosh k_{ij}^{+}(h+z)}{\cosh k_{ij}^{+} h} \frac{D_{ij}^{+}}{(\sigma_i + \sigma_j)} \sin(\psi_i + \psi_j) \qquad (3\text{-}45)$$

in which

$$D_{ij}^{-} = \frac{(\sqrt{R_i} - \sqrt{R_j})\left\{\sqrt{R_j}\,(k_i^2 - R_i^2) - \sqrt{R_i}\,(k_j^2 - R_j^2)\right\}}{(\sqrt{R_i} - \sqrt{R_j})^2 - k_{ij}^{-} \tanh k_{ij}^{-} h}$$

$$+ \frac{2(\sqrt{R_i} - \sqrt{R_j})^2(\vec{k}_i \cdot \vec{k}_j + R_i R_j)}{(\sqrt{R_i} - \sqrt{R_j})^2 - k_{ij}^{-} \tanh k_{ij}^{-} h} \qquad (3\text{-}46)$$

$$D_{ij}^{+} = \frac{2(\sqrt{R_i} + \sqrt{R_j})^2(\vec{k}_i \cdot \vec{k}_j - R_i R_j)}{(\sqrt{R_i} + \sqrt{R_j})^2 - k_{ij}^{+} \tanh k_{ij}^{+} h}$$

$$+ \frac{(\sqrt{R_i} + \sqrt{R_j})\left\{\sqrt{R_i}\,(k_j^2 - R_j^2) + \sqrt{R_j}\,(k_i^2 - R_i^2)\right\}}{(\sqrt{R_i} + \sqrt{R_j})^2 - k_{ij}^{+} \tanh k_{ij}^{+} h} \qquad (3\text{-}47)$$

By substituting for the first order potential $\phi^{(1)}$ and water elevation $\eta^{(1)}$, and the second order potential $\phi^{(2)}$, represented by Equations (3-26), (3-28) and (3-49) respectively, in Equation (3-25), we obtain the second order corrections for water surface elevation :

$$\eta^{(2)} = \frac{1}{4}\sum_{i=1}^{\infty}\sum_{j=1}^{\infty} a_i a_j \Big[\Big\{ \frac{D_{ij}^{-} - (\vec{k}_i \cdot \vec{k}_j + k_i k_j)}{\sqrt{k_i k_j}} + (k_i + k_j) \Big\} \cos(\psi_i - \psi_j)$$

$$+ \Big\{ \frac{D_{ij}^{+} - (\vec{k}_i \cdot \vec{k}_j - k_i k_j)}{\sqrt{k_i k_j}} + (k_i + k_j) \Big\} \cos(\psi_i + \psi_j) \Big] \qquad (3\text{-}48)$$

An alternative form of this is

$$\eta^{(2)} = \frac{1}{4}\sum_{i=1}^{\infty}\sum_{j=1}^{\infty} a_i a_j \Big[\Big\{ \frac{D_{ij}^{-} - D_{ij}^{+} - 2 k_i k_j}{\sqrt{k_i k_j}} \Big\} \sin\psi_i \sin\psi_j$$

$$+ \Big\{ \frac{D_{ij}^{-} + D_{ij}^{+} - 2 \vec{k}_i \cdot \vec{k}_j}{\sqrt{k_i k_j}} + 2(k_i + k_j) \Big\} \cos\psi_i \cos\psi_j \qquad (3\text{-}49)$$

The skewness kernel as defined in Equation (2-22) is

$$K(\vec{k}_i, \vec{k}_j) = \frac{D_{ij}^{-} + D_{ij}^{+} - 2 \vec{k}_i \cdot \vec{k}_j}{4\sqrt{k_i k_j}} + \frac{1}{2}(k_i + k_j) \qquad (3\text{-}50)$$

For infinite depth the generalized derivation readily reduces to the equations derived by Longuet-Higgins (1963) for deep water. For $\vec{k}_i = \vec{k}_j$ and N=1, the formulas for potential function and water surface profile reduce to the familiar Stokes second order equations. Another check on the equations has been provided by deriving equations for velocity potential and water surface elevation for the short-crested wave system considered by Chappelear (1961)

CHAPTER 4

STATISTICAL RELATIONS FOR A LINEAR DIRECTIONAL SEA AND ASSOCIATED WAVE FORCES

Some of the statistical relations for the linear directional sea have been derived and will be presented and discussed in this chapter. In particular, formulas will be presented for the correlations and probability density for the water particle kinematics, probability distribution of force per unit length of a pile, and for the drag dominant case a closed form solution for the joint probability density of x and y force components for a three dimensional random sea.

In directional sea simulation, certain difficulties can be encountered due to adding the same frequency components with random independent phases. A discussion of this problem is followed by an investigation into the effects of finite time simulation on the mean square value of a random realization, and on the correlations amongst the simulated variables.

4.1 Probability Distribution of Water Particle Kinematics

A linear random sea is assumed to be represented as

$$\eta(\vec{x},t)=\sum_{m=1}^{M}\sum_{n=1}^{N}\sqrt{C_\nu\, S(\sigma_m)\,\Delta\sigma_m\,\Delta\theta_n}\,\cos^{\nu}\!\left(\theta_n-\frac{\pi}{2}\right)\cos\psi_{mn}\,, \qquad (4\text{-}1)$$

$$\psi_{mn} = \vec{k}_m\,\vec{x} - \sigma_m t + \epsilon_{mn}(\sigma_m,\theta_n)$$

$$0<\sigma_1<\sigma_2<\cdots\cdots<\sigma_M<\infty$$

$$-\frac{\pi}{2}<\theta_1<\theta_2<\cdots\cdots<\theta_N<\frac{\pi}{2}$$

which is a finite sum analogue of the pseudo-integral in Equation (2-1) with a directional distribution given as Equation (2-28). In the above the y direction is the predominant direction and θ_n is the direction in which each component propagates with respect to the x-axis. As mentioned in Chapter 2, Pierson (1955) has given a proof that Equation (4-1) in the limit represents a three dimensional Gaussian process.

The velocity field corresponding to the above is given by

$$\vec{u}(\vec{x},z,t)=\vec{\nabla}\,\phi(\vec{x},z,t) \qquad (4\text{-}2)$$

In particular the velocity in the x-direction is

$$u(\vec{x},z,t) = \frac{\partial \phi}{\partial x} = \sum_{m=1}^{M} \sum_{n=1}^{N} \sqrt{c_\nu \, S(\sigma_m) \, \Delta\sigma_m \, \Delta\theta_n} \; \cos^{\nu}\left(\theta_n - \frac{\pi}{2}\right)$$

$$\cos\psi_{mn} \, \frac{g\, k_m}{\sigma_m} \, \frac{\cosh k_m(h+z)}{\cosh K_m h} \cos\theta_n \tag{4-3}$$

This can be represented in abbreviated form as

$$\sum_{m=1}^{M} \sum_{n=1}^{N} B(k_m) \sqrt{C_\nu \, \Delta\sigma_m \, \Delta\theta_n} \; \cos^{\nu}\left(\theta_n - \frac{\pi}{2}\right)\left(-\sin\left(\theta_n - \frac{\pi}{2}\right)\right)\cos\psi_{mn} \tag{4-4}$$

in which

$$B(k_m) = \frac{\sqrt{S(\sigma_m)} \cdot g\, k_m \cosh k_m(h+z)}{\sigma_m \cosh K_m h} \tag{4-5}$$

$$\psi_{mn} = \vec{k}_m \cdot \vec{x} - \sigma_m t + \epsilon_{mn} \tag{4-6}$$

The average velocity is

$$\bar{u} = 0 \tag{4-7}$$

The mean square velocity in the x-direction is

$$\overline{u^2} = E\left\{ \left(\sum_{m=1}^{M} \sum_{n=1}^{N} B(K_m) \sqrt{C_\nu \, \Delta\sigma_m \, \Delta\theta_n} \right. \right.$$
$$\left. \cos^{\nu}(\theta_n - \tfrac{\pi}{2}) \left(-\sin(\theta_n - \tfrac{\pi}{2})\right) \cos\psi_{mn} \right) \cdot$$
$$\left(\sum_{m'=1}^{M} \sum_{n'=1}^{N} B(K_{m'}) \sqrt{C_\nu \, \Delta\sigma_{m'} \, \Delta\theta_{n'}} \right.$$
$$\left. \left. \cos^{\nu}(\theta_{n'} - \tfrac{\pi}{2}) \left(-\sin(\theta_{n'} - \tfrac{\pi}{2})\right) \cos\psi_{m'n'} \right) \right\} \qquad (4-8)$$

Since the linear system represented by Equation (4-1) is Gaussian only if the phases are independent, the average of the cross products is zero and the contribution to the sum is from the terms containing $\cos^2\psi_{mn}$ and the above reduces to

$$\overline{u^2} = \sum_{m=1}^{M} \sum_{n=1}^{N} B^2(K_m) \; C_\nu \, \Delta\sigma_m \, \Delta\theta_n$$
$$\cos^{2\nu}(\theta_n - \tfrac{\pi}{2}) \; \sin^2(\theta_n - \tfrac{\pi}{2}) \cos^2\psi_{mn} \qquad (4-9)$$

In the limit $N \to \infty$ and $\Delta\theta \to 0$

$$\overline{u^2} = \sum_{m=1}^{M} \tfrac{1}{2} \, B^2(K_m) \; \Delta\sigma_m \left(1 - \frac{C_\nu}{C_{\nu+1}}\right) \qquad (4-10)$$

Similarly for the velocity v in the y-direction

$$\overline{v} = 0 \tag{4-11}$$

and $$\overline{v^2} = \sum_{m=1}^{M} \tfrac{1}{2} B^2(k_m)\, \Delta\sigma_m \frac{C_\nu}{C_{\nu+1}} \tag{4-12}$$

Thus $$\overline{u^2} + \overline{v^2} = \sum_{m=1}^{M} \tfrac{1}{2} B^2(k_m)\, \Delta\sigma_m \tag{4-13}$$

The correlation between u and v is

$$\overline{uv} = E\Big[\Big\{\sum_{m=1}^{M}\sum_{n=1}^{N} B(k_m)\sqrt{C_\nu\,\Delta\sigma_m\,\Delta\theta_n}\,\cos^\nu(\theta_n-\tfrac{\pi}{2})(-\sin(\theta_n-\tfrac{\pi}{2}))\cos\psi_{mn}\Big\}\cdot$$

$$\cdot\Big\{\sum_{m'=1}^{M}\sum_{n'=1}^{N} B(k_{m'})\sqrt{C_\nu\,\Delta\sigma_{m'}\,\Delta\theta_{n'}}\,\cdot$$

$$\cos^\nu(\theta_{n'}-\tfrac{\pi}{2})\cos(\theta_{n'}-\tfrac{\pi}{2})\cos\psi_{m'n'}\Big\}\Big] \tag{4-14}$$

Since the phases are independent, only the diagonal terms survive and

$$\overline{uv} = \sum_{m=1}^{M}\sum_{n=1}^{N} B^2(k_m)\, C_\nu\, \Delta\sigma_m\,\Delta\theta_n\,\cdot$$

$$\cdot\cos^{2\nu+1}(\theta_n-\tfrac{\pi}{2})(-\sin(\theta_n-\tfrac{\pi}{2}))\cos^2\psi_{mn} \tag{4-15}$$

As $\overline{\cos^2 \psi_{mn}} = \frac{1}{2}$, we obtain for

$$\overline{uv} = \sum_{m=1}^{M} \frac{1}{2} B^2(k_m)\ c_\nu \Delta\sigma_m$$

$$\cdot \sum_{n=1}^{N} \cos^{2\nu+1}(\theta_n - \tfrac{\pi}{2})(-\sin(\theta_n - \tfrac{\pi}{2}))\ \Delta\theta_n \qquad (4\text{-}16)$$

In the limit $N \to \infty$, and $\Delta\theta_n \to 0$ the summation of the terms involving θ is equal to zero. Therefore,

$$\overline{uv} = 0 \qquad (4\text{-}17)$$

Similarly $\overline{u\dot{u}}$, $\overline{u\dot{v}}$, $\overline{\dot{u}v}$, $\overline{\dot{u}\dot{v}}$ and $\overline{v\dot{v}}$ are found to be equal to zero. Thus the marginal distributions for the velocities u and v, and the accelerations $\dot{u}$ and $\dot{v}$ are

$$u \sim N(0, \sigma_u^2) \qquad \dot{u} \sim N(0, \sigma_{\dot{u}}^2)$$

$$v \sim N(0, \sigma_v^2) \qquad \dot{v} \sim N(0, \sigma_{\dot{v}}^2) \qquad (4\text{-}18)$$

and the correlations are

$$\rho_{uv} = \rho_{u\dot{u}} = \rho_{\dot{u}v} = \rho_{u\dot{v}} = \rho_{v\dot{v}} = \rho_{\dot{u}\dot{v}} = 0 \qquad (4\text{-}19)$$

and the joint probability density function is

$$f(u, v, \dot{u}, \dot{v}) = \frac{EXP\left\{-\frac{1}{2}\left(\frac{u^2}{\sigma_u^2} + \frac{v^2}{\sigma_u^2} + \frac{\dot{u}^2}{\sigma_{\dot{u}}^2} + \frac{\dot{v}^2}{\sigma_{\dot{v}}^2}\right)\right\}}{(2\pi)^2\ \sigma_u\, \sigma_v\, \sigma_{\dot{u}}\, \sigma_{\dot{v}}} \qquad (4\text{-}20)$$

4.2 Probability Distribution of Force Components

The horizontal force per unit length of pile in complex notation is:

$$F_x + jF_y = C_1(u + jv)\,|u + jv| + C_2(\dot{u} + j\dot{v}) \tag{4-21}$$

in which C_1 and C_2 are given by Equations (2-35) and (2-36) and $j=\sqrt{-1}$. The x and y components of the forces are

$$\begin{aligned} F_x &= C_1 u (u^2+v^2)^{\frac{1}{2}} + C_2 \dot{u} \\ F_y &= C_1 v (u^2+v^2)^{\frac{1}{2}} + C_2 \dot{v} \end{aligned} \tag{4-22}$$

The drag force components are

$$\begin{aligned} D_x &= C_1 u (u^2+v^2)^{\frac{1}{2}} \\ D_y &= C_1 v (u^2+v^2)^{\frac{1}{2}} \end{aligned} \tag{4-23}$$

and the inertia force components are

$$\begin{aligned} I_x &= C_2 \dot{u} \\ I_y &= C_2 \dot{v} \end{aligned} \tag{4-24}$$

From the known joint distribution of u, $\dot{u}$, v and $\dot{v}$ given by Equation (4-20), it is proposed to find the joint distribution for D_x, D_y, I_x and I_y. The inverse relations for the transformation are

$$\dot{u} = \frac{I_x}{C_2}$$
$$\dot{v} = \frac{I_y}{C_2} \qquad (4\text{-}25)$$

$$u = \frac{D_x}{\sqrt{C_1}\,(D_x^2 + D_y^2)^{\frac{1}{4}}}$$
$$v = \frac{D_y}{\sqrt{C_1}\,(D_x^2 + D_y^2)^{\frac{1}{4}}} \qquad (4\text{-}26)$$

The Jacobian of the transformation is

$$J\left(\frac{u, v, \dot{u}, \dot{v}}{D_x, D_y, I_x, I_y}\right) = \frac{1}{2\,C_1\,C_2^2\,(D_x^2 + D_y^2)^{\frac{1}{2}}} \qquad (4\text{-}27)$$

Therefore, the joint probability density function for D_x, D_y, I_x and I_y is

$$f\,(D_x, D_y, I_x, I_y)$$

$$= \frac{EXP\left[-\left\{\dfrac{\dfrac{D_x^2}{2\sigma_u^2} + \dfrac{D_y^2}{2\sigma_v^2}}{C_1 (D_x^2 + D_y^2)^{\frac{1}{2}}}\right\} - \left\{\dfrac{I_x}{2C_2^2\sigma_{\dot{u}}^2} + \dfrac{I_y}{2\sigma_{\dot{v}}^2 C_2^2}\right\}\right]}{2C_1 C_2^2\,(D_x^2 + D_y^2)^{\frac{1}{2}}\,(2\pi)^2\,\sigma_u\,\sigma_v\,\sigma_{\dot{u}}\,\sigma_{\dot{v}}} \qquad (4\text{-}28)$$

Separating terms involving drag and inertia components

$$f(D_x,D_y)\cdot f(I_x,I_y) = \frac{e^{-\frac{\frac{D_x^2}{\sigma_u^2}+\frac{D_y^2}{\sigma_v^2}}{2c_1\,(D_x^2+D_y^2)^{\frac{1}{2}}}}}{4\pi\, C_1\,(D_x^2+D_y^2)^{\frac{1}{2}}\,\sigma_u\,\sigma_v}\,\cdot$$

$$\cdot\,\frac{e^{-\frac{I_x^2}{2c_2^2\,\sigma_{\dot u}^2}-\frac{I_y^2}{2c_2^2\,\sigma_{\dot v}^2}}}{2\pi\;C_2^2\;\sigma_{\dot u}\;\sigma_{\dot v}} \qquad (4-29)$$

It may be noted that the marginal joint probabilty density of the inertia force components is a bivariate Gaussian density with zero mean and variance $c_2^2\sigma_{\dot u}^2$ and $c_2^2\sigma_{\dot v}^2$. The marginal density of the drag force components is given by $f(D_x\,,\;D_y)$ and has been plotted in Figure (4-1). It is noted that the density function has a singularity at the point (0,0).

4.3 Variation in the Mean Square of a Random Realization

In the simulation of linear directional seas, components with the same frequency but with different amplitudes and phases occur. The following derivation will be helpful in understanding some features of the simulation method.

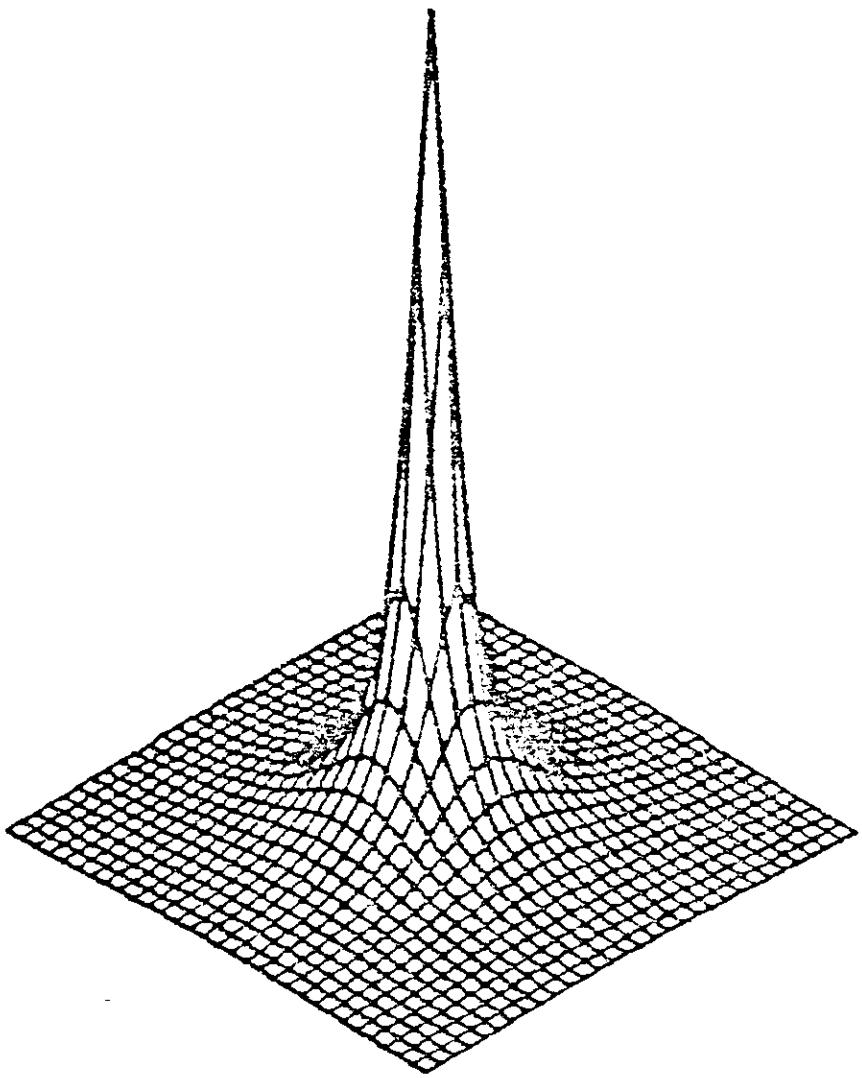

Figure 4-1. Marginal Joint Probability Density of Drag Force Components.

Let the water elevation be represented by

$$\eta = a_1 \cos(\sigma t + \epsilon_1) + a_2 \cos(\sigma t + \epsilon_2) + \cdots + a_n \cos(\sigma t + \epsilon_n) \quad (4\text{-}30)$$

Expanding the cosine and simplifying yields

$$\eta = \cos \sigma t \left(\sum_{i=1}^{n} a_i \cos \epsilon_i \right) + \sin \sigma t \left(\sum_{i=1}^{n} a_i \sin \epsilon_i \right) \quad (4\text{-}31)$$

The mean value estimated from a record of length τ is

$$\bar{\eta} = \frac{1}{\tau} \int_0^{\tau} \eta \, dt$$

$$= \frac{\sin \sigma\tau}{\sigma\tau} \left(\sum_{i=1}^{n} a_i \cos \epsilon_i \right) + \frac{1 - \cos \sigma\tau}{\sigma\tau} \left(\sum_{i=1}^{n} a_i \sin \epsilon_i \right) \quad (4\text{-}32)$$

which has an expected value equal to zero and tends to zero as the length of record increases.

The mean square value estimated from a record of length τ is

$$\hat{\overline{\eta^2}} = \frac{1}{\tau} \int_0^{\tau} \eta^2 \, dt \quad (4\text{-}33)$$

On substituting for η from Equation (4-30), we obtain

$$\hat{\overline{\eta^2}} = \left(\sum_{i=1}^{n} a_i \cos \epsilon_i \right)^2 + \left(\sum_{i=1}^{n} a_i \sin \epsilon_i \right)^2$$

$$- \frac{\cos 2\sigma\tau - 1}{2\sigma\tau} \left(\sum_{i=1}^{n} a_i \cos \epsilon_i \right)^2 \left(\sum_{i=1}^{n} a_i \sin \epsilon_i \right) \quad (4\text{-}34)$$

On simplifying the preceding yields

$$\hat{\eta}^2 = \sum_{i=1}^{n} a_i^2 + \sum_{i=2}^{n} \sum_{j=1}^{i-1} 2a_i a_j \cos(\epsilon_i - \epsilon_j) - \frac{\cos 2\sigma\tau - 1}{2\sigma\tau}\left(\sum_{i=1}^{n} a_i \cos\epsilon_i\right)\left(\sum_{i=1}^{n} a_i \sin\epsilon_i\right) \quad (4-35)$$

The expected value is

$$E(\hat{\eta}^2) = \frac{1}{2}\sum_{i=1}^{n} a_i^2 \quad (4-36)$$

The variance of the estimate is

$$E\left\{\hat{\eta}^2 - E\hat{\eta}^2\right\}^2 = E\left\{\sum_{i=2}^{n}\sum_{j=1}^{i-1} 2a_i a_j \cos(\epsilon_i - \epsilon_j) - \frac{\cos 2\sigma\tau - 1}{2\sigma\tau}\left(\sum_{i=1}^{n} a_i \cos\epsilon_i\right)\left(\sum_{i=1}^{n} a_i \sin\epsilon_i\right)\right\}^2 \quad (4-37)$$

On simplifying we have

$$Var(\hat{\eta}^2) = \left\{\sum_{i=2}^{n}\sum_{j=1}^{i-1} 2a_i a_j \cos(\epsilon_i - \epsilon_j)\right\}^2$$

$$-E\left\{2\sum_{i=2}^{n}\sum_{j=1}^{i-1} 2a_i a_j \cos(\epsilon_i - \epsilon_j)\frac{\cos 2\sigma\tau - 1}{2\sigma\tau}\left(\sum_{i=1}^{n} a_i \cos\epsilon_i\right)\left(\sum_{i=1}^{n} a_i \sin\epsilon_i\right)\right\}$$

$$+ E\left\{\frac{\cos 2\sigma\tau - 1}{2\sigma\tau}\left(\sum_{i=1}^{n} a_i \cos\epsilon_i\right)\left(\sum_{i=1}^{n} a_i \sin\epsilon_i\right)\right\}^2 \quad (4-38)$$

If τ is reasonably large in the simulated records, the last term is of the order $\frac{1}{\tau^2}$ and is negligible. For this case, the second term is equal to zero and the first term is

$$\sum_{i=2}^{n} \sum_{j=1}^{i-1} \frac{a_i^2 \; a_j^2}{2}$$

Therefore, the variance of the mean square value of the simulated record is

$$Var(\hat{\eta^2}) = \sum_{i=2}^{n} \sum_{j=1}^{i-1} \frac{a_i^2 \; a_j^2}{2} \tag{4-39}$$

4.4 Effect of Finite Length Simulation on Correlations

The correlations computed in the first section of this chapter are true only for a record of infinite length. Simulation is usually of finite length, particularly in this case, records of 200 seconds have been simulated. The remainder of this chapter is devoted to exploring the effects of the finite length record on the correlations amongst the simulated variables.

Considering two variables η_1 and η_2 being represented by

$$\eta_1 = a_1 \cos(\sigma_1 t + \epsilon_1) \tag{4-40}$$

$$\eta_2 = a_2 \cos(\sigma_2 t + \epsilon_2) \tag{4-41}$$

The estimated correlation between the two variables is

$$\widehat{\overline{\eta_1 \eta_2}} = \frac{1}{\tau} \int_0^{\tau} \eta_1 \eta_2 \, dt$$

$$= \frac{1}{\tau} \int_0^{\tau} a_1 a_2 \cos(\sigma_1 t + \epsilon_1) \cos(\sigma_2 t + \epsilon_2) \, dt \tag{4-42}$$

After simplifying we obtain

$$\widehat{\overline{\eta_1 \eta_2}} = \frac{a_1 a_2}{\tau(\sigma_1^2 - \sigma_2^2)} \Big[\sigma_1 \sin(\sigma_1 \tau + \epsilon_1) \cos(\sigma_2 \tau + \epsilon_2)$$

$$- \sigma_2 \cos(\sigma_1 \tau + \epsilon_1) \sin \sigma_2$$

$$- \sigma_1 \sin \epsilon_1 \cos \epsilon_1 + \sigma_2 \cos \epsilon_1 \sin \epsilon_2 \Big] \tag{4-43}$$

The expected value of the estimated correlation is zero. Also, as the record length increases the estimated value tends to zero. The variance of the estimated correlation is

$$Var\left(\widehat{\eta_1 \eta_2}\right) = E\left[\frac{a_1^2 a_2^2}{\tau^2(\sigma_1^2-\sigma_2^2)}\left\{\sigma_1 \sin(\sigma_1\tau+\epsilon_1)\cos(\sigma_2\tau+\epsilon_2)\right.\right.$$

$$-\sigma_2 \cos(\sigma_1\tau+\epsilon_1)\sin(\sigma_2\tau+\epsilon_2)$$

$$\left.\left.-\sigma_1 \sin\epsilon_1 \cos\epsilon_2 + \sigma_2 \cos\epsilon_1 \sin\epsilon_1\right\}^2\right] \tag{4-44}$$

Carrying out the variance determination requires calculation of the following expectations:

$$E\left\{\sin(\sigma_1\tau+\epsilon_1)\sin\epsilon_1\right\} = \frac{1}{2}\cos\sigma_1\tau \tag{4-45}$$

$$E\left\{\sin(\sigma_1\tau+\epsilon_1)\cos\epsilon_1\right\} = \frac{1}{2}\sin\sigma_1\tau \tag{4-46}$$

$$E\left\{\cos(\sigma_1\tau+\epsilon_1)\sin\epsilon_1\right\} = -\frac{1}{2}\sin\sigma_1\tau \tag{4-47}$$

$$E\left\{\cos(\sigma_1\tau+\epsilon_1)\cos\epsilon_1\right\} = \frac{1}{2}\cos\sigma_1\tau. \tag{4-48}$$

Substituting the values of these expectations into Equation (4-44) we find

$$Var\left(\widehat{\eta_1 \eta_2}\right) = \frac{a_1^2 a_2^2}{\tau^2(\sigma_1^2-\sigma_2^2)^2} \left\{ \frac{1}{4}\left(\sigma_1^2+\sigma_2^2+\sigma_1^2+\sigma_2^2\right) \right.$$

$$- \sigma_1^2 \cdot \frac{1}{2}\cos\sigma_1\tau \cdot \frac{1}{2}\cos\sigma_2\tau + \sigma_1\sigma_2 \cdot \frac{1}{2}\sin\sigma_1\tau\left(-\frac{1}{2}\sin\sigma_2\tau\right)$$

$$\left. + \sigma_1\sigma_2\left(-\frac{1}{2}\sin\sigma_1\tau\right)\frac{1}{2}\sin\sigma_2\tau - \sigma_2^2 \cdot \frac{1}{2}\cos\sigma_1\tau\,\frac{1}{2}\cos\sigma_2\tau \right\} \qquad (4\text{-}49)$$

On simplifying

$$Var\left(\widehat{\eta_1 \eta_2}\right) = \frac{a_1^2 a_2^2}{2\tau^2(\sigma_1^2-\sigma_2^2)^2} \left\{ \sigma_1^2+\sigma_2^2 \right.$$

$$- \frac{1}{2}\left(\sigma_1^2+\sigma_2^2\right)\cos\sigma_1\tau\cos\sigma_2\tau$$

$$- \sigma_1\sigma_2\sin\sigma_1\tau\sin\sigma_2\tau \qquad (4\text{-}50)$$

from which it can be seen that the variance approaches zero as the inverse square of the simulated record length.

CHAPTER 5

SIMULATION METHOD

The second order perturbation solution developed in Chapter 3 should characterize a real wave field including nonlinearities reasonably accurately. From the second order potential solution obtained by adding Equations (3-26) and (3-45), water particle kinematics at every point (x,y,z) in the wave field can be calculated. Using these wave field kinematics in an analytical wave force computation results in a cumbersome solution. To gain an insight into the behavior of the exact solution, the potential solution correct to the second order has been simulated and wave forces computed for further study.

5.1 Procedure for Simulation

The procedure for simulating a random directional second order sea surface and associated wave forces is summarized below:

(1) The linear Gaussian approximation to a random sea surface is represented by the discrete counterpart

of Equation (2-1)

$$\eta(\vec{x},t)=\sum_{m=1}^{M}\sum_{n=1}^{N}\sqrt{S(\sigma_m,\theta_n)\,\Delta\sigma_m\,\Delta\theta_n}\;\cos(\vec{k}_m\cdot\vec{x}-\sigma t+\epsilon_{mn}) \qquad (5\text{-}1)$$

Thus if M frequencies and N directions are selected (not necessarily at equal intervals), then the linear approximation to the wave field has MN components. Pierson (1955) has given proof that the above finite sum tends to the pseudo-intergral in Equation (2-1) as M and N tend to infinity and it represents a three dimensional stationary Gaussian process.

(2) Using Equations (3-45) and (3-48), second order corrections are calculated. There are (MN)**2 second order correction components. The phases of these nonlinear components are related to the phases of the linear components. Thus the process represented by the sum of the linear and the nonlinear components is no longer Gaussian. Departure from Gaussian process is appropriately indicated by the skewness.

(3) The time history of water elevation η is obtained by summing all the components and taking the

inverse Fast Fourier Transform.

(4) Velocities and accelerations at any point are computed as follows

(a) Velocities and accelerations due to each component are resolved along the x and y axes.

(b) The contribution from each component is added to obtain the Fourier coefficients a_n and b_n.

(c) Using the inverse Fast Fourier Transform, the time domain realizations for velocities and accelerations in the x and y directions are obtained.

(5) These velocities and accelerations are used in the Morison formula to compute wave forces per unit length on a pile.

(6) The total force on the pile is obtained by numerically integrating the force up to the free water surface obtained in Step 3.

(7) Similar force histories can be obtained for the pile at any other desired point. Thus forces on a group of piles can be studied.

5.2 Algorithm for Simulation

The above simulation method has been implemented into a set of Fortran programs. The essential features of the computation scheme are depicted in the flow chart in Figure 5-1 and are summarized below:

(1) The given or assumed directional spectrum $S(\sigma,\theta)$ is discretized so that the sea surface is represented by

$$\eta(\vec{x},t) = \sum_{i=1}^{M} \sum_{j=1}^{N} a_{ij} \cos(\vec{k}_i \cdot \vec{x} - \sigma_i t + \epsilon_{ij}) \tag{5-2}$$

where $a_{ij} = \sqrt{2 S(\sigma_i, \theta_j) \Delta\sigma_i \Delta\theta_j}$ (5-3)

(2) Second order interaction components are computed by Equations (3-45) and (3-48).

(3) The position of the pile in the x-y plane is selected. This step is essential for simulating the total force on a group of piles.

(4) A set of uniform random phases lying between $(0,2\pi)$ is selected for the linear components. The phases of the nonlinear components are derived from these phases (Equation 3-48).

(5) Fourier coefficients for water elevation are obtained by adding Fourier coefficients for each of the linear and nonlinear components.

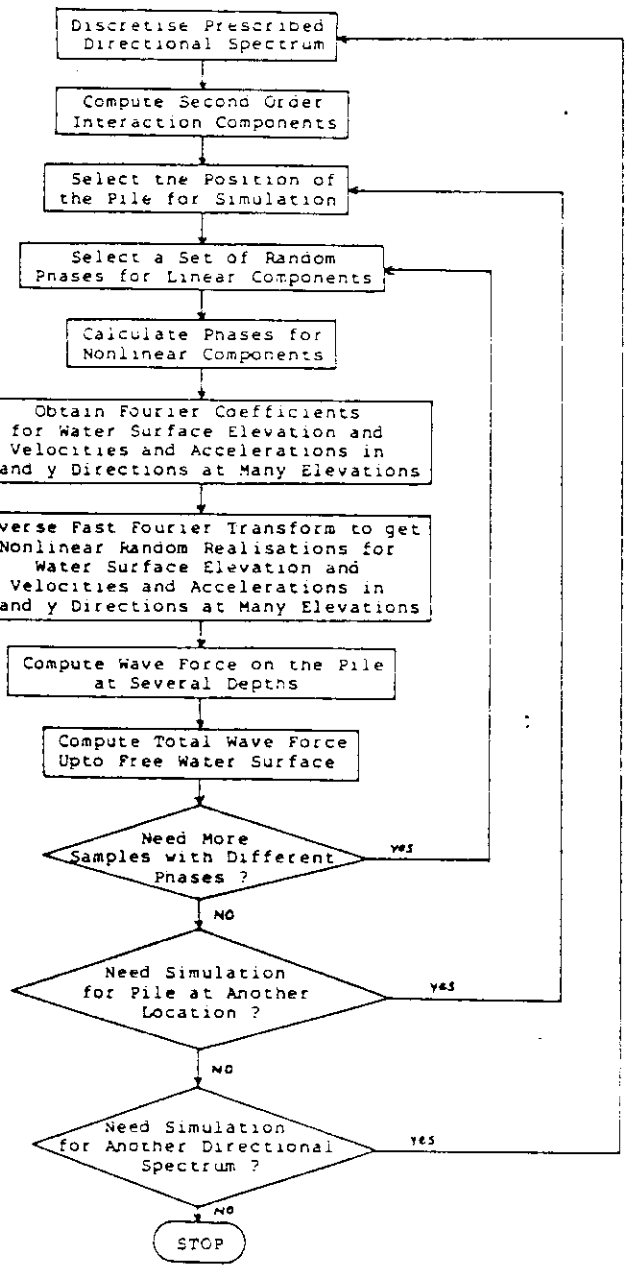

Figure 5-1. Flow Chart for Computer Programs for Simulating Second Order Directional Sea and Associated Wave Forces.

(6) Similarly Fourier coefficients are obtained for velocities and accelerations in the x and y directions at several depths.

(7) Using the inverse Fast Fourier Transform, nonlinear random realizations for water surface elevation and velocities and accelerations in the x and y directions at several depths are obtained.

(8) Wave forces at several depths are computed by the Morison formula.

(9) The total force on the pile up to the free surface is finally computed.

5.3 Comparison with Other Methods

The nonlinear random sea simulation method implemented by Hudspeth (1974,1975) first determines the unidirectional second order sea surface realization, but the water particle kinematics are computed by the linear filtering method due to Reid (1958). A stretched vertical coordinate was used to take into account the displacement of the free surface. In the present method, second order directional sea surface and associated kinematics are simulated retaining the linear phases and the related nonlinear phases. Also the force is computed up to the free surface without the use of the stretched coordinates.

The present method yields results very similar to Dean's more intuitive hybrid method (1977), particularly up to the second order. As will be evidenced in the next chapter numerical results from the two methods are quite similar.

Some of the more notable features of the present method may be summarized as follows:

(1) Randomness depicted by the spectral densities, probabilty densities and intercorrelations amongst various variables like water surface elevation and velocities and accelerations in the x and y directions at several points have been fully represented.

(2) Nonlinearities correct up to second order have been included.

(3) Phases of the nonlinear contributions have been retained.

(4) Any reasonable distribution of the directional energy spectrum of a realistic sea can be simulated.

(5) The skewness of the simulated water surface displacement is realistically represented without any artificial means. The skewnesses of other

variables of interest are also maintained.

(6) The total wave force has been computed by considering the appropriate displacement of the free surface.

A set of very efficient Fortran programs have been developed to implement the above simulation method. In the next chapter some of the many important results derived from the simulation method are presented and discussed.

CHAPTER 6

APPLICATION OF SIMULATION

The methods of the last chapter have been applied to simulate linear and nonlinear realizations of the random sea surface for the Bretschneider spectrum and four different directional spreads. The nonlinearity as represented by the skewness has been computed in each case. It has been found that the skewness is greatest for a narrow directional spread because for the given two wave numbers the skewness kernel is largest for the small included angles. The reasons for this phenomenon and the possible occurrence of negative skewness in the field have been discussed.

The simulation method has been further applied to compute total wave forces on a single pile and a multiple pile group. The total force on a pile reduces by a factor of 1 to 0.61 with the increase in the directional spread of the energy spectrum from unidirectional to omnidirectional. For the four pile group with 60 feet separation the reduction factors are similar to those for the single pile case. However, for the four pile group with one pile at each corner of a 300 feet square the reduction factor varies from 0.79 to 0.39 for the directional spectrum varying from unidirectional to omnidirectional.

6.1 Discrete Directional Spectra

In this study the directional spectrum has been assumed to be given by

$$S(\sigma, \theta) = S(\sigma) \cdot D(\theta) \tag{6-1}$$

in which the Bretschneider spectrum representation has been utilized for $S(\sigma)$, i.e.

$$S(\sigma) = \frac{5\, E_f}{\sigma_0} \left(\frac{\sigma}{\sigma_0}\right)^{-5} e^{-\frac{5}{4}\left(\frac{\sigma}{\sigma_0}\right)^4} \tag{6-2}$$

in which

E_f is total energy given by

$$\int_0^{\infty} S(\sigma)\, d\sigma \tag{6-3}$$

σ_0 is the angular frequency of the peak of spectrum

and the directional spreading function $D(\theta)$ was assumed to be given by Equation (2-28).

Simulation was carried out for twelve different directional spectra formed by permuting three different total energies with four different directional spreads corresponding to the values of the directional spreading parameter ν equal to 0, 1, 5, and 5000. The shapes of the directional spreading function $D(\theta)$ for three different values of spreading parameter ν are presented in Figure 6-1. A value of ν equal to zero corresponds to the case when the energy is equally distributed in all directions (omnidirectional). A value of ν equal to 5000 approximates a unidirectional sea. Values of ν equal to 1 and 5 represent intermediate directional spreads which possibly correspond to realistic seas. For a value of ν equal to 5, 91.8 % of the total energy is concentrated within an angle of 60 degrees.

The continuous directional spreading function has been replaced by twenty equidistant discrete directions in the range 0 to 180 degrees. Similarly the linear continuous spectral density $S(\sigma)$ has been represented by 60 cosine components with the discrete frequencies ranging from .005 Hertz to 0.30 Hertz at an equal interval of 0.005 Hertz.

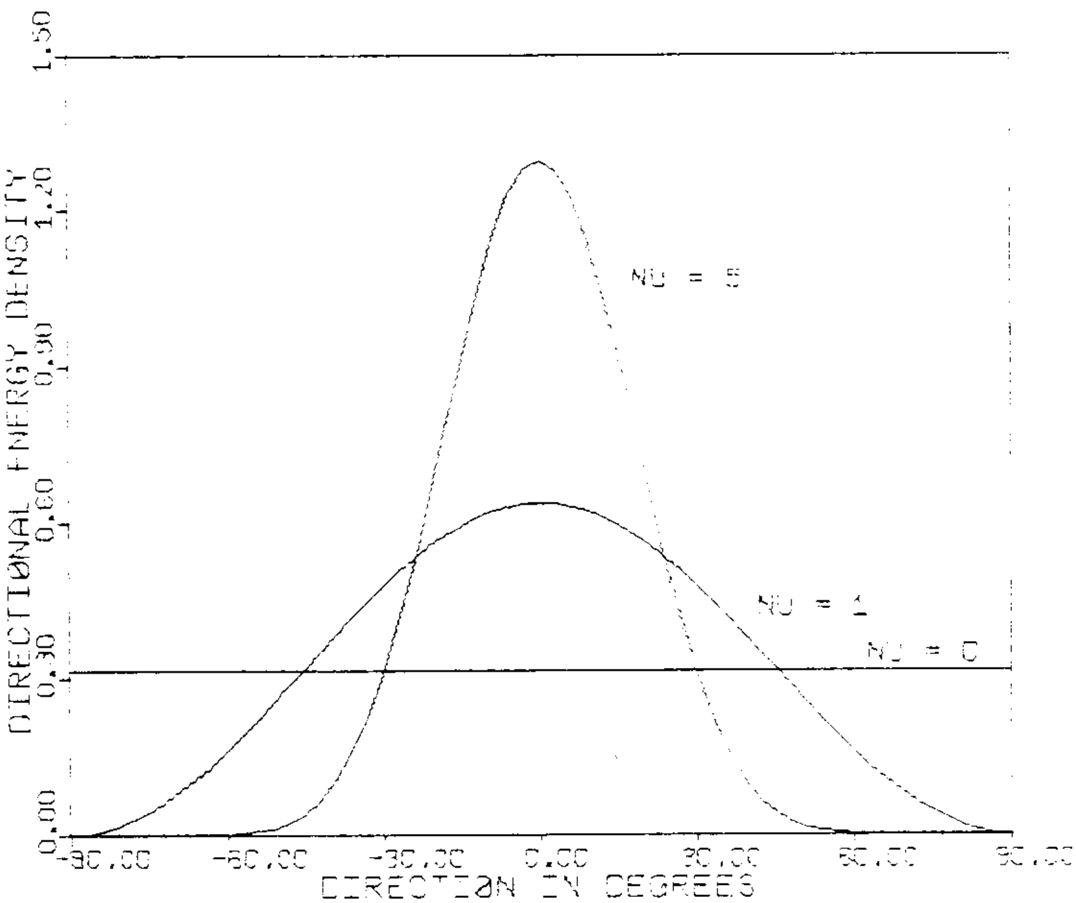

Figure 6-1. Directional Energy Spreading Factors for Directional Parameter ν Equal to 0, 1, and 5 in Equation 2-28.

Each of the 1200 cosine components, obtained by permuting 60 discrete frequencies and 20 discrete directions, are assigned one random phase drawn independently from an identically uniform distribution between 0 and 360 degrees. Before using the phases, the set of 1200 phases have been tested for suitability in the simulation.

6.2 The Random Phases

The set of 1200 random phases has been generated by using the random number generator available at the University of Delaware Computing Center. The frequency distribution of the 1200 random numbers used in the simulation is presented in Table 6-1.

The percentage varies from 8.17% to 11.75% compared to the theoretical percentage of 10%. The computed value of chi-square is 0.1385 which is acceptable at commonly used significance levels. Therefore, it is reasonable to believe that the 1200 random phases belong to a uniform distribution.

For detecting any periodicity in the set, the fast Fourier transform has been used to compute the periodogram of the 1200 random numbers. A cumulative

TABLE 6-1

The Frequency Distribution of

the Sample Random Phases

Interval No.	Range of Interval in Degrees	No. of Occurrences	% of Total
1	0-36	141	11.75
2	36-72	122	10.17
3	72-108	114	9.5
4	108-144	126	10.50
5	144-180	110	9.17
6	180-216	98	8.17
7	216-252	139	11.58
8	252-288	103	8.58
9	288-324	134	11.17
10	324-360	113	9.42
Total	360	1200	100.01

periodogram has been computed and has been normalized by the variance of the random numbers. Normalized frequencies have been formed by dividing frequencies by the Nyquist frequency. The normalized cumulative periodogram has been plotted in Figure 6-2 against the normalized frequency. The bounding lines, corresponding to the confidence limits for 5% significance level in the Kolmogorov-Smirnov test of the hypothesis that the observations are drawn from white noise, have also been shown on the figure. At a 5% significance level it is reasonable to accept that the random numbers are uncorrelated and without any hidden periodicity.

6.3 Linear and Nonlinear Random Sea Surfaces

The 1200 cosine component waves, consisting of 60 discrete frequencies, and propagating in 20 discrete directions in 100 feet of water, and having independent random phases, have been combined to obtain linear realizations of 200 seconds duration for the sea surface elevation and water particle kinematics at several depths.

Linear components with significant energy only have been used in calculating the nonlinear components. 20 frequencies from 0.05 Hertz to 0.15 Hertz and 20

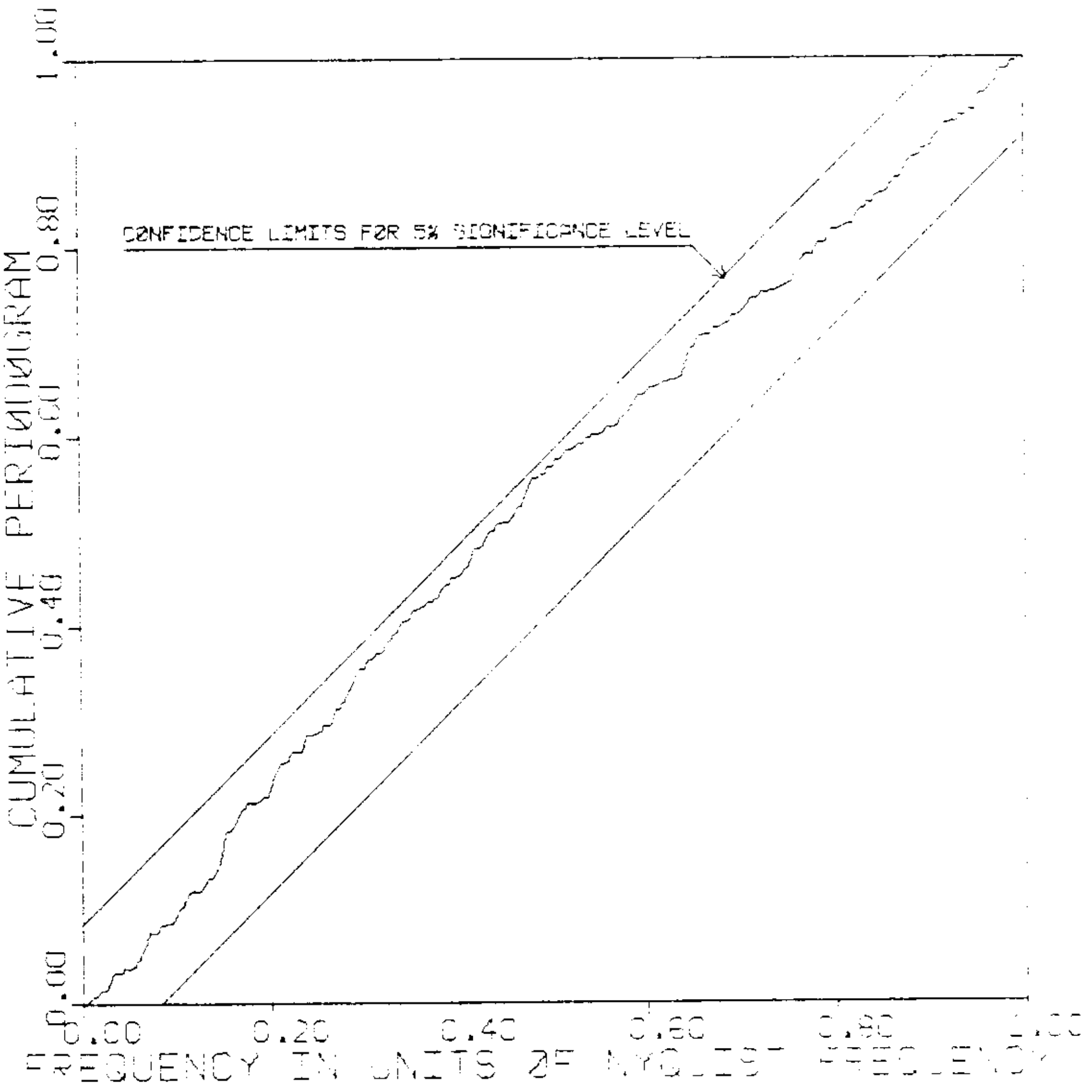

Figure 6-2. Cumulative Periodogram for Random Phases. (The Bounding Lines Represent Confidence Limits for 5% Significance Level in Kolmogorov-Smirnov Test)

directions have been combined to yield 160,000 nonlinear components. Adding these to the linear components, we obtain the nonlinear random realizations for the sea surface and the water particle kinematics at the depths of interest.

The linear and the nonlinear random sea surface realizations have been computed for four different directional spectra with the same total energy. Figures 6-3 to 6-6 show typical linear and nonlinear sea surface realizations for values of the directional distribution parameter ν equal to 0, 1, 5, and 5000. The lower parts of the figures show the linear (solid line) and the nonlinear (dashed line) realizations for the sea surface elevations. As expected the nonlinear contributions, shown for clarity in the upper part of the figures, flatten the troughs and cause the crests to be more peaked. The wave height and period of the individual waves are practically the same for the linear and the nonlinear realizations. But the more peaked crests, caused by nonlinear corrections, in general result in increased velocities below the crests and hence, increased maximum drag forces.

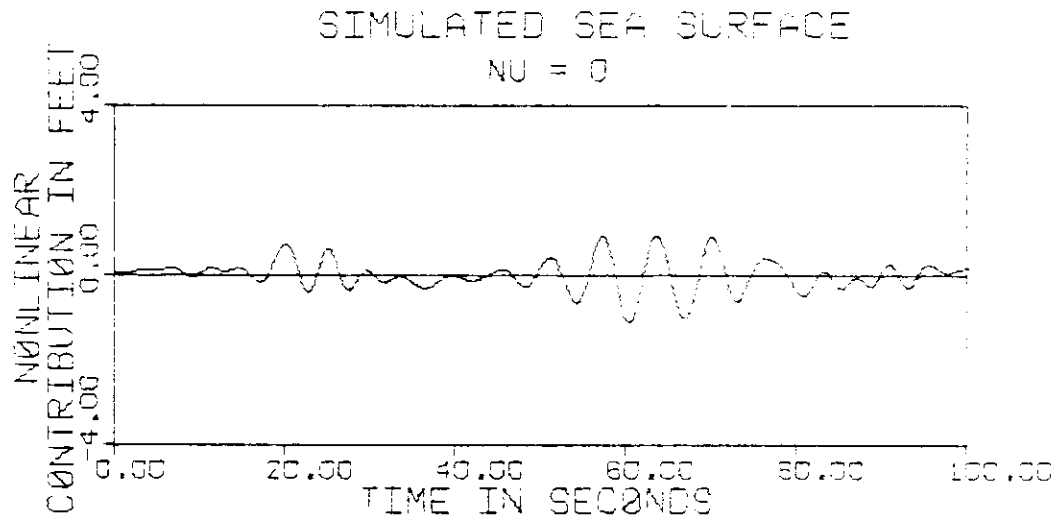

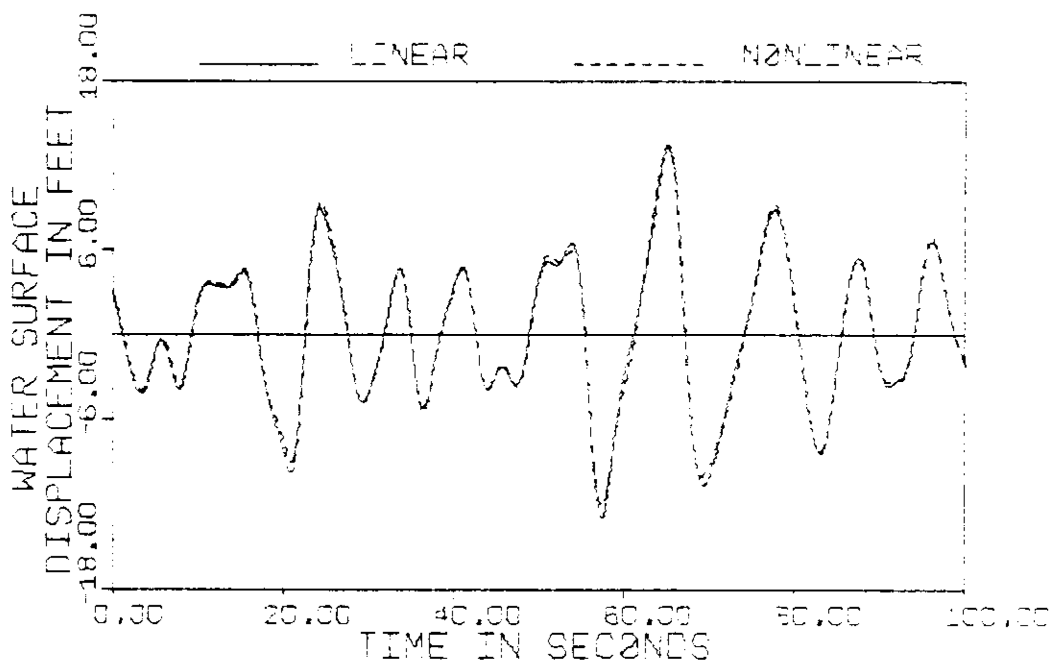

Figure 6-3. Linear and Nonlinear Random Sea Surface Realizations for Uniform Energy Density Over a 180 Degree Sector. (Water Depth = 100 Feet, Total Energy = 22.3 Feet^2)

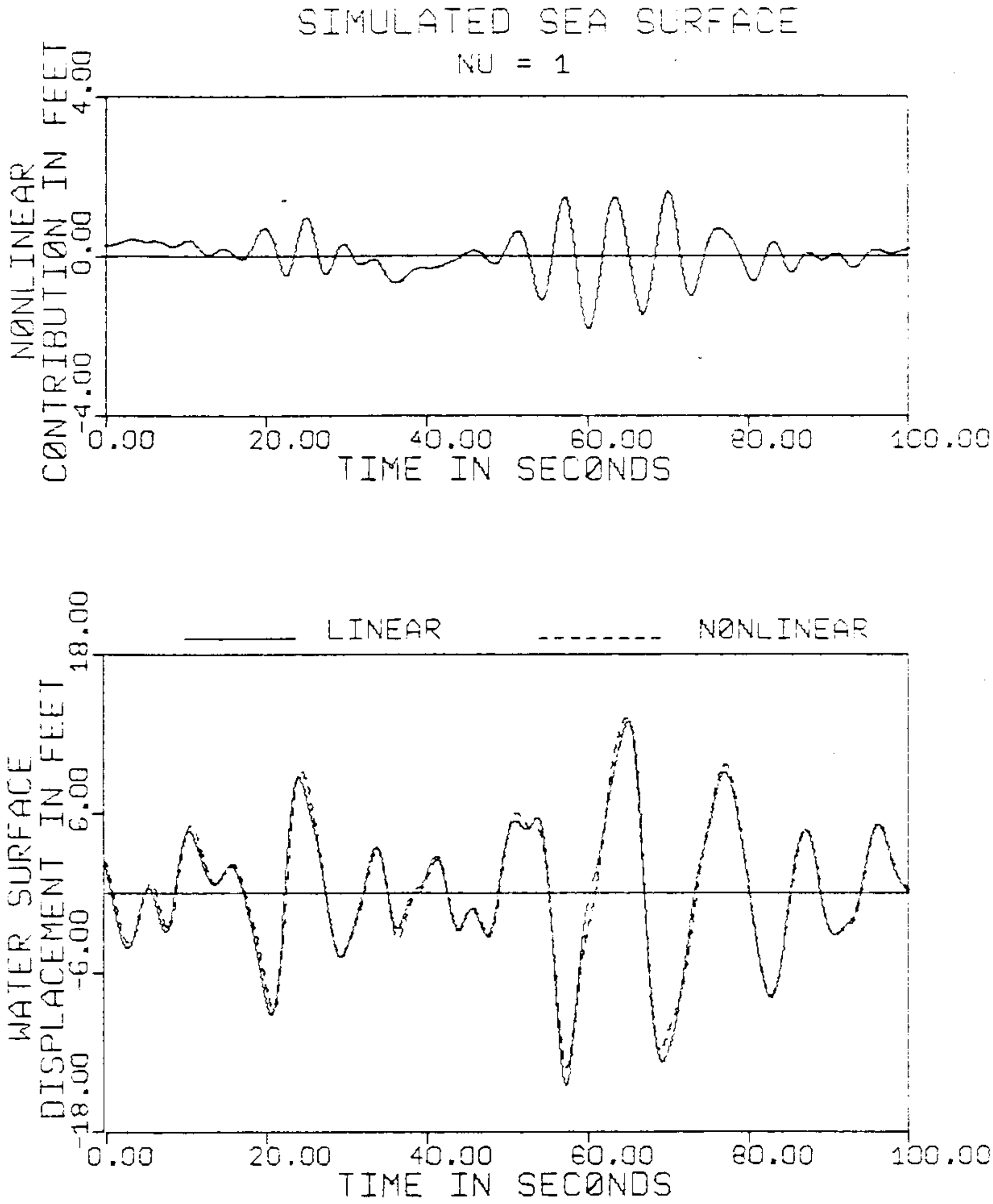

Figure 6-4. Linear and Nonlinear Random Sea Surface Realizations for ν = 1. (Water Depth = 100 Feet, Total Energy = 22.3 Feet^2)

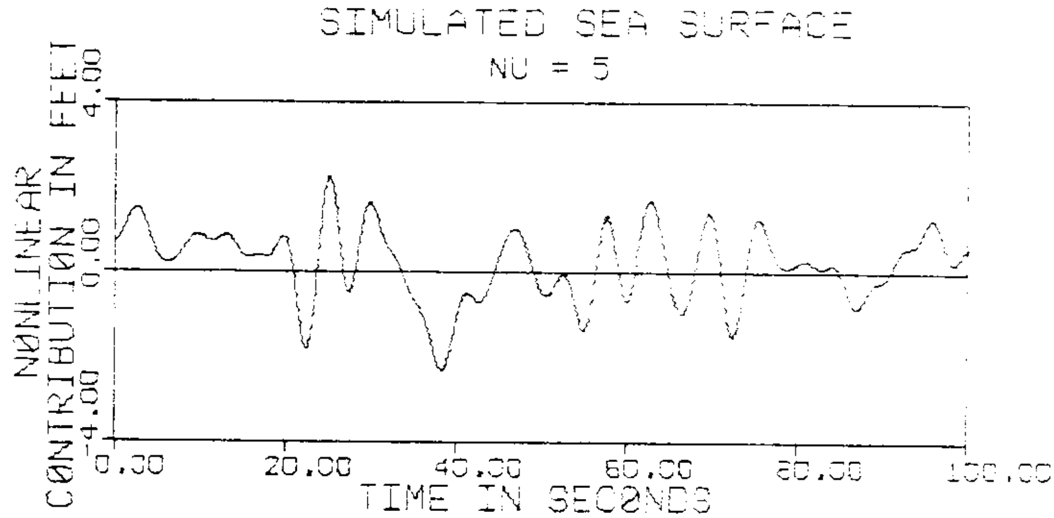

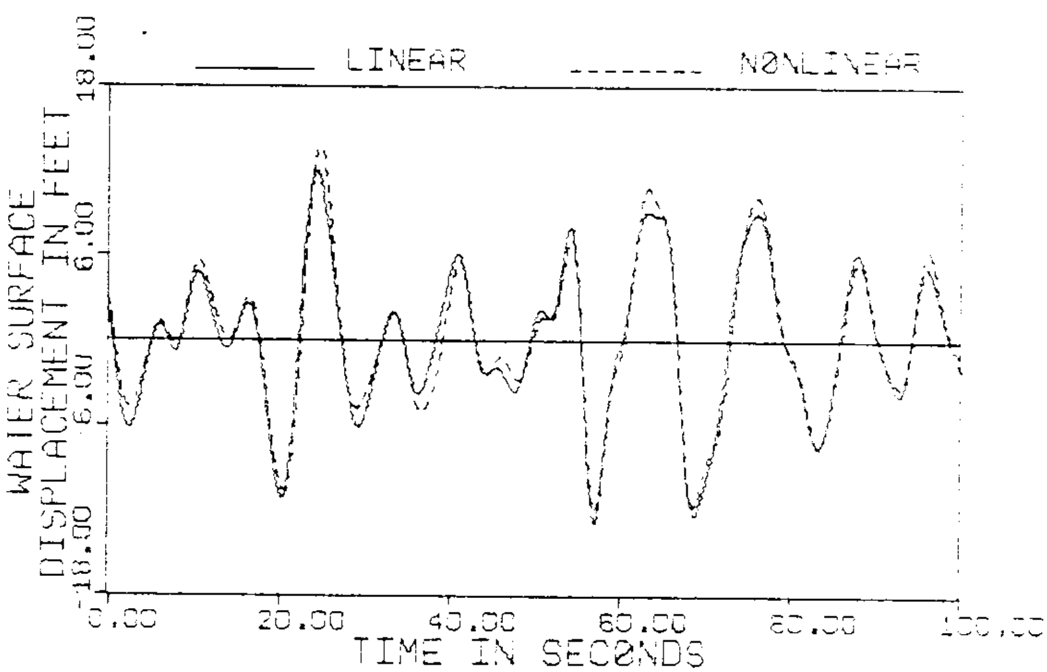

Figure 6-5. Linear and Nonlinear Random Sea Surface Realizations for $\nu = 5$. (Water Depth = 100 Feet, Total Energy = 22.3 Feet^2)

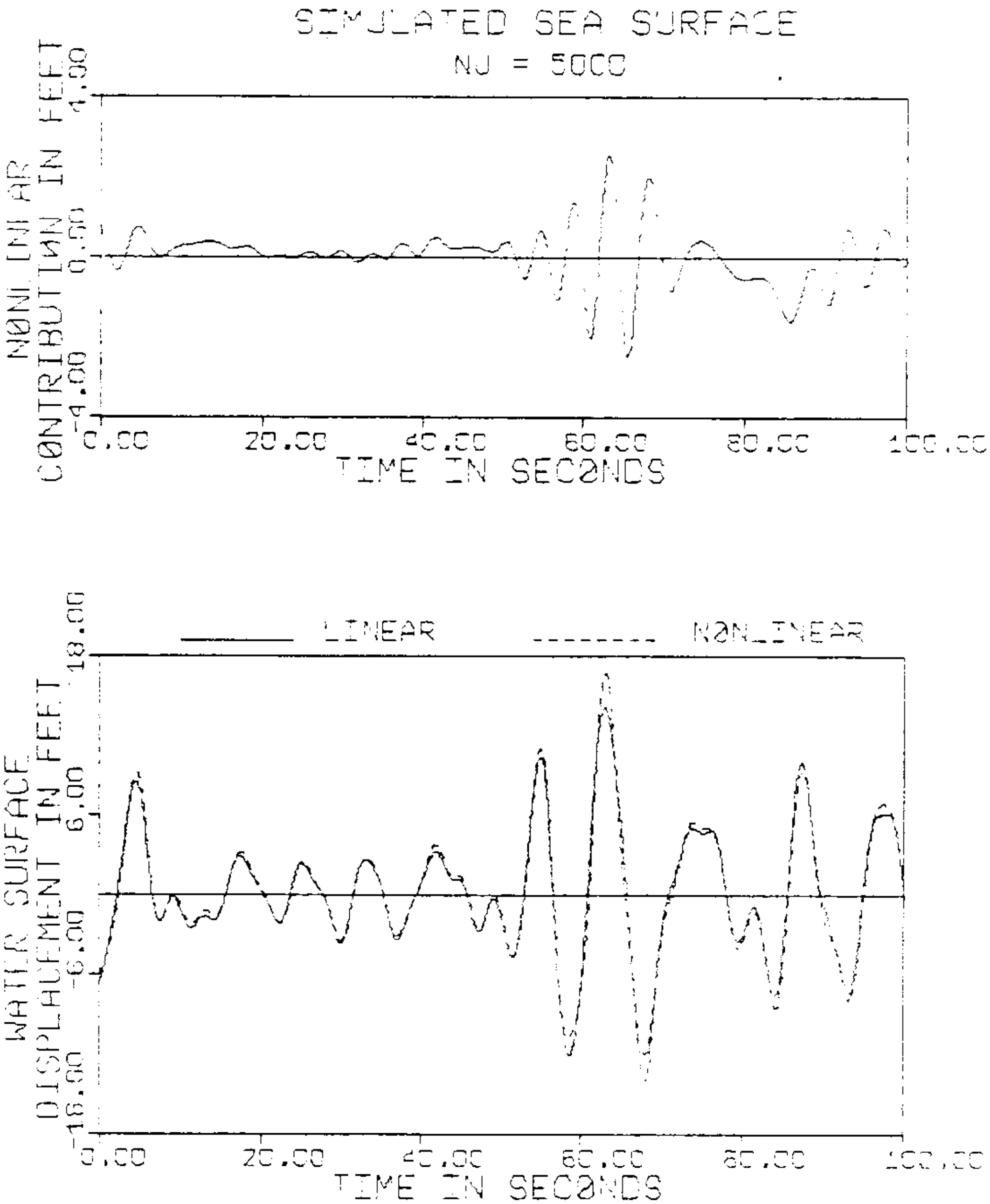

Figure 6-6. Linear and Nonlinear Random Sea Surface Realizations for Unidirectional Sea. (Water Depth = 100 Feet, Total Energy = 22.3 Feet^2)

6.4 Linear and Nonlinear Random Sea Surface Spectra

The spectral densities of the linear and nonlinear sea surface realizations for the four values of the directional spreading parameter ν are presented in Figures 6-7 to 6-10. The linear spectral densities are presented as solid lines. On the same figures the selected Bretschneider spectra have been plotted. The assumed and simulated linear spectra are represented by the same solid lines. This has been achieved by selecting the phases carefully as guided by the derivations in Section 4-3 and testing them for suitability (Section 6-2) before using them.

The broken curves on these figures represent the spectral densities of the nonlinear realizations. A small peak in the vicinity of twice the frequency of peak energy density can be noticed in the nonlinear spectra. Similar peaks have been reported in the spectral densities of random waves measured in the field and laboratory.

The nonlinear spectra have small energy in the subharmonic frequency bands in which the corresponding linear spectra have no energy at all. The energy in the very low frequencies has been observed in the field as

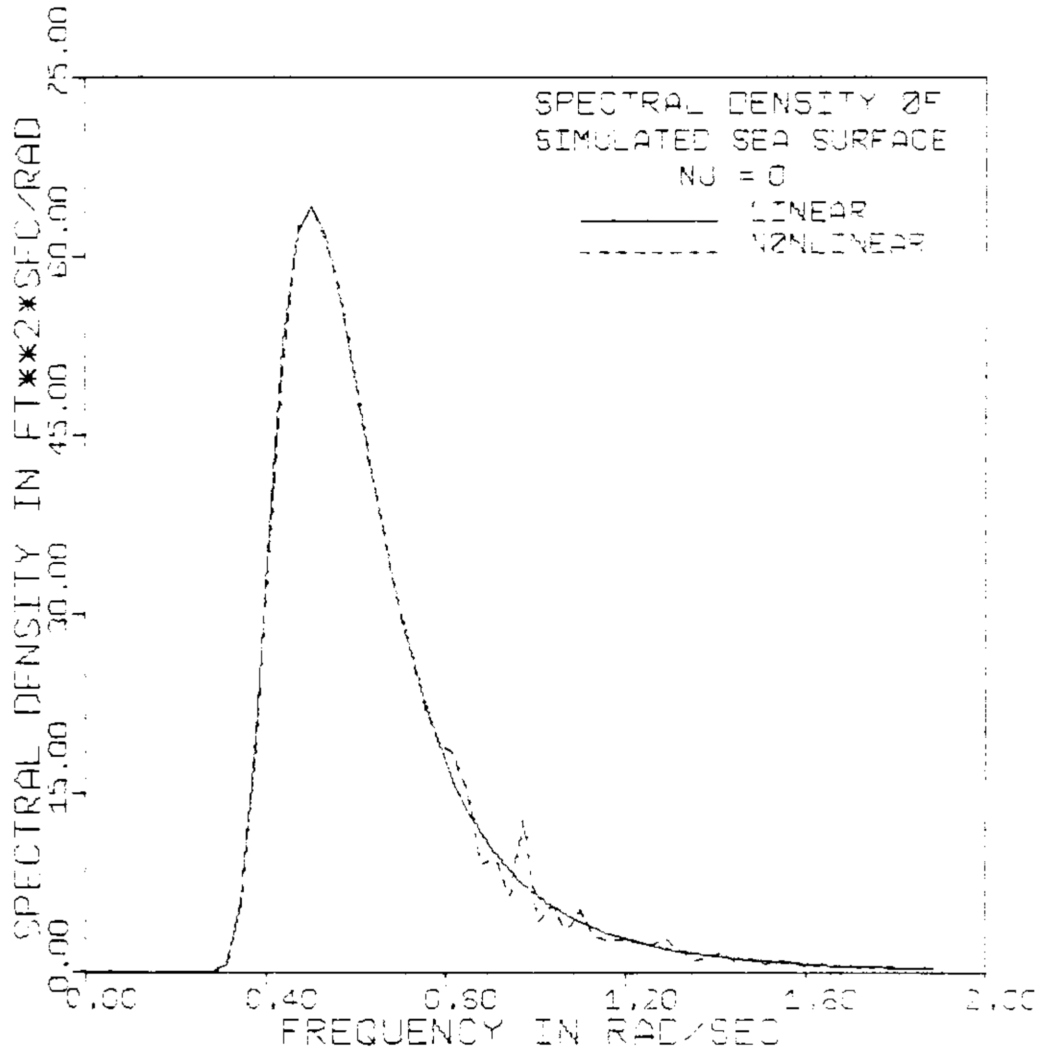

Figure 6-7. Spectral Densities of Simulated Linear and Nonlinear Random Sea Surface Realization for Uniform Energy Density Over a 180 Degree Sector. (ν = 0, Water Depth =100 Feet, Total Energy = 22.3 Feet^2)

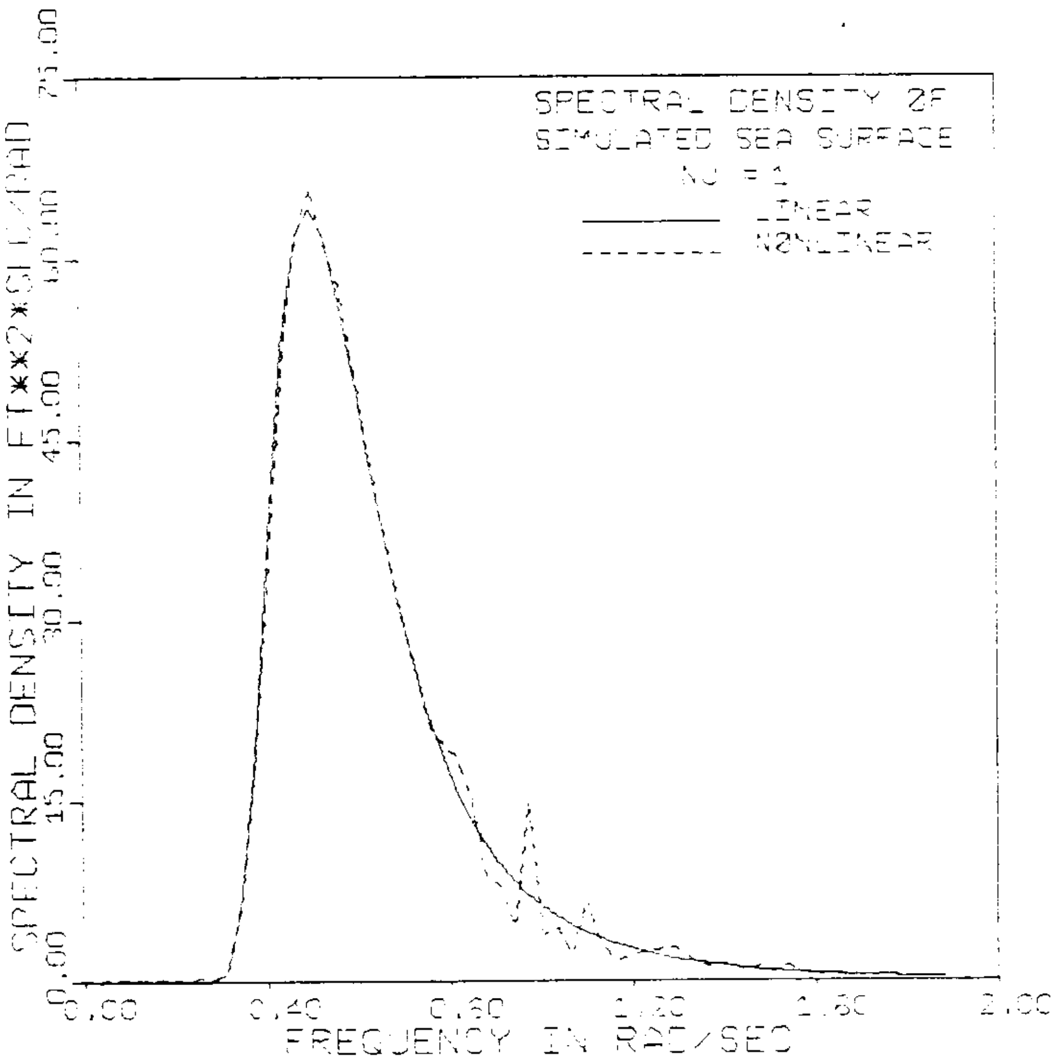

Figure 6-8. Spectral Densities of Simulated Linear and Nonlinear Random Sea Surface for Directional Energy Distribution Parameter ν = 1. (Water Depth = 100 Feet, Total Energy = 22.3 Feet^2)

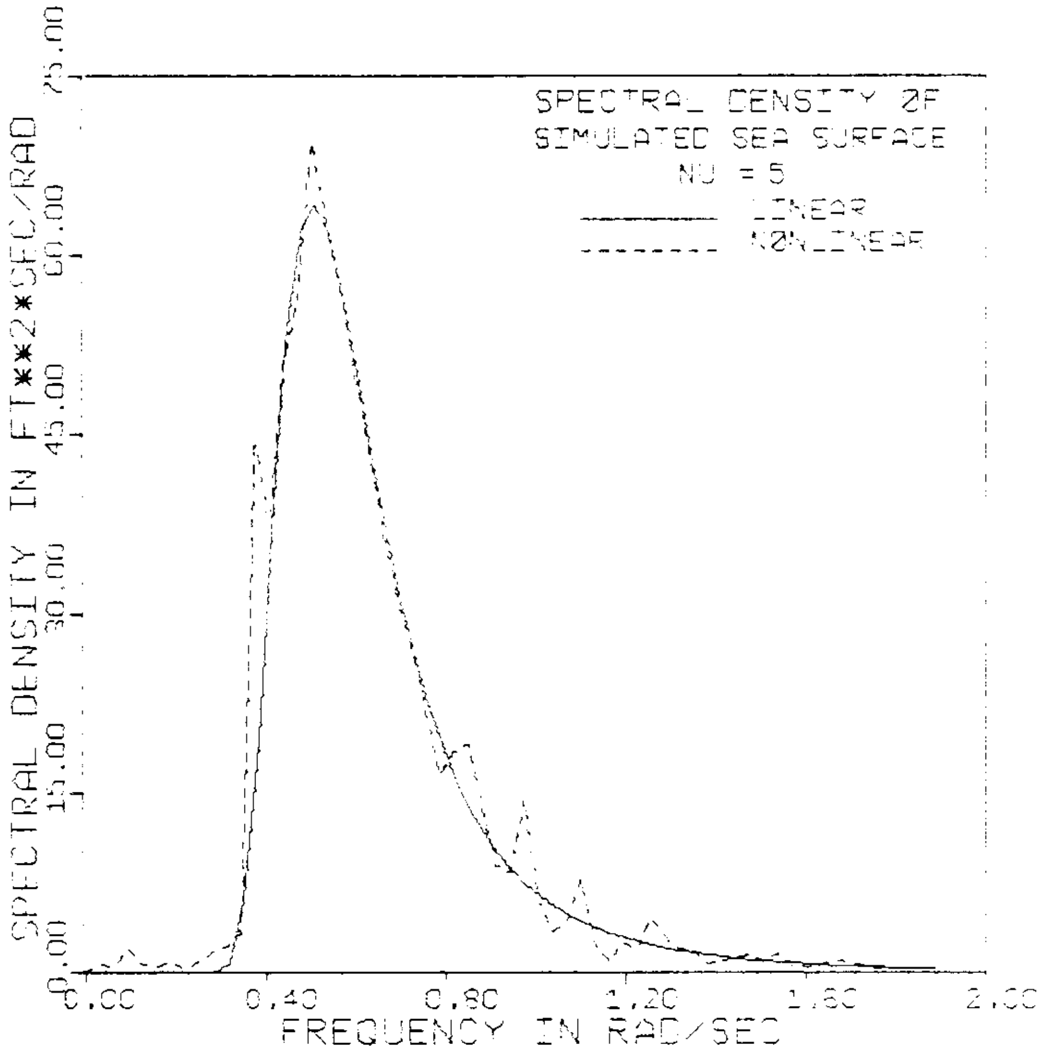

Figure 6-9. Spectral Densities of Simulated Linear and Nonlinear Random Sea Surface for Directional Energy Distribution Parameter ν = 5. (Water Depth = 100 Feet, Total Energy = 22.3 Feet^2)

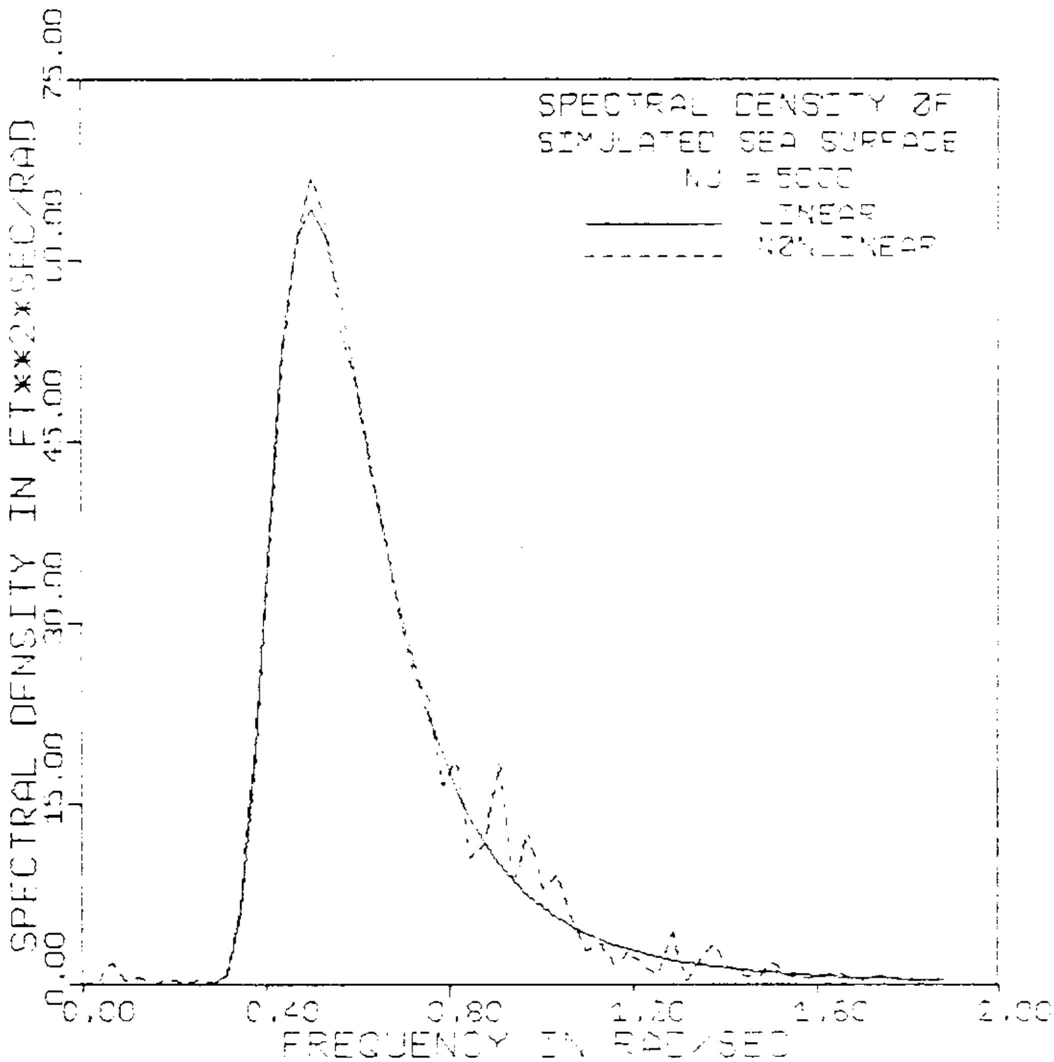

Figure 6-10. Spectral Densities of Simulated Linear and Nonlinear Random Sea Surface for a Long Crested Sea. (ν = 5000, Water Depth = 100 Feet, Total Energy = 22.3 Feet^2)

surf beats and the second order interaction theory has been used to explain the occurrence of surf beats in the nearshore zone (Gallagher, 1971). Thus the present method has been able to model two of the observed features of nonlinear waves.

In the preceding paragraphs some of the important features of the time domain realizations of the sea surface have been discussed. It is evident that different directional spreads do not cause identical nonlinear effects. Skewness has been known to be a sensitive and representative parameter depicting nonlinearity. In the following section the skewness and its kernel are discussed.

6.5 Skewness and Its Kernel

The dimensionless skewness coefficients, defined as the mean cube divided by the cube of the standard deviation, have been computed for 11 values of the directional parameter ν and are presented in Table 6-2. Figure 6-11 shows the same data graphically. For the directional spreading function used in this study, it can be seen that an intermediate spreading of energy causes maximum skewness. The unidirectional waves represented by a value of ν equal to 5000 have the least skewness. With

TABLE 6-2

Variation in Skewness with
Change in the Directional Spread

ν	Skewness
5000	0.1286
500	0.1286
50	0.1581
7	0.1800
6	0.1803
5	0.1803
4	0.1797
1	0.1647
0.1	0.1470
0.01	0.1447
0	0.1447

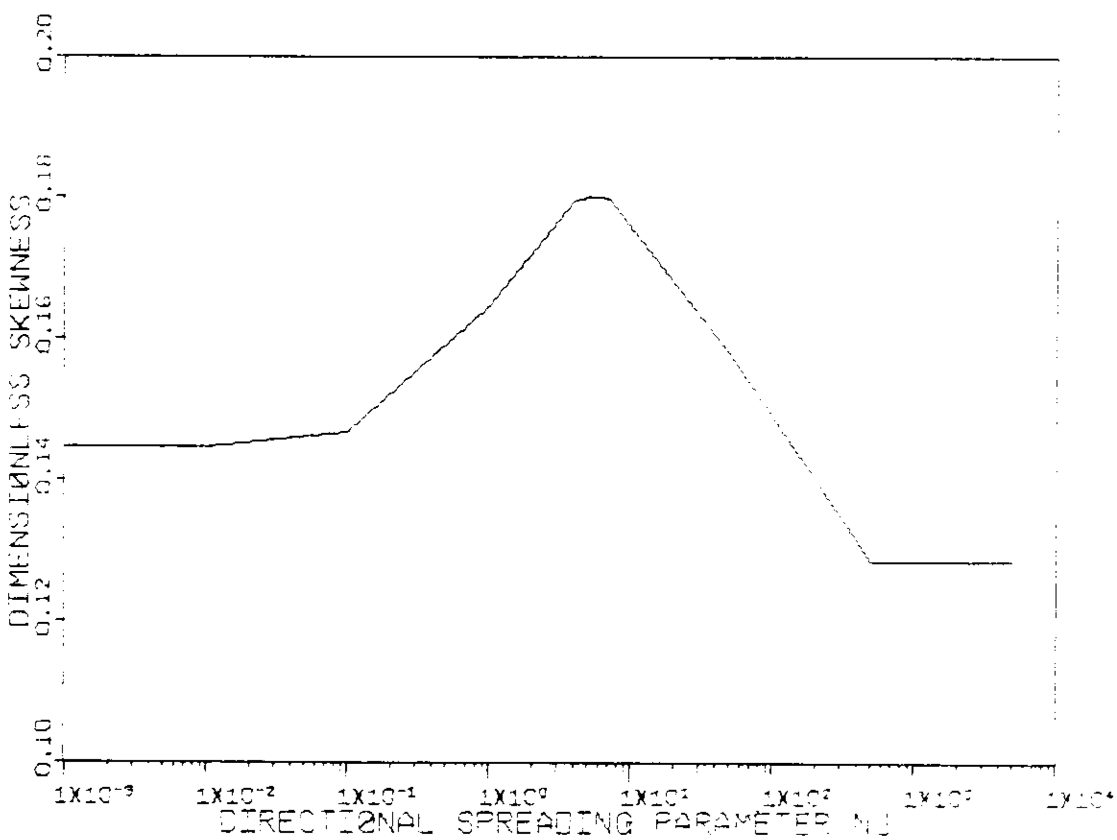

Figure 6-11. Variation in Dimensionless Skewness with Directional Spreading Parameter ν.

the wave directions spread uniformly over a 180 degrees sector, the skewness is less than the maximum but greater than for the case of unidirectional waves. Table 6-2 and Figure 6-11 represent cases of random waves, each with total energy equal to 22.3 feet square in a water depth of 100 feet. In lesser water depth and for greater wave energy the skewness would be greater.

It is of interest to consider the nature and cause of the maximum skewness calculated for the narrow directional spread. This is particularly significant because the limited directional spectrum estimates of a number of real wave systems indicate that the value of the spreading parameter ν lies between 1 and 2. In the extreme case, if we model a sea having a directional spread corresponding to a value of ν equal to 5 by a unidirectional sea, the skewness is reduced by 28%. Similar reductions are realized in the skewnesses of the water particle kinematics at several depths. As the drag force is proportional to the square of the velocities, the skewness of force is reduced by a greater percentage than for the sea surface.

In order to appreciate the manner in which the skewness is affected by the directional spreading in wave energy, it is helpful to examine the skewness kernel carefully. The skewness kernel for the infinite depth case has been presented by Longuet-Higgins (1963) and has been reproduced as Equation 2-23. The corresponding relation for the finite depth case has been derived in Chapter 3 (Equation 3-50). Analytically it has not been possible to show that the skewness kernel is always positive for the finite depth case as has been shown by Longuet-Higgins (1963) for the infinite depth case. However the numerical computations have shown that the skewness kernel for the finite depth case is positive for the frequency range 0.05 to 0.15 Hertz and water depths of 1, 10, and 100 feet. The calculations also indicate that the skewness increases as the water depth decreases. Table 6-3 presents values of the skewness kernel for three depths and two collinear waves of frequencies 0.075 and 0.080 Hertz.

These findings conform to the results and observations of other investigators. The waves become steeper and more asymmetric as they propagate into shallower water. The actual waves, however, are limited in amplitude and steepness because of other physical considerations. Therefore, in computing actual skewness coefficients, only physically realizable waves for the deptn under consideration should be used.

TABLE 6-3

Skewness Kernel Values for Two Collinear Waves

of Frequencies 0.075 and 0.08 Hertz

Depth in Feet	Skewness Kernel
1	0.251
10	0.026
100	0.0039

The variation in the skewness kernel with frequency and direction is much more interesting. The result of Longuet-Higgins (1963) for the infinite depth case was discussed in Chapter 2. The simulation method has been used to recalculate the kernel values for the deep water case by using a very large value for the water depth. The results of a typical computation are presented in Figure 6-12 as a surface plot. The plotted surface pertains to the values of the skewness kernel for a frequency of 0.075 Hertz interacting with 21 frequencies ranging from 0.05 to 0.15 Hertz and propagating from 36 directions ranging from 0 to 175 degrees. It can be noticed immediately that the point corresponding to the

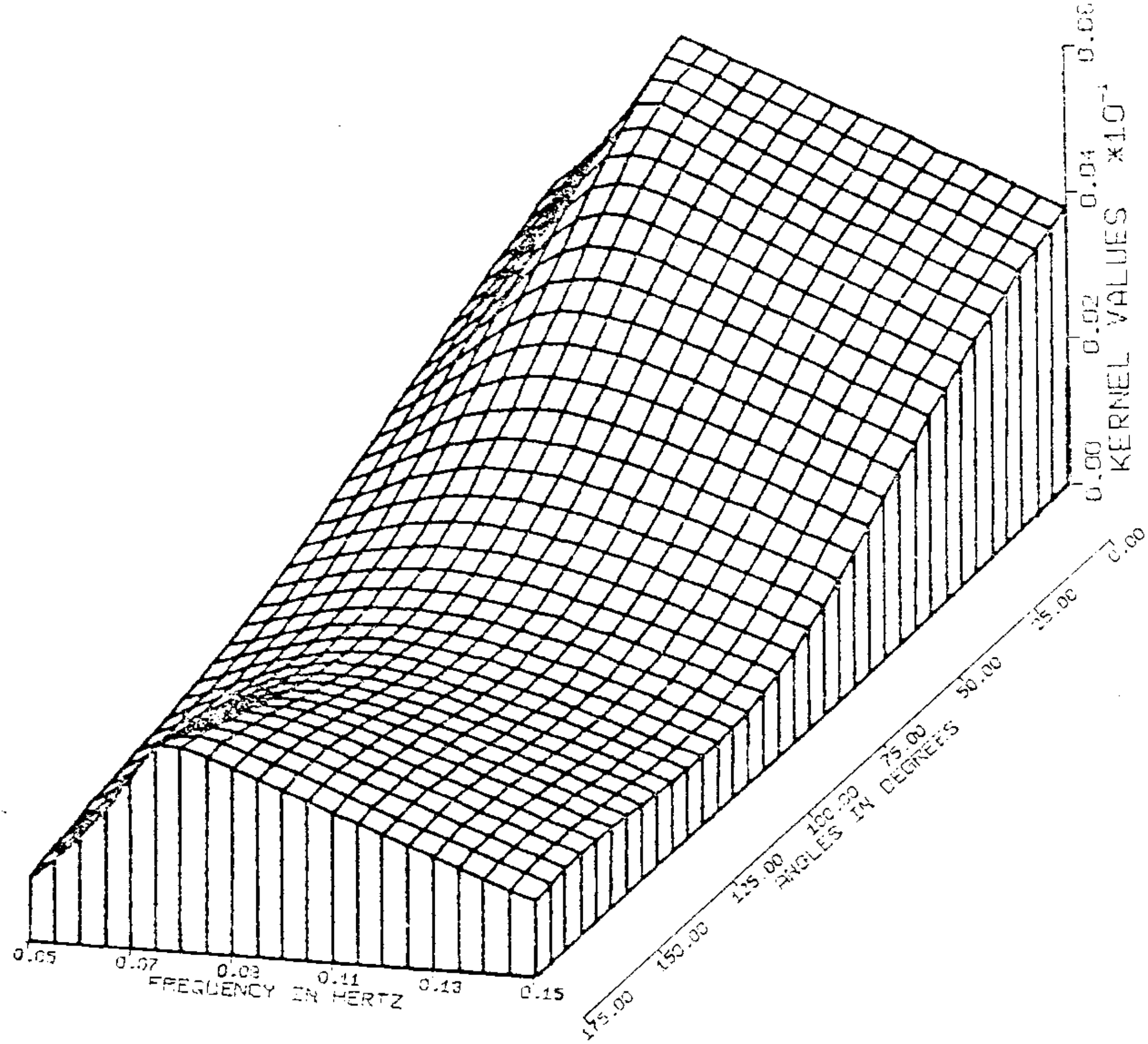

Figure 6-12. An Oblique View of a Surface Plot of the Skewness Kernel for a 0.075 Hertz Wave Interacting with 21 Waves of Frequencies Ranging from 0.05 to 0.15 Hertz Propagating at 36 Angles Ranging from 0 to 175 Degrees in Water of Infinite Depth.

self-interaction is the most prominent feature on the kernel surface. For the given two frequencies the kernel value for the collinear case is greater than those for almost all other included angles. It will be seen later that there is a weak peak for an included angle of about 9 degrees. For a given pair of waves the interaction is the least for the nearly orthogonal directions. These features are similar to those discussed by Longuet-Higgins (1963).

Similar calculations have been carried out for the finite depth case. The skewness kernel for 100 feet depth has been plotted to evaluate any special features. Figure 6-13 shows the surface plot of skewness kernel for a wave of 0.075 Hertz frequency interacting with waves of 21 frequencies ranging from 0.05 to 0.15 Hertz and propagating at 36 angles ranging from 0 to 175 degrees in a water depth of 100 feet. Self-interaction is the most prominent feature even in the case of finite depth. For included angles between 0 and 60 degrees, the interaction in shallow water is much stronger than in the deep water. For included angles between 60 and 175 degrees, interactions in the two cases are very similar. In this range of included angles the interaction for the shallow water is marginally greater than that for the deep water

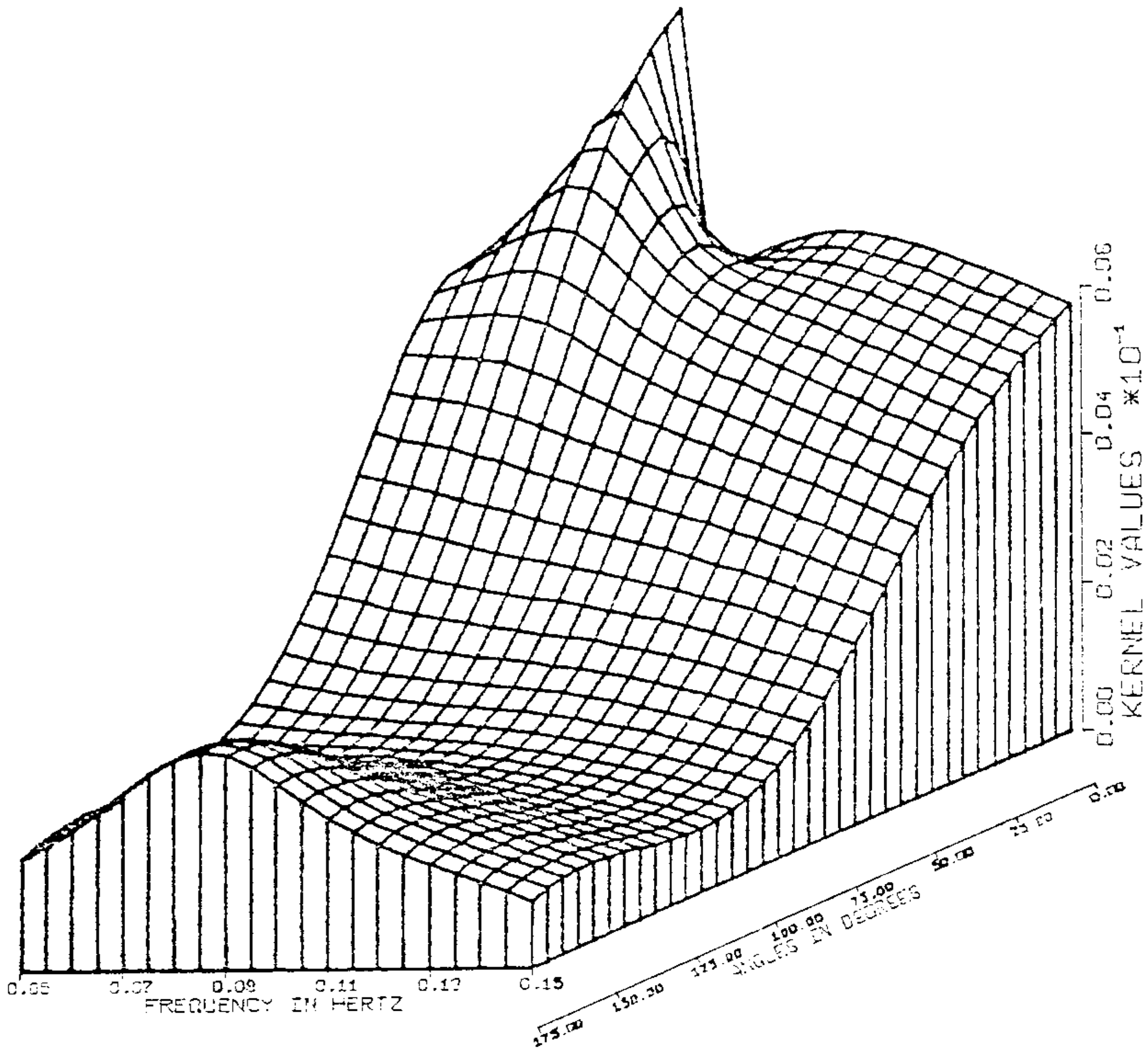

Figure 6-13. An Oblique View of a Surface Plot of the Skewness Kernel for a 0.075 Hertz Wave Interacting with 21 Waves of Frequencies Ranging from 0.05 to 0.15 Hertz Propagating at 36 Angles Ranging from 0 to 175 Degrees in a Water Depth of 100 Feet.

case. For frequencies much greater than 0.075 Hertz, the strongest interaction occurs when the waves are collinear. This feature is similar to the infinite depth case. But in the neighborhood of 0.075 Hertz, interaction in a direction other than the collinear one has the maximum value.

The skewness kernel values for a 0.075 Hertz wave interacting with a 0.08 Hertz wave propagating over a directional range varying from 0 to 180 degrees have been computed and plotted in Figure 6-14. The solid line is for the deep water case. The curve is nearly symmetrical about 95 degrees. There is a weak maximum around an included angle of 9 degree. For comparing this curve with that of Longuet-Higgins for the deep water case, the dimensionless parameter defined in Equation 2-24 has been computed. Its value in the present case is equal to 1.00085. The curve corresponding to this value in Figure 2-1 is the same as the solid line in Figure 6-14 except for a factor.

The broken line in Figure 6-14 shows the variation in the skewness kernel for the same frequencies and directions but in 100 feet water depth. For small included angles the kernel value is low. This sharply

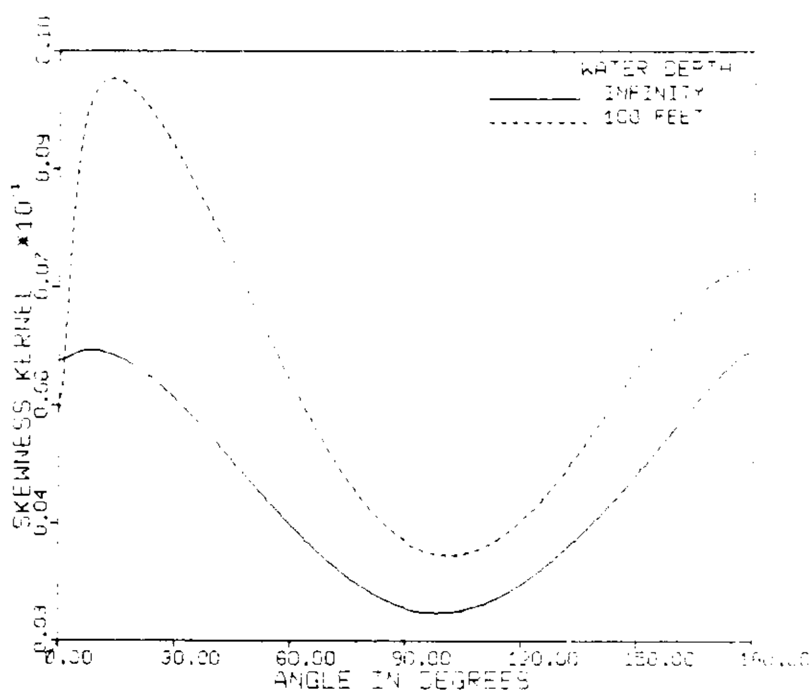

Figure 6-14. Variation in Skewness Kernel Values with Change in Included Angle for Two Waves of Frequencies Equal to 0.075 and 0.08 Hertz.

rises to a maximum around 13 degrees. It gradually descends to a minimum value around 100 degrees, then slowly increases to a maximum at 180 degrees. The value at 180 degrees is higher than that at 0 degrees. For the approximate range 0 to 60 degrees the kernel values for the 100 feet depth case are much higher than those for the deep water case. For about 60 degrees to 180 degrees the kernel values for the 100 feet depth case are greater than, but much closer to those for the infinite depth case.

The second order correction is partly the result of the quadratic velocity effect in the dynamic free surface boundary condition. It can be shown easily that in the case of two waves intersecting at an angle, the quadratic velocity correction is maximum when the two waves are collinear. When the two waves have nearly the same frequency and travel at a small angle, their crests propagate nearly in phase. This causes strong interaction similar to the self-interaction effects. Thus for two waves of nearly equal frequencies, greater interaction occurs at a small intersecting angle rather than at zero angle.

The previous discussion of the skewness kernel is now used to explain the simulated result that the skewness of the sea surface is greatest for a narrow directional spread of a random sea. As discussed in the previous paragraphs, for the 100 feet depth the skewness kernel has much higher values for angles ranging from 0 to 60 degrees than those for angles encompassing 60 to 180 degrees. In the 0 to 60 degree range the kernel value has a sharp peak around 13 degrees. Thus if all the energies are concentrated in one direction, the skewness is small. As the directional spread increases, more wave interactions take place at angles around 13 degrees, thus resulting in higher skewness. Further increase in the directional spread results in more waves interacting at angles other than 13 degrees and also at angles greater than 60 degrees for which skewness kernel values are lower than those for angles 0 to 60 degrees. This means lower skewness for greater than an optimum directional spread. For the directional spreading model used in this study the maximum skewness occurs for a narrow directional spread corresponding to the directional spreading parameter ν equal to 5.

Any discussion of skewnesses would be incomplete without referring to the negative skewnesses measured in the field and the laboratory.

6.6 Observed Negative Skewnesses

The nonlinear wave theories and almost all the observations in the field and laboratory indicate that water waves have positive skewnesses. However, some of the observations of Kinsman (1960) have negative skewnesses. These observed negative skewnesses are generally ascribed to errors in data gathering, and in numerical computation, particularly due to the finite length of record. During the course of this study, a possible mechanism for the occurrence of negative skewnesses has been developed.

As found in Chapter 3, the second order components have frequencies equal to the sums and the differences of the linear component frequencies. The components obtained by summing the frequencies cause positive skewness, because they sharpen the crests and flatten the troughs. The components obtained by taking differences of the linear frequencies are better known as "beat" frequencies. These beat frequencies are 180 degrees out of phase with the wave group envelope. The beat profile has a minimum corresponding to the peak in the wave envelope and vice-versa, thereby reducing the mean cube value and the skewness of the sea surface displacement. As the wave group moves into shallower water, the energy in the beat frequency bands increases, thus decreasing the skewness. The individual waves at the same time steepen and increase skewness. But they soon become unstable particularly in the presence of an overlying wind and break into smaller waves. Thus growth of positive skewness may be limited by the physical considerations.

From the above discussion it can be concluded that the presence of proportionately high energy in the beat frequency bands, which are 180 degrees out of phase, indicates the possibility of the presence of very low or negative skewnesses. The data of Kinsman (1960) have been examined in this light. The spectral densities of 16 data sets have relatively small energy in the very low frequency bands. These records have skewnesses varying from 0.138 to 0.438. But 9 data sets have varying amounts of energy in the beat frequency bands. The computed skewnesses for these records are all very low, between -0.092 and 0.088, three of them being negative. Record No. 083 has skewness equal to -0.004. The spectral density of this record has been reproduced in Figure 6-15. It can be seen that a large fraction of the total energy is in the low frequency bands for this case.

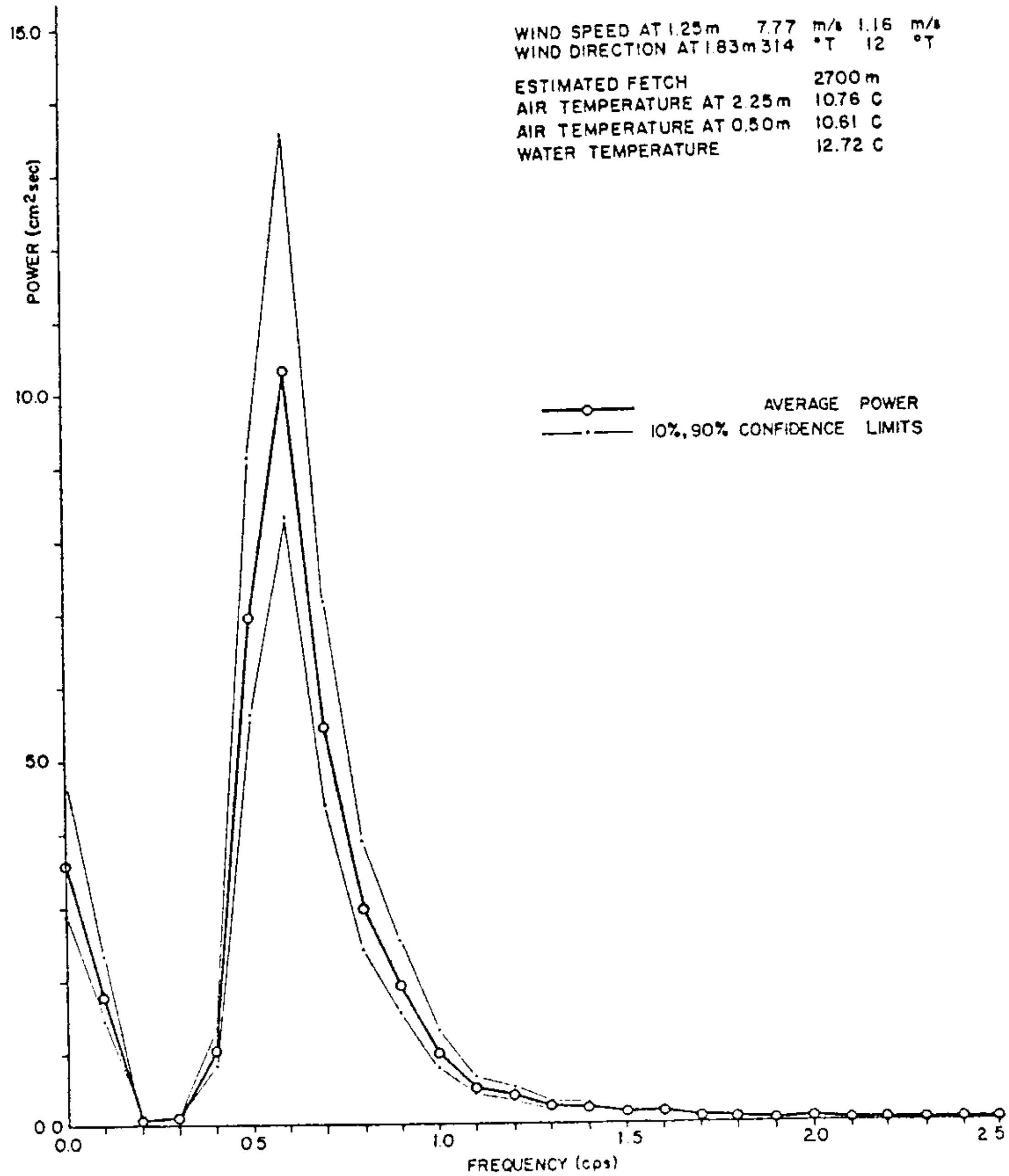

Figure 6-15. Spectral Density of Wave Record No. 83
(Reproduced from Kinsman 1960).

The previous brief discussion about skewness has not only theoretical importance but has practical significance in wave force computations because the skewness of the wave forces is higher than that of the sea surface and an increase in the skewness of force alters the distribution of the extreme forces. This and other aspects of wave force simulation have been discussed in the rest of this chapter.

6.7 Wave Force Simulation

For the four directional spreads, wave forces per unit length of pile at five levels have been computed using the Morison formula with drag and inertia coefficients suggested by Dean and Aagaard (1970). For even a small directional spread, large forces in the direction normal to the dominant direction have occurred in the simulation. Total forces on the length of the pile below water have been computed. The maximum force in a simulated wave has been compared with the maximum force computed by the Stokes second order theory for a wave of the same period and wave height. The average ratios of the forces computed by the Stokes second order theory and the simulation method vary from 0.95 to 1.62 for unidirectional and omnidirectional energy distributions respectively. Similar ratios are indicated by the hybrid method (Dean 1977) for a drag dominant case.

By strict superposition of the kinematics due to each linear and second order nonlinear components, the accelerations and the velocities in the x and y directions have been computed at five levels in a water depth of 100 feet which is nearly equal to the water depth of 98.8 feet associated with Wave Force Project II measurements. The resultant horizontal force per unit length was computed by the Morison formula using the computed kinematics and the modified Dean and Aagaard (1970) resultant force coefficients reproduced in Table 6-4. The Reynolds number was determined using a value for kinematic viscosity equal to 0.000014 feet squared/second, a pile diameter of 3.71 feet, (which is equal to the diameter of the instrumented pile in the Wave Force Project II) and a density of sea water of 2.0 slugs/cubic feet.

TABLE 6-4

Modified Drag and Inertia Coefficients for the Resultant Pressure Forces per Unit Length (Dean and Aagaard, 1970)

Reynolds No. (X 10)	Coefficient of Drag, C	Coefficient of Inertia, C
Re < 3	1.34	1.18
3 < Re < 10	0.98	1.18
Re > 10	0.92	1.18

6.8 Linear and Nonlinear Random Pressure Forces

The force per unit length has been computed for five levels in a water depth of 100 feet. The force per unit length in the predominant direction (inline) and a direction normal to it (transverse direction) for a level 75 feet above bottom were computed and plotted for the four directional distributions used in this study. Figure 6-16 presents computed wave forces for the unidirectional waves for which the transverse direction forces are identically equal to zero. Figure 6-17 shows the forces

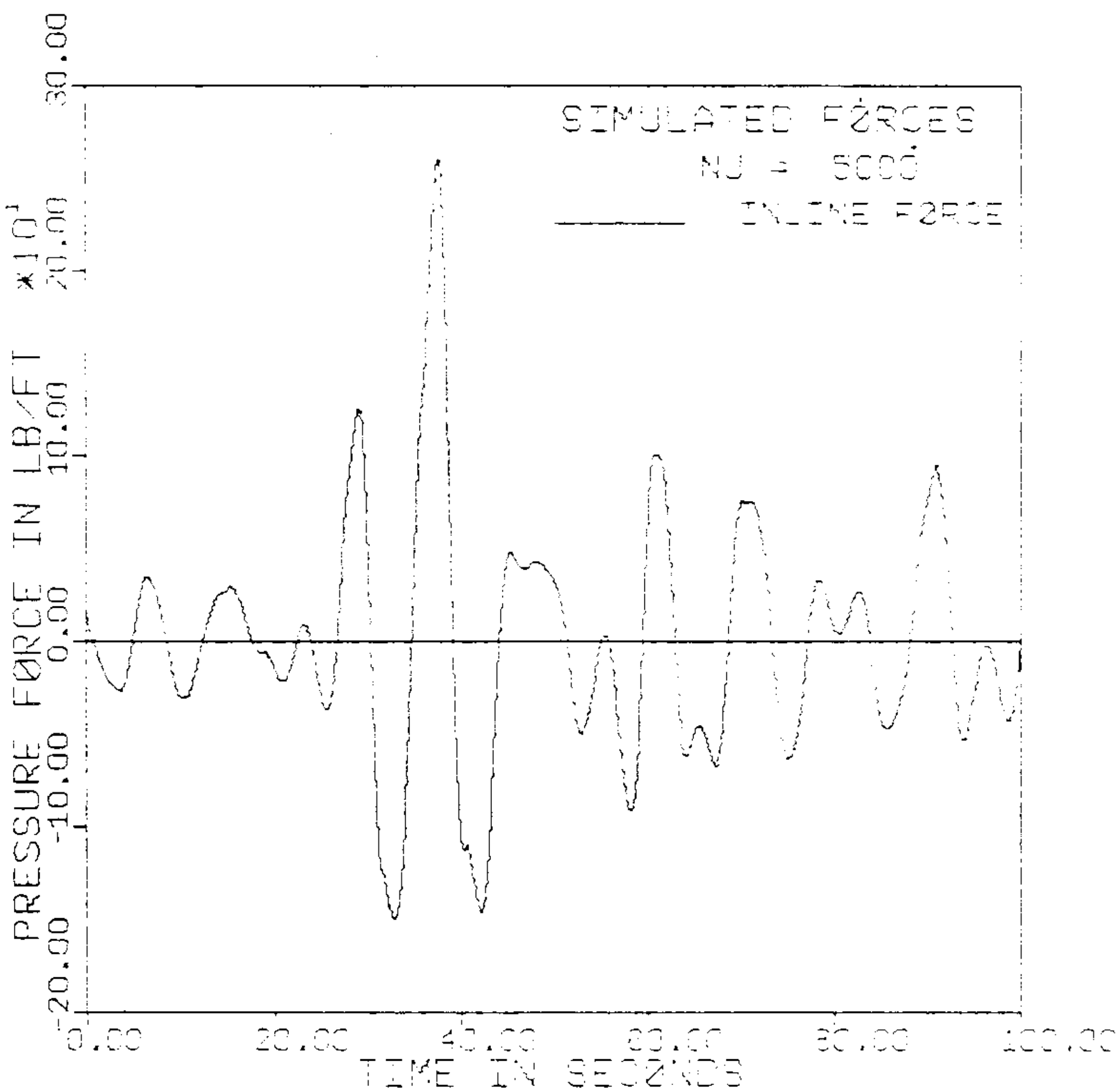

Figure 6-16. Simulated Variation of Force per Unit Length on a 3.7 Feet Diameter Pile at a Level 75 Feet from Base in a Water Depth of 100 Feet for Unidirectional Waves.

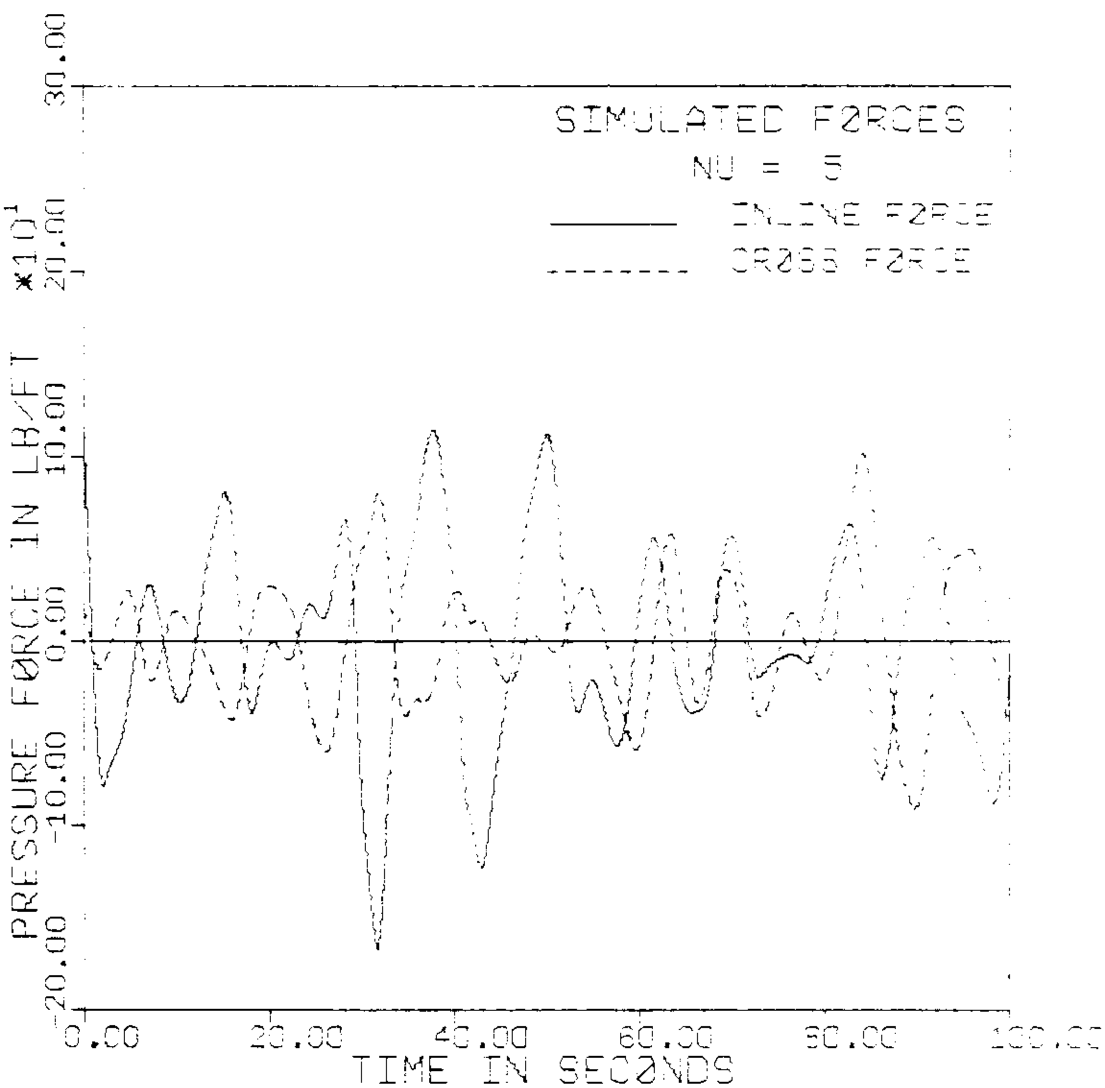

Figure 6-17. Simulated Variation of Force per Unit Length on a 3.7 Feet Diameter Pile at a Level 75 Feet from Base in a Water Depth of 100 Feet for a Directional Distribution of Wave Energy Given by $\cos^{10}\theta$.

for a narrow directional distribution of energy corresponding to a value of ν equal to 5. The solid line shows the instantaneous force per unit length in the predominant direction. The dashed line shows the instantaneous force per unit length in the transverse direction. It can be seen that the forces in the transverse direction are of the same order of magnitude as in the predominant direction. It appears that the instantaneous resultant force occurs from all directions. In the case of ν equal to 1 (Figure 6-18) and the homogeneous wave field case (ν equal to 0, Figure 6-19), the forces in the transverse direction are as large as those in the predominant direction.

The Wave Force Project II field data for the wave forces show very large forces in the transverse direction. It has been suggested that these large transverse forces are due to the vortex shedding effects. In the present study vortex shedding effects were not considered yet large transverse forces have occurred in the simulation of directional seas. The results of this study show that the large transverse forces can be caused by a directional distribution of wave energy.

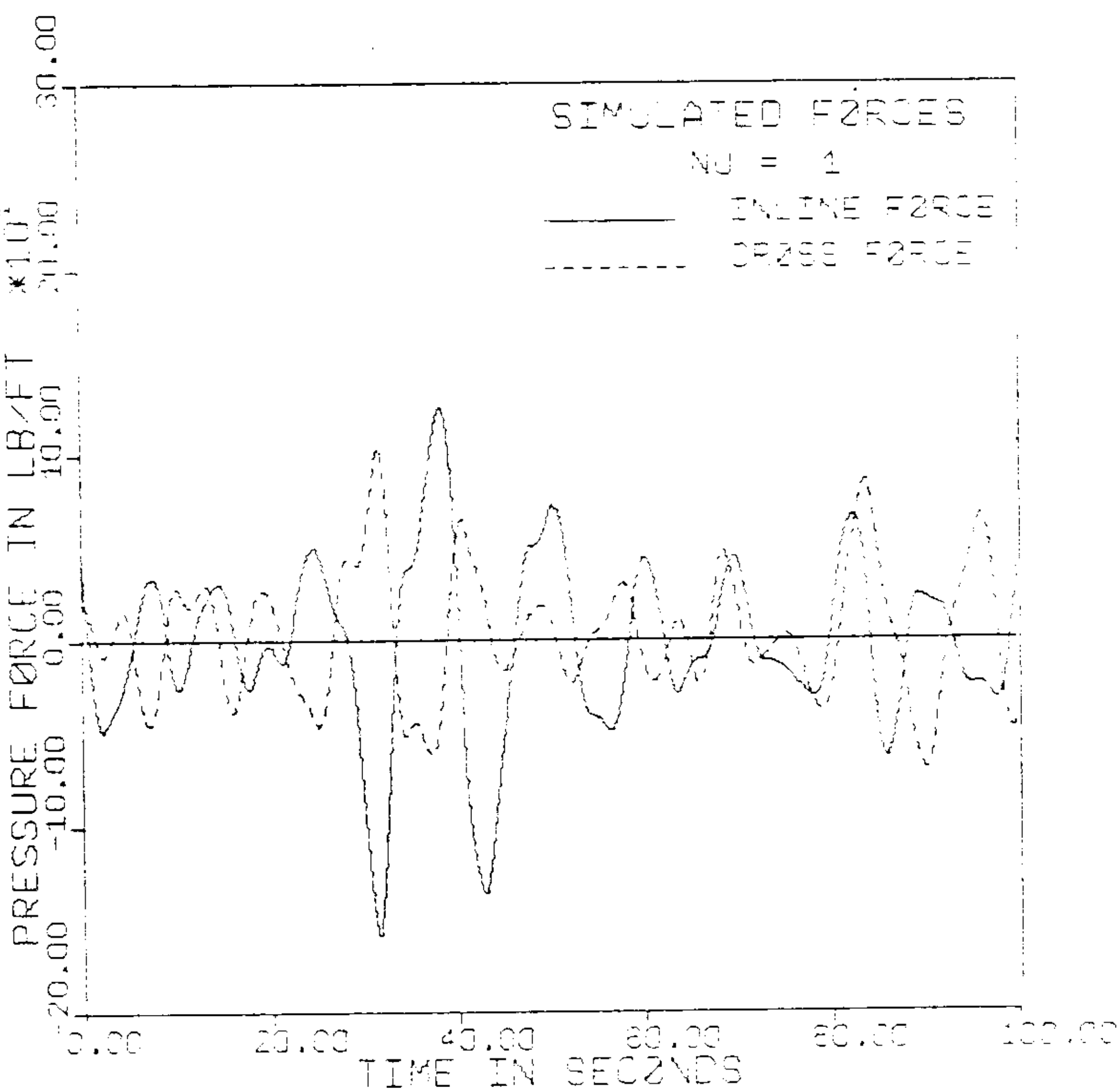

Figure 6-18. Simulated Variation of Force per Unit Length on a 3.7 Feet Diameter Pile at a Level 75 Feet from Base in a Water Depth of 100 Feet for a Directional Distribution of Wave Energy Given by $\cos^2 \theta$.

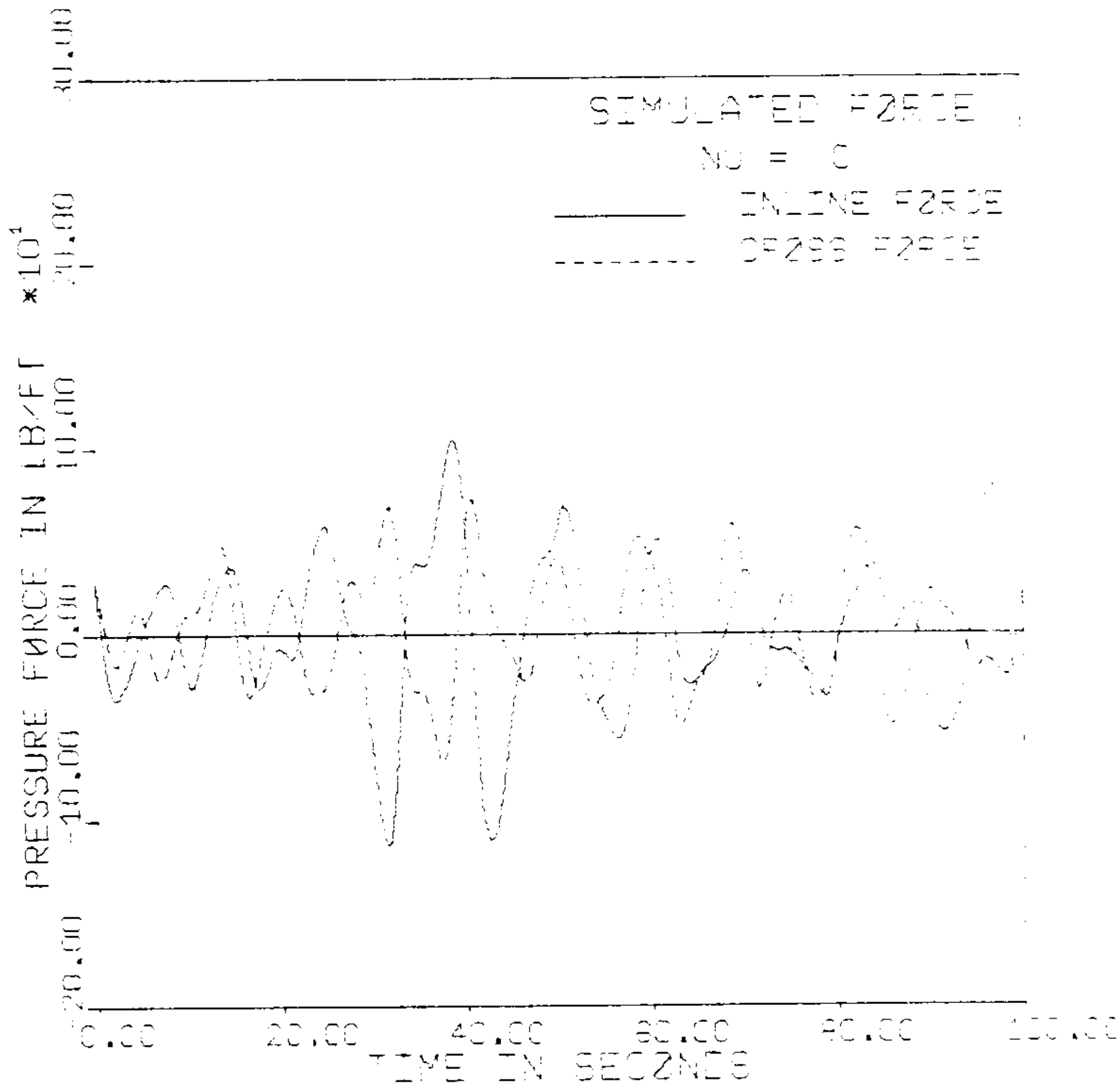

Figure 6-19. Simulated Variation of Force per Unit Length on a 3.7 Feet Diameter Pile at a Level 75 Feet from Base in a Water Depth of 100 Feet for an Omnidirectional Distribution of Wave Energy ($\nu = 0$).

6.9 Spectral Densities of the Simulated Pressure Forces

The spectral densities of the force per unit length in the predominant direction and a direction normal to it for a level 75 feet above the bottom have been computed and plotted for the four directional distributions used in this study. Figure 6-20 shows the spectral density of the force per unit length in the case of unidirectional waves. The highest peak in the figure corresponds to the peak in the wave spectral density (Figure 6-16). There are two other smaller peaks corresponding to the frequencies equal to 1.5 and 2 times the frequency corresponding to the principal peak.

Figure 6-21 shows the spectral densities of the inline and the transverse forces at 75 feet above the bottom for a directional distribution given by $\cos^2\theta$. The spectral density for the inline force is similar to the unidirectional case, except that it has a small peak at about the third subharmonic of the frequency corresponding to the principal peak. The broken line shows the spectral density of the forces in the transverse direction. This does not have a peak at the frequency for which there are peaks in the spectral densities of the sea elevation and the inline forces. The

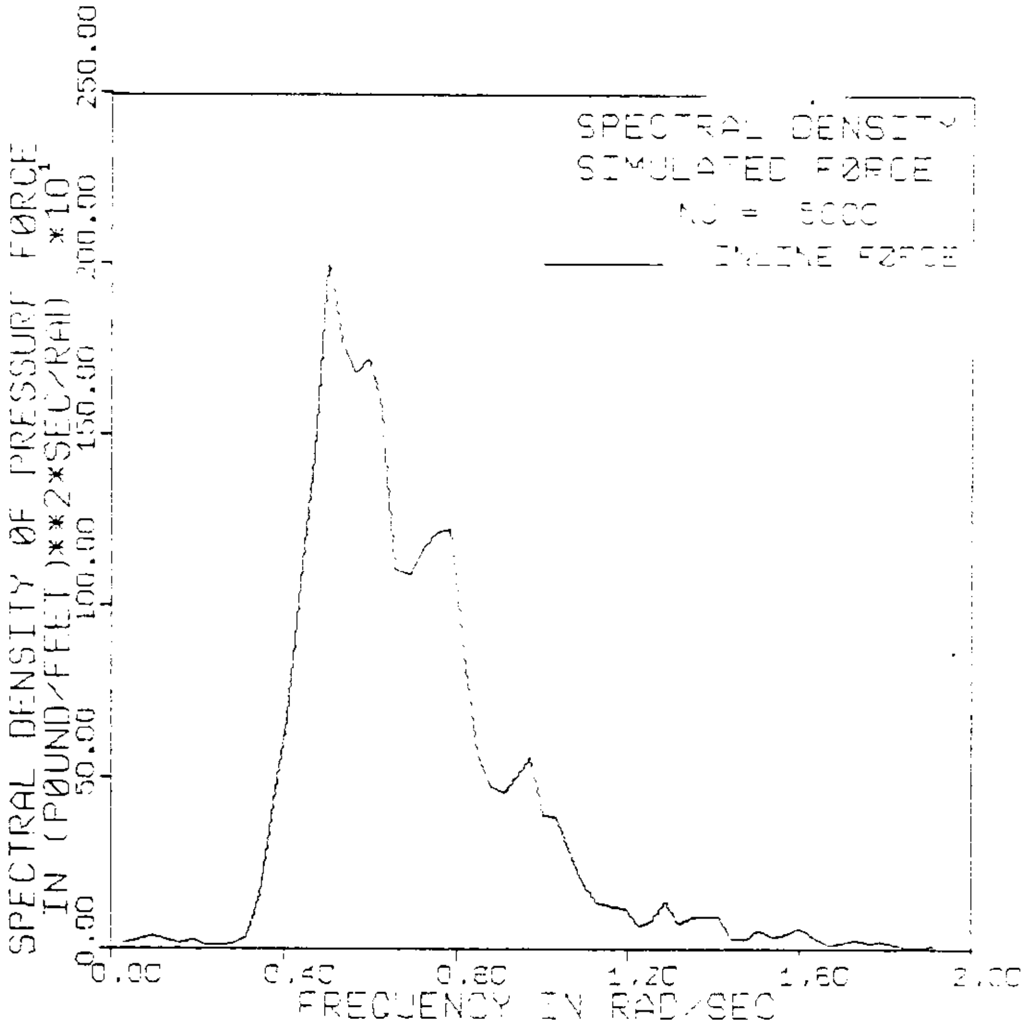

Figure 6-20. Spectral Density of Simulated Force per Unit Length at a Level 75 Feet Above the Bottom for Unidirectional Waves.

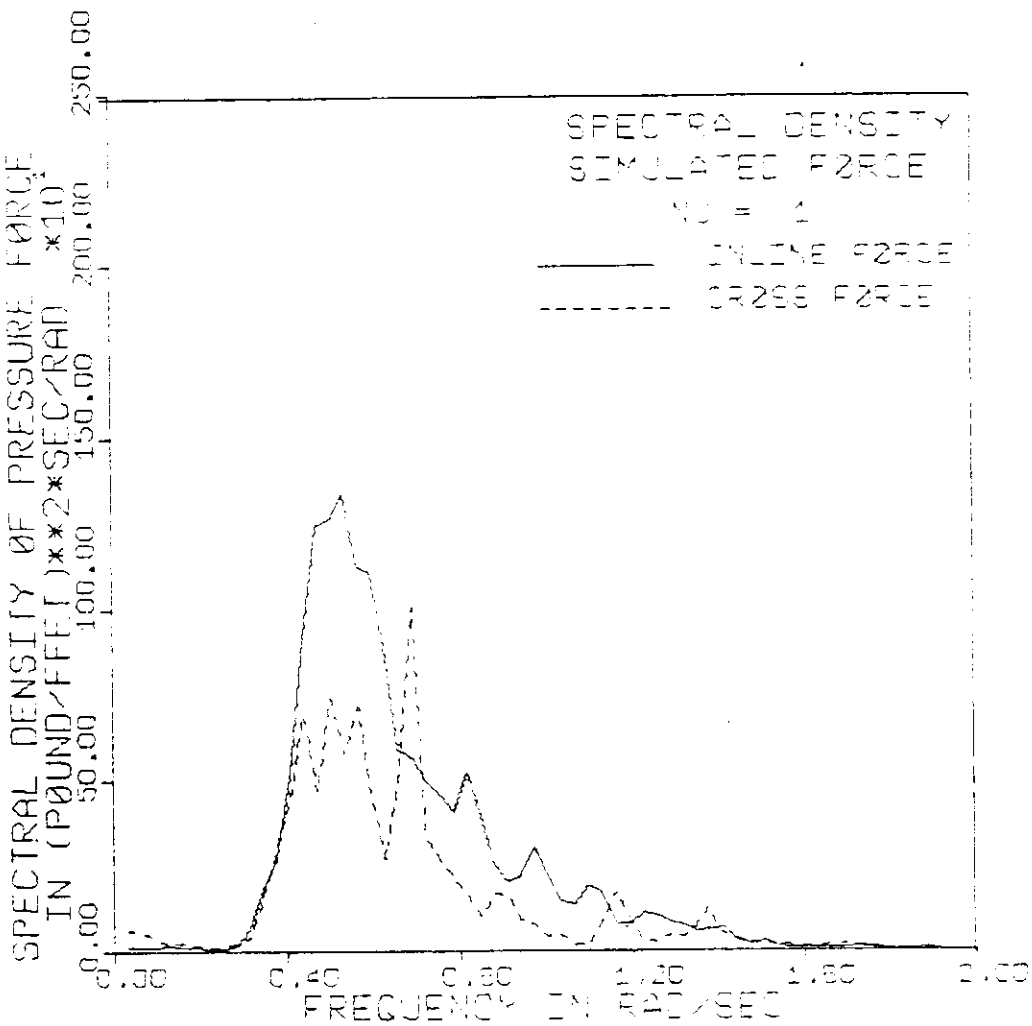

Figure 6-21. Spectral Density of Simulated Force per Unit Length at a Level 75 Feet Above the Bottom for a Directional Distribution of Energy Given by $\cos^2\theta$.

spectral density of the transverse forces is rather broad band in the range 0.4 to 0.8 radians/second. The mean square value of the transverse forces is smaller than that of the inline force.

The spectral densities of the inline and the transverse forces for the directional distribution given by $\cos^{10}\theta$ (Figure 6-22) are similar to those for the directional distribution given by $\cos^{2}\theta$, except that the small peak at the third subharmonic is not present. The mean square value of the inline force is substantially greater than that of the transverse force.

In the case of the completely homogeneous sea, the mean square values of the inline and the transverse forces are nearly equal (Figure 6-23). In other words, there is no predominant force direction. The transverse forces have significant energy in the beat frequency bands, while the inline forces do not.

Several interesting features have been noticed in the force spectra. The presence of peaks in the inline force spectra at the frequencies equal to that corresponding to the peaks in the sea elevation spectra are expected results. In addition peaks have occurred at the third subharmonic frequency and at 1.5 times the

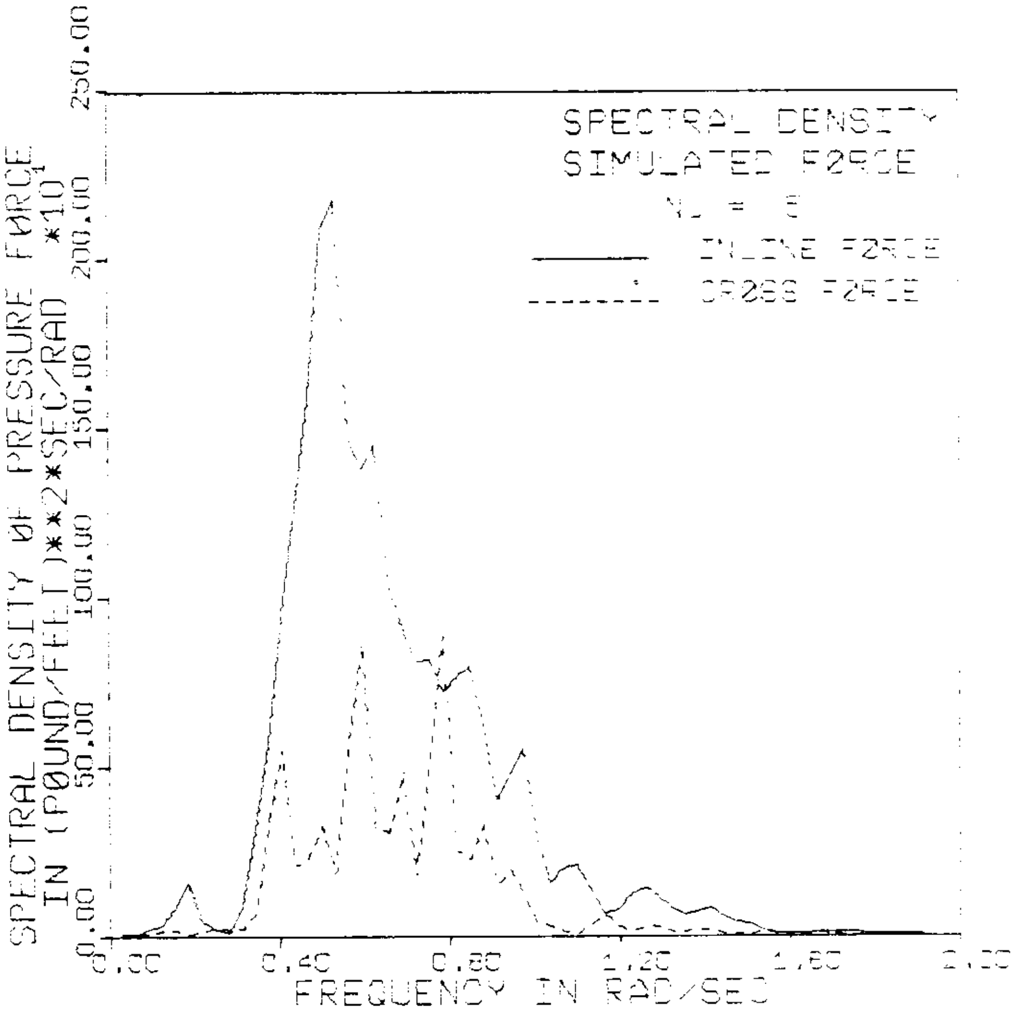

Figure 6-22. Spectral Density of Simulated Force per Unit Length at a Level 75 Feet Above the Bottom for a Directional Distribution of Energy Given by $\cos^{10}\theta$.

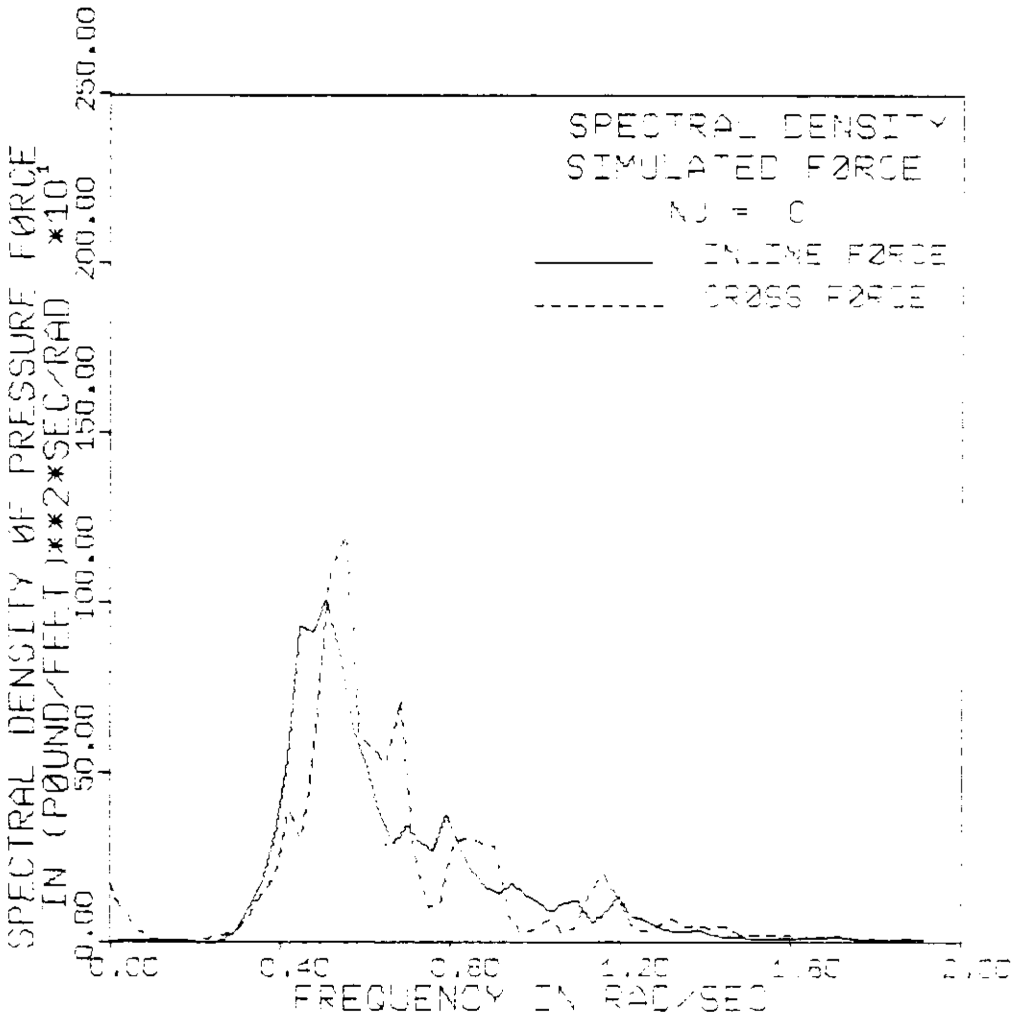

Figure 6-23. Spectral Density of Simulated Force per Unit Length at a Level 75 Feet Above the Bottom for Uniform Energy Density Over a 180 Degree Sector (ν = 0).

fundamental frequency. These seem to have been generated through the nonlinearity associated with the wave force (drag component). The transverse force spectra are broad band for the two narrow directional distributions used in this study. For the completely homogeneous sea the transverse force spectral density is similar to the inline spectral density except for significantly greater energy in the beat frequency bands.

6.10 Comparison with Hybrid Method for Single Pile

The total force on a piling has been computed by numerically integrating the force per unit length up to the free water surface. From the record of the water surface elevation, 17 to 28 waves with single peaks have been selected (Figure 6-24). For each of these waves, the following were tabulated:

(i) the wave height, defined as the difference between the crest level and the average of the adjoining trough elevations;

(ii) wave period, defined by the time between two consecutive upward zero crossings; and

(iii) the maximum simulated force occurring during each of the selected waves.

For each of these waves, the total force on the pile has also been computed using the Stokes second order wave

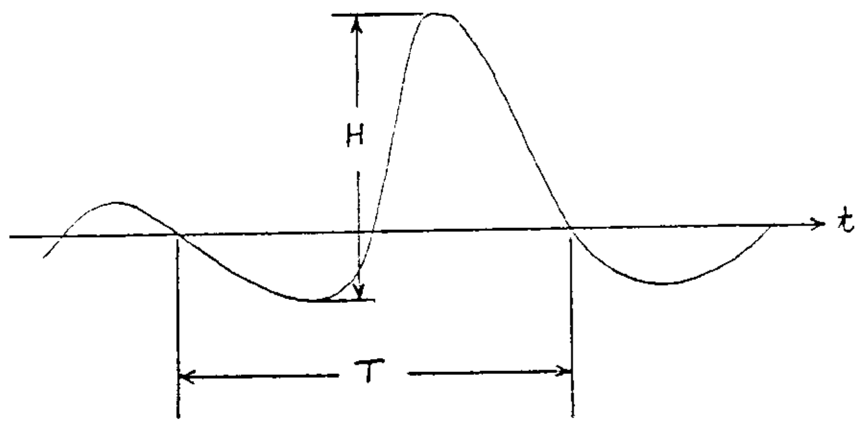

Figure 6-24. Definition Sketch for Obtaining Wave Height and Wave Period from a Random Sea Elevation Record.

theory. An appropriate reduction factor from the Hybrid method has been applied to obtain the computed maximum total force on the pile. For a directional spread corresponding to a value of ν equal to 1, the total forces obtained in this manner are plotted against those obtained directly from the simulation method in Figure 6-25. There is reasonable agreement with the line of equivalence. Since the simulated waves are not symmetrical about the crest as are the Stokes waves, the forces computed by the two methods do not agree on a one-to-one basis.

Similar computations have been carried out for the four directional distributions. A ratio has been computed for each wave by dividing the force obtained by simulation into the force calculated by the Stokes second order theory. The average ratio for the four directional spreads has been presented in Table 6-5. In the same table, ratios recommended by the Hybrid method for the inertia dominant and the drag dominant cases have been given for comparison. It is seen that the ratios calculated by the simulation method are very close to the ratios suggested by the Hybrid method for the drag dominant case. The force ratios vary from 0.95 to 1.62 for the directional distribution changing from the

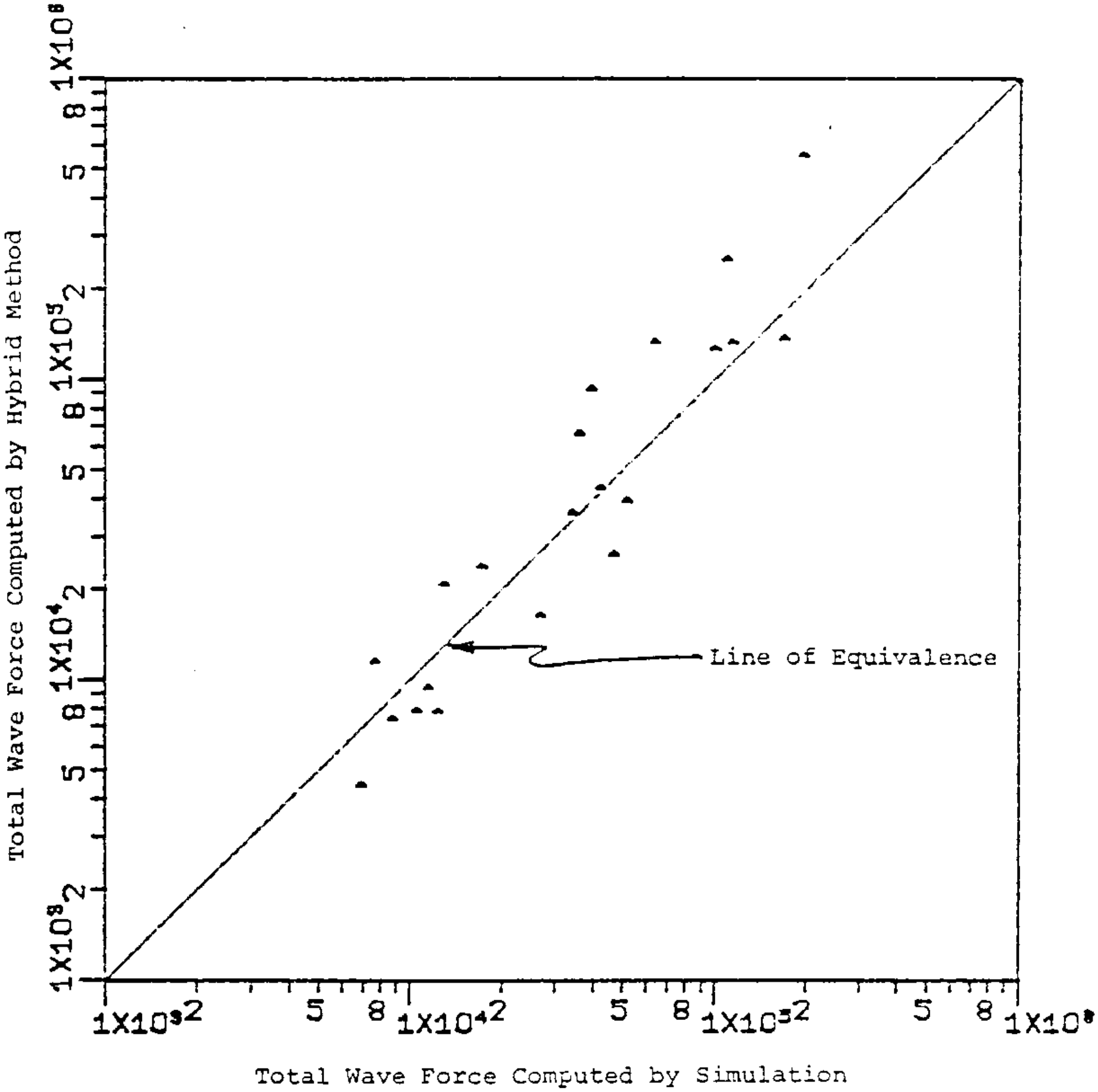

Figure 6-25. Comparison of Total Wave Force on a Pile in 100 Feet of Water Computed by Hybrid Method and Simulation Method (Directional Spread Given by $\cos^2\theta$).

TABLE 6.5

COMPARISON OF TOTAL FORCES ON A SINGLE PILING

OBTAINED BY SECOND ORDER SIMULATION AND THE HYBRID METHOD

(Water Depth = 100 ft.)

Exponent ν in Spreading Function: $\cos^{2\nu}\theta$	Hybrid Method: Ratio of Non-Linear Wave Force for Unidirectional and Directional Seas		Simulation Method	
	Inertia Dominant	Drag Dominant	Average Ratio of Forces Computed by Stokes Second Order Theory and Simulation Method	No. of Force Ratios Included in Average
∞ (Unidirectional)	1.0	1.0	.95	17
5	1.04	1.09	1.13	19
1	1.15	1.33	1.48	21
0 (Omnidirectional)	1.30	1.69	1.62	28

unidirectional to the omnidirectional case. Thus in the extreme case of a completely confused sea, the second order Stokes theory predicts wave forces which are approximately 60 percent greater than those obtained by the simulation of a second order directional sea.

6.11 Comparison of Total Forces on a Four Pile Group

The total forces on a four pile group with one 3.7 feet diameter pile at each corner of a square (Figure 6-26) were computed by the simulation method for the four directional distributions of energy. The maximum force in a number of waves has been compared with the maximum force computed by the second order Stokes theory using the wave height and period of the corresponding simulated waves. The average ratios of forces computed by the Stokes second order theory and the simulation method have been computed for the each of the four directional distributions. Table 6-6 presents the average ratios for two cases: one for a pile separation of 60 feet and the second for a pile separation of 300 feet. It is seen that for the 60 feet case the ratios are the same as the ones for the single pile case. But for piling that are 300 feet apart, the average ratios range from 1.26 to 2.54. Thus for the four piles 300 feet apart the second order

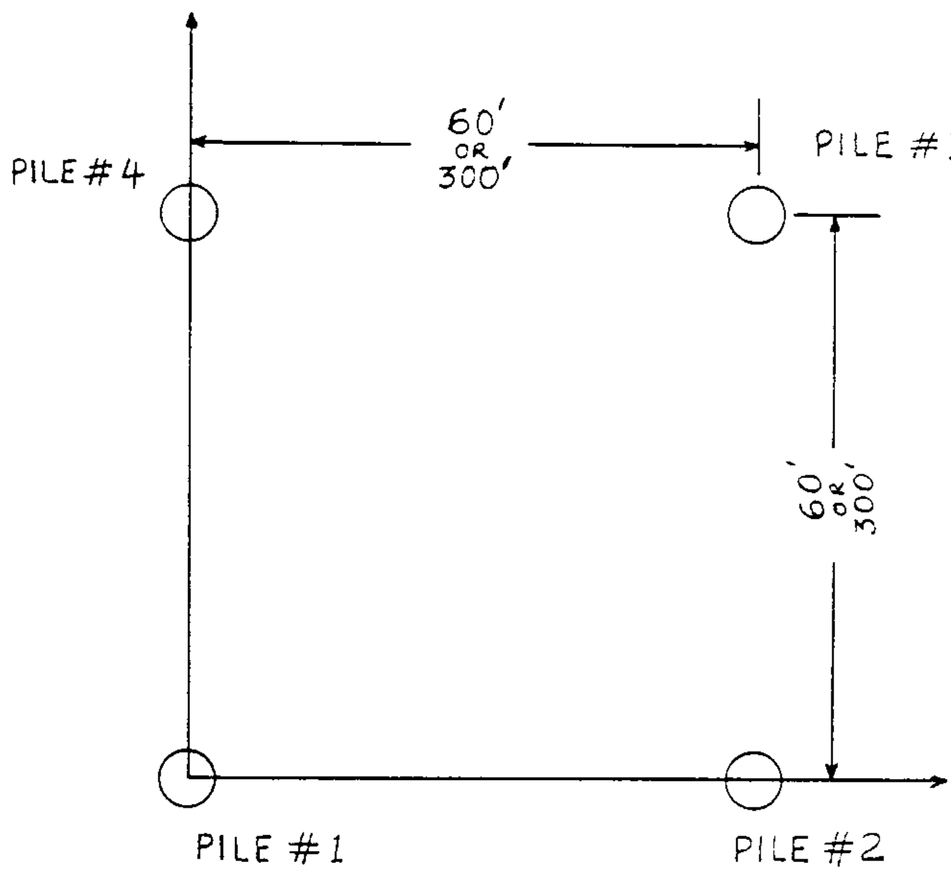

Figure 6-26. Plan View of Pile Groups Considered in This Study.

TABLE 6-6

Comparison of Total Forces on a Four Pile Group Obtained by the Second Order Stokes Theory and the Second Order Directional Simulation

ν	Average Ratio of Forces Computed by Stokes Second Order Theory and Simulation Method		
	Separation in feet		Sample
	60	300	Size
5000	1.02	1.26	17
5	1.13	1.53	19
1	1.50	2.54	21
0	1.63	2.46	28

Stokes theory yields forces which are 26 percent to 154 percent greater than those obtained by a simulation of the second order directional random sea.

The four pile group with 60 feet separation is not very different from the single pile case, because the wave lengths associated with the predominant wave energy, are nearly ten times the separation distance. Therefore, the crests of high waves occur nearly simultaneously at the four piles. Hence, the maximum total force on the pile group is approximately equal to four times the maximum total force on a single pile.

The separation distance of 300 feet is more interesting because it is approximately equal to half the wave length of the waves associated with the predominant wave energy propagating in y direction. Hence, the simultaneous occurrence of the crests of high waves at the four piles is very rare. The correlation amongst the sea surface elevations at the four piles is either very small or negative. Table 6-7 depicts the correlation matrix for the water surface elevation at the four piles for the directional distribution of energy given by $\cos^2\theta$

TABLE 6-7

Correlation Matrix for the Sea Surface Elevation at the Four Piles for the Directional Distribution Given by $\cos^2\theta$

Pile No.	1	2	3	4
1	1.0	-0.323	0.033	-0.389
2	-0.323	1.0	-0.390	0.055
3	0.033	-0.390	1.0	-0.233
4	-0.389	0.055	-0.233	1.000

Similar correlations exist for the forces. Therefore, the forces on the piles cancel one another resulting in a smaller total force on the pile group.

These results suggest that considerable economy can be realized in the design of large structures by incorporating the directional effects of a real sea.

CHAPTER 7

SUMMARY AND CONCLUSIONS

In the present study the nonlinearities, randomness and directionality (all important elements of ocean waves) have been retained. The twofold nonlinearity, one due to the nonlinear boundary conditions at the surface and the second due to the drag force relationship, prevent a closed form solution for the wave forces from being obtained. In order to study the effect of the directional spread of wave energy and the distance between piles in a pile group on the extreme wave forces on a pile, a methodology has been developed to simulate three dimensional nonlinear random seas and the associated wave forces.

The boundary value problem with the appropriate boundary conditions for a three dimensional nonlinear random wave field is presented in Chapter 3. Using perturbation techniques, the nonlinear problem is converted into linear (in the unknowns of that order) boundary value problems. These are solved for the finite depth case in terms of finite Fourier sums. Relationships for the second order interaction components are derived in Section 3-4. The results obtained were verified with prior solutions due to Longuet-Higgins (1963) and Chappelear (1961) for more specialized cases.

Some of the statistical relations for the linear directional sea are presented and discussed in Chapter 4. In particular formulas are presented for the correlations and probability density for the water particle kinematics, distribution of force per unit length of a pile, and, for the drag dominant case, a closed form solution for the joint probability density of x and y force components for three dimensional random seas.

In directional sea simulation, certain difficulties may be encountered because of adding the same frequency components with random independent phases. A discussion of this problem is followed by an investigation into the effects of finite time simulation on the mean square value of a random realisation, and on the correlations amongst the simulated variables.

The method for simulating a three dimensional nonlinear random wave field is described in Chapter 5. Wave forces due to a directional nonlinear random sea are simulated via the following steps:

(i) a linear directional sea is represented by a number of discrete frequencies and at each frequency there are several wave components with independent phases propagating in several directions;

(ii) second order perturbation components including all fundamental interactions are computed according to the analytical formulation developed for the finite depth case;

(iii) water particle kinematics are computed from the linear and nonlinear second order perturbation components; and

(iv) the wave forces are computed from the water particle kinematics and the Morison formula using suitable drag and inertia coefficients suggested by Dean and Aagaard (1970).

Some of the more notable features of the present method may be summarized as follows:

(1) Randomness depicted by the spectral densities, probabilty densities and intercorrelations amongst various variables such as water surface elevation

and velocities and accelerations in x and y directions at several points have been fully represented.

(2) Nonlinearities correct up to second order are included.

(3) Phases of the nonlinear contributions are retained.

(4) Any reasonable form of the directional energy spectrum for a realistic sea can be simulated.

(5) The skewness of the simulated water surface displacement is realistically represented without any artificial means. The skewnesses of other variables of interest are also maintained.

(6) The total wave force is computed by considering the appropriate displacement of the free surface.

A set of very efficient Fortran programs have been developed to implement the above simulation method. In the last chapter some of the many important results derived from the simulation method were presented and discussed. The methods of Chapter 5 have been applied to simulate the linear and nonlinear realizations of the sea surface for the Bretschneider spectrum and four different directional spreads. The nonlinearity represented by the skewness has been computed in each case. It was found that the skewness is greatest for a narrow directional spread because for the given two wave numbers the skewness kernel is largest for small included angles. The reasons for this phenomenon and the possibile occurrence of negative skewness in the field have been discussed.

The simulation method has been further applied to compute total wave forces on a single pile and a multiple pile group. The total force on a pile reduces by a factor of 1 to 0.61 with the increase in the directional spread of the energy spectrum from unidirectional to omnidirectional. For the four pile group with 60 feet separation the reduction factors are similar to those for the single pile case. These results are nearly the same as those obtained by the Hybrid method (Dean 1977) for a drag dominant case. For the four pile group with one pile at each corner of a 300 feet square the reduction factor varies from 0.79 to 0.39 for the directional spectrum varying from unidirectional to omnidirectional respectively.

These results suggest that considerable economy can be realized in the design of large structures by incorporating the directional effects of a real sea.

REFERENCES

Birkhoff, G., and Kotik, J., "Fourier Analysis of Wave Trains," Gravity Waves, National Bureau of Standards, Circular No. 521, 1951, pp. 221-234.

Borgman, L. E., "Random Hydrodynamic Forces on Objects," Annals of Mathematical Statistics, Vol. 38, 1967, pp. 37-51.

Borgman, L. E., "Spectral Analysis of Ocean Wave Forces on Piling," J. Waterways and Harbor Div., Proc. ASCE, V. 93, WW2, 1967, pp. 126-156.

Borgman, L. E., "Directional Spectra Models for Design Use," Preprint First Offshore Technology Conference, V. I, Paper No. OTC 1069, May, 1969, pp. 721-747.

Borgman, L. E., "Statistical Model for Ocean Waves and Wave Forces," in Advances in Hydrosciences, Vol. 8, ed. by V. T. Chow, Academic Press, New York, 1972, pp. 139-181.

Chappelear, J. E., "On the Description of Short-Crested Waves," Beach Erosion Board Technical Memorandum No. 125, 1961.

Chappelear, J. E., "Direct Numerical Calculation of Wave Properties," Journal Geophysical Research, Vol. 66, No. 2, February, 1961, pp. 501-508.

Dalrymple, R. A., "A Finite Amplitude Wave on a Linear Shear Current," Journal of Geophysical Research, Vol. 79, No. 30, October 20, 1974.

Dean, R. G., "Stream Function Representation of Nonlinear Ocean Waves," Journal of Geophysical Research, V. 70, No. 18, September 15, 1965, pp. 4561-4572.

Dean, R. G., "Directional Spectra: Some Applications and Storage," Proc. of International Symposium on Ocean Wave Measurement and Analysis, ASCE New Orleans, September 9-11, 1974, pp. 23-39.

Dean, R. G., "Hybrid Method of Computing Wave Loading," Proceedings of Ninth Offshore Technology Conference, Paper No. OTC 3029, May 1977, pp. 483-492.

Dean, R. G. and Aagaard, P. M., "Wave Forces: Data Analysis and Engineering Calculation Method," Journal of Petroleum Technology, March 1970, pp. 368-375.

Gallagher, B., "Generation of Surf Beat by Nonlinear Wave Interactions," Journal of Fluid Mechanics, V. 49, 1971, pp. 1-20.

Hasselmann, K., "On the Nonlinear Energy Transfer in a Gravity Wave Spectrum, Part I, General," Journal of Fluid Mechanics, V. 12, 1962, pp. 481-500.

Hasselmann, K., "On the Nonlinear Energy Transfer in a Gravity-Wave Spectrum, Part 2, Conservation Theorems, Wave Particle Correspondence, Irreversibility," Journal of Fluid Mechanics, Vol. 15, 1963, pp. 273-281.

Hasselmann, K., "On the Nonlinear Energy Transfer in a Gravity-Wave Spectrum, Part 3, Computation of the Energy Flux and Swell-Sea Interaction for a Neumann Spectrum," Journal of Fluid Mechanics, Vol. 15, 1963, pp. 383-398.

Hudspeth, R. T., "Prediction of Wave Forces from Nonlinear Random Sea Simulations," Ph.D. Dissertation submitted to the University of Florida, June 1974.

Hudspeth, R. T., "Wave Force Predictions from Nonlinear Random Sea Simulations," Proceedings 1975 Offshore Technology Conference, Paper No. OTC 2193, May 1975, pp. 471-485.

Hudspeth, R. T., Dalrymple, R. A., and Dean, R. G., "Comparison of Wave Forces Computed by Linear and Stream Function Methods," Preprints 1974 Offshore Technology Conference, Vol. II, Paper No. OTC 2037, May 6-8, 1974, pp. 17-32.

Kinsman, B., "Surface Waves at Short Fetches and Low Wind Speeds - a Field Study, Vols. 1-3," Chesapeake Bay Institute, Technical Report No. XIX, Ref. 60-1, 1960, 581 pp.

Laitone, E. V., "The Second Approximation of Cnoidal and Solitary Waves," Journal of Fluid Mechanics, Vol. 9, Part 3, November, 1960, pp. 430-444.

Longuet-Higgins, M. S., "Statistical Properties of a Moving Wave-Form," Proceedings Cambridge Philosophical Society, Vol. 52, No. 2, 1956, pp. 234-245.

Longuet-Higgins, M. S., "The Statistical Analysis of a Random, Moving Surface," Phil. Trans. Royal Society, Series A, Vol. 249, February, 1957, pp. 321-387.

Longuet-Higgins, M. S., "The Statistical Geometry of Random Surfaces," Proc. Symposium Applied Mathematics, Vol. 13, 1961, pp. 105-143.

Longuet-Higgins, M. S., "Resonant Interactions Between Two Trains of Gravity Waves," Journal of Fluid Mechanics, Vol. 12, No. 3, 1962, pp. 321-332.

Longuet-Higgins, M. S., "The Effect of Nonlinearities on Statistical Distributions in the Theory of Sea Waves," Journal of Fluid Mechanics, Vol. 17, 1963, pp. 459-80.

Malhotra, A. K., and Penzien, J., "Response of Offshore Structures to Random Wave Forces," Journal of Structural Division, Proc. American Society of Civil Engineers, Vol. 96, No. ST10, October, 1970, pp. 2155-2173.

Phillips, O. M., "On the Dynamics of Unsteady Gravity Waves of Finite Amplitude, Part 1. The Elementary Interactions," Journal of Fluid Mechanics, Vol. 9, No. 2, 1960, pp. 193-217.

Phillips, O. M., "On the Dynamics of Unsteady Gravity Waves of Finite Amplitude, Part 2, Local Properties of a Random Wave Field," Journal of Fluid Mechanics, Vol. 11, No. 1, 1961, pp. 143-155.

Pierson, W. J., Jr., "Wind Generated Gravity Waves," Advances in Geophysics, Vol. 2, Academic Press, 1955, pp. 93-178.

Pierson, W. J., Jr., and Holmes, P., "Irregular Wave Forces on a Pile," Journal of Waterways and Harbor Division, Proc. American Society of Civil Engineers, Vol. 91, No. WW4, 1965, pp. 1-10.

Reid, R. O., "Correlation of Water Level Variations with Wave Forces on a Vertical Pile for Nonperiodic Waves," Proc. VI Conference on Coastal Engineering, Santa Barbara, 1958, pp. 749-786.

Rice, S. O., "Mathematical Analysis of Random Noise," Bell System Technical Journal, Vol. 23, 1944, pp. 282-332, and Vol. 24, 1945, pp. 46-156. Reprinted in Selected Papers on Noise and Stochastic Processes, ed. by N. Wax, Dover Publications Inc., New York, 1954, pp. 133-294.

Rudnick, P., "Correlograms for Pacific Ocean Waves," Proceedings of Second Berkeley Symposium on Mathematical Statistics and Probability, Berkeley, 1951, University of California Press, pp. 627-638.

Skjelbreia, L., and Hendrickson, J. A., "Fifth Order Gravity Wave Theory," Proceedings of Seventh Conference on Coastal Engineering, Chapter 10, 1961, pp. 184-196.

Tick, L. J., "A Nonlinear Random Model of Gravity Waves I," Journal of Mathematics and Mechanics, Vol. 8, 1959, pp. 643-651.

Tick, L. J., "The Estimation of 'Transfer Functions' of Quadratic

Systems," Technometrics, Vol. 3, No. 4, November, 1961, pp. 563-567.

Tick, L. J., "Nonlinear Probability Model for Ocean Waves," in Ocean Wave Spectra, Prentice Hall Inc., Englewood Cliffs, N. J., 1963, pp. 163-169.

Tung, C. C., and Huang, N. E., "Wave-Current Force Spectra," Center for Marine and Coastal Studies Report No. 72-2, North Carolina State University, Raleigh, N. C., December 1972.

Tung, C. C., and Huang, N. E., "Influence of Current on Some Statistical Properties of Waves," Center for Marine and Coastal Studies Report No. 73-3, North Carolina State University, Raleigh, N. C., December 1973.

Von Schwind, J. J., and Reid, R. O., "Characteristics of Gravity Waves of Permanent Form," Journal of Geophysical Research, Vol. 73, No. 3, January, 1972, pp. 420-433.

Wheeler, J. D., "Method for Calculating Forces Produced by Irregular Waves," Preprints 1969 Offshore Technology Conference, Vol. I, Paper No. OTC 1007, May 18-21, 1969, pp. 83-94.